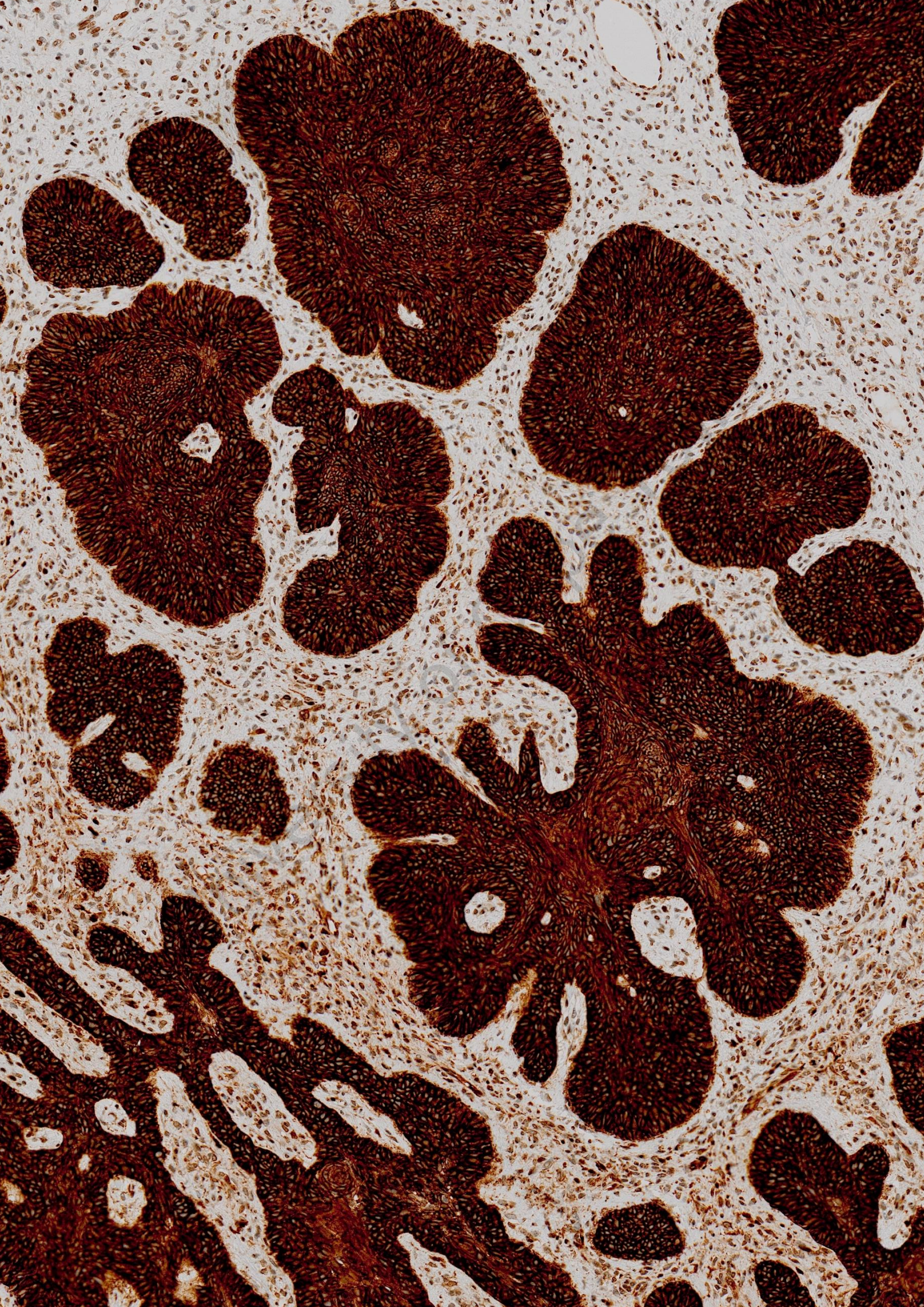

Basal cell carcinoma: A digital immunohistochemical analysis of BCL-2, p53 and CD138 expression in low- and high-risk histological patterns

by

Janet de Stadler

RBLJAN001

Supervisor: Dr Riyaadh Roberts

Co-supervisor: Dr Amsha Ramburan

A dissertation submitted to the Faculty of Health Sciences

University of Cape Town

In partial fulfilment of the requirements

for Master of Medicine (Anatomical Pathology)

January 2023

Declaration

I, Janet Lyndsay de Stadler, hereby declare that the work on which this dissertation/thesis is based is my original work (except where acknowledgements indicate otherwise) and that neither the whole work nor any part of it has been, is being, or is to be submitted for another degree in this or any other university.

I empower the university to reproduce for the purpose of research either the whole or any portion of the contents in any manner whatsoever.

Signature:

Signed by candidate

Date: 09/01/2023

Dedication

This dissertation is dedicated to my late grandparents: Professor John Cameron Holmes, Mrs Ellen Miller Holmes, Mr Antonio Xavier Gomez Rebelo and Mrs Grace Rebelo; as well as Ms Mary Thelander.

For their love, guidance, and financial support.

Acknowledgements

I wish to acknowledge the following individuals for the roles they played in my thesis:

- My supervisor, Dr Riyaadh Roberts, for sharing his research ideas with me and agreeing to supervise my MMed. In addition, for his ongoing guidance each step of the way, including the critical appraisal of my protocol and dissertation writing, as well as assistance with data collection.
- Dr Amsha Ramburan, my co-supervisor, for her critical appraisal of my dissertation and valuable feedback.
- Mr Jurgen Geitner, for performing whole slide scanning and digital analysis.
- Mr Raymond Kriel, for assisting with the immunohistochemical staining.
- Ms Nafiesa Allie, for answering all my antibody related questions and for assistance with the protocols and optimisation of the primary antibodies.
- Mr Samir Jacobs and his team, for the retrieval of slides and tissue blocks from archives.
- Dr Nadia Ikumi for her assistance with the statistical analysis and enthusiasm for my research. Ms Michelle Henry and Mr Ebrahim Steenkamp for their statistical support.
- My colleagues in D7, for their support during the write-up process of my dissertation.
- Dr Jarryd Lunn, for his assistance with Mendeley in the early part of my dissertation.
- The National Health Laboratory Services, for funding of my research through the Research Trust grant.
- My family and friends for their endless encouragement and support.
- My husband, Shane de Stadler, the master encourager, and ultimate data capturer. Thank you for always encouraging my dreams and for the sacrifices you have made along the way.

Abstract

Introduction

Basal cell carcinoma (BCC) is the leading cancer in males and the second commonest cancer in females in South Africa. The cost to the health sector is expected to rise given the increasing global incidence rates, particularly of aggressive BCCs. Improved understanding of BCC is paramount to enhance early detection and screening which could potentially offset these rising costs. Specific histological patterns of BCC have been defined as high-risk for recurrence by the World Health Organisation. The different BCC subtypes are not simply architectural patterns but may represent differences in aetiopathogenesis and protein expression, and impact future targeted therapies. Upregulation of the Hedgehog pathway and *TP53* inactivation are the two most common events in the development of BCCs. High-risk BCC patterns have been observed to show increased expression of tumoural p53 and decreased expression of BCL-2 and CD138 compared with low-risk patterns. In addition, peritumoural expression of CD138 has been noted to increase in the stroma of high-risk BCCs. These observations have largely been made by light microscopy rather than with digital analysis.

Methods

A retrospective, laboratory-based, observational study of 104 BCCs excised between January 2016 to December 2019 was undertaken at the National Health Laboratory Services (NHLS) Anatomical Pathology Laboratory, Groote Schuur Hospital (GSH), Cape Town, South Africa. BCCs with either pure or mixed histological patterns were included. Immunohistochemical staining for p53, BCL-2 and CD138 was performed, followed by whole slide scanning and digital analysis of set quantitative parameters using QuPath software. Statistical analyses were performed using STATA version 17.0 and R.

Results

104 BCCs were evaluated. Sixty were categorised as low-risk and 44 as high-risk BCCs.

BCL-2 was expressed in 78.33% of BCCs, most commonly with weak intensity staining. High-risk BCCs had significantly lower BCL-2 labelling compared to low-risk BCCs ($p = 0.04$). Overall, 90.83% of BCCs expressed p53. Expression was most commonly of strong intensity. There was no significant difference in mean p53 scores between low-risk and high-risk BCCs ($p = 0.82$).

All BCCs expressed tumoural CD138 with either moderate or strong intensity, and the mean expression was higher in low-risk compared to high-risk BCCs ($p = 0.0035$). In addition, high-risk BCCs showed increased stromal expression of CD138 compared to low-risk BCCs ($p < 0.0001$).

Conclusion

BCL-2 is expressed by most BCCs in keeping with the cell of origin, albeit with weak and focal staining. The lower expression of BCL-2 seen in high-risk BCCs may be the result of loss of heterozygosity of the *BCL-2* gene or due to down regulation of the BCL-2 protein due to other mutations. In addition, p53 is expressed by the majority of BCCs regardless of risk category and is typically strong and diffuse. This may reflect either underlying *TP53* mutations or an upregulation of WT p53 due to oncogenic stressors. Furthermore, the lower expression of CD138 in high-risk BCCs is thought to be due to a decrease in tumoral protease activity and/or transcriptional- or posttranscriptional regulation. Lastly, the increased expression of CD138 in the stromal matrix of high-risk BCCs is in keeping with its recognition as a poor prognostic indicator in most tumour types.

Table of contents

List of Tables

List of Figures

List of Annexures

Abbreviations

BCC	Basal cell carcinoma
BCL-2	B-cell lymphoma-2
DNA	Deoxyribonucleic acid
ECM	Extracellular matrix
FDA	Food and Drug Administration
FFPE	Formalin fixed paraffin embedded
GLI-1	Glioma-associated oncogene family member 1
GSH	Groote Schuur Hospital
H&E	Haematoxylin and eosin
HH	Hedgehog
HREC	Human Research Ethics Committee
IHC	Immunohistochemistry
ISGYP	The International Society of Gynaecological Pathologists
LM	Light microscopy
mRNA	Messenger ribonucleic acid
MMed	Masters of Medicine
NBCCS	Nevoid basal cell carcinoma syndrome
NCCN	National Comprehensive Cancer Network
NCR	National Cancer Registry
NHLS	National Health Laboratory Services
NMSC	Non-melanoma skin cancer
PTCH-1	Patched homolog 1
PUVA	Psoralen plus ultraviolet radiation type A
SCC	Squamous cell carcinoma
SD	Standard deviation
SHH	Sonic Hedgehog
SMO	Smoothened
TAH	Tygerberg Academic Hospital
UCT	University of Cape Town

UVB	Ultraviolet radiation type B
UVR	Ultraviolet radiation
WHO	World Health Organisation
WSI	Whole slide imaging
WT	Wild-type
XP	Xeroderma pigmentosum

Chapter 1: Literature review

1.1 Introduction

The World Health Organisation (WHO) defines basal cell carcinoma (BCC) as a carcinoma arising from the basal cells of either the hair follicle or interfollicular epidermis.(1) Some of the earliest described cases in literature date back to the early 1800s in Ireland, when it was observed that BCCs were slow growing tumours with a low metastatic potential.(2) BCC is now recognised as the most common cancer in White populations globally, with incidence rates exceeding 1000/100 000 person-years in high risk regions such as Australia. Many countries report a rise in the incidence of BCC despite concerns of underreporting.(3,4)

In South Africa, according to the 2014 National Cancer Registry (NCR), BCC is the leading cancer in males and the second commonest cancer in females across all four ethnic groups combined; with age standardised incidence rates of 55.55 and 28.59/100 000 person-years respectively.(5) Although these rates are lower than many other countries,(3) when stratified according to ethnicity and sex, the incidence increases dramatically to 223.19/100 000 person-years in White males, the most affected group.(5) Of the skin cancers, BCC is the most common across three of South Africa's ethnic groups (Asian, Coloured, and White populations) with the exception of the Black population.(6)

These results are reflected by a local study in the Western Cape Province of South Africa; where BCC was also the most common skin cancer across the White, Coloured and Asian ethnic groups in an analysis of malignant skin biopsies at Tygerberg Academic Hospital (TAH).(7) Findings of a study in the Northern Cape Province of South Africa found BCC to be the commonest skin malignancy in the White population only; although possible underestimation of BCC amongst the other ethnic groups due to the lack of histologic confirmation was a recognised limiting factor of the study.(8)

The cost of non-melanoma skin cancer (NMSC) in 2015 was estimated at ZAR 81.6 million per annum; a costly expense related to the treatment and follow-up of patients.(9) Although cost of treatment per BCC is not as high as those of other cancers, the high number of patients

translates into increased overall cost.(10) In addition, although the recurrence rates of BCC in South Africa are currently low (3.7% over three years)(11) there is recent data from Sweden showing that there is a faster increase in the incidence of aggressive compared with non-aggressive BCC.(4) This was recognised as an economic health challenge in a developed nation;(4) and is of great concern given the frequent delay in BCC diagnosis of more than one year.(11,12) Mohs micrographic surgery is the gold standard of treatment for high-risk BCC, but is expensive compared to other treatment options with limited availability in certain South African settings.(11,12) Given these factors, BCCs are currently relevant and costly to the South African health sector, with expenditure likely to increase in the future. Early detection by screening and appropriate treatment, including emerging therapies, can potentially off-set this cost.(12,13)

1.2 Risk factors

BCC arises due to interactions of genetic, phenotypic and environmental factors; with each factor contributing a small, incremental risk to its' development.(14)

1.2.1 Ultraviolet radiation (UVR)

UVR, particularly intense and intermittent solar UV type B (UVB) exposure in childhood, is a major environmental risk factor for BCC.(14,15) Exposure may occur outdoors due to occupational or recreational activities; or alternatively due to indoor tanning or therapy, such as a high number of psoralen plus UVA radiation (PUVA) or UVB treatments for psoriasis (> 100 and 300 treatments respectively).(14) Chronic actinic damage; including melanocytic nevi, freckles, solar elastosis, solar lentigines and actinic keratosis are also predictors of BCC.(10) The association of UVR and BCC is borne out by the following observations:

i) The majority of BCCs occur in sun-exposed regions, such as on the head and neck (53.5-95.9%).(4,15–17) Similar findings were reported across all four South African ethnic groups in both males and females (59.09 – 68.8%).(6,11)

ii) Melanin plays an important photoprotective role.(15) BCCs increase in frequency with decreasing skin pigmentation; occurring most commonly in White, followed by Coloured, Asian and Black ethnic groups in a South African analysis.(6) Within the White population; Fitzpatrick phototype I and II skins are more at risk than III and IV skins.(15) The Fitzpatrick scale is used to type skin colour according to its' tanning potential.(18)

iii) Variations in incidence rates between countries are also attributed to differences in geographic latitude and altitude; with decreasing latitude and increasing altitude being associated with increased rates of BCC due to more intense UVR exposure(3,4) South Africa has a low latitude (22-35^0) and a high inland altitude.(6)

Different types of sun exposure may influence BCC subtype. For example, superficial BCC is associated with a truncal location; a site which is generally sun unexposed or receives intermittent sun exposure. Other BCC subtypes, such as nodular, are proposed to be associated with cumulative sun-exposure.(10,19) That being said, as an overall group, BCC are more strongly associated with intermittent rather than constant sun-exposure. In addition, unlike

squamous cell carcinomas (SCC), the risk of BCC does not continue to rise with a cumulative duration of sun exposure; but instead reaches a plateau after a set number of hours.(20)

1.2.2 Other confirmed environmental risk factors

Other important environmental risk factors include the exposure to ionising radiation from a variety of sources, particularly if young of age at the time of exposure or having a susceptible phenotypic skin type; chronic arsenic exposure; and systemic immunosuppression (persons with chronic immunosuppression and increased longevity such as with organ transplant recipients)(14)

1.2.3 Phenotypic risk factors

Phenotypic risk factors include increasing age, attributed to an accumulation of UVR-induced deoxyribonucleic acid (DNA) damage over time and due to reduced repair capabilities; personal and/or family history of skin cancer; fair skin, inability to tan, light hair and eye colour (Fitzpatrick phototypes I and II), and male sex.(5,10,14) In a local South African study, the median age of patients with BCC was 70 years and there was a slight male predominance (55.7%).(11) Although a study in France showed a slight predominance of BCC in females; they attributed this to the increased age of the study population with males having more likely succumbed to other illnesses, thus skewing the data.(21) However, the true incidence rate in females is noted to be increasing, for various proposed reasons including an increase in sunbed use, a change in sunbathing habits and clothing.(4,10)

1.2.4 Genetic risk factors

Certain germline mutations are associated with increased risk and early onset of BCCs. These include Xeroderma pigmentosum (XP); autosomal dominant naevoid basal cell carcinoma syndrome (NBCCS) and other genodermatoses.(10,13,22) In addition, germline polymorphisms also contribute to BCC risk. These include variations in *melanocortin 1 receptor* gene; single nucleotide polymorphisms in the pigmentation pathway e.g. tyrosine or agouti signalling protein; amongst other genes, such as those involved in detoxification of oxidative stress products.(13,14)

1.2.5 Other

In one study, 28.2% of patients did not have any reported sun exposure, other UVB risk factors, or a predisposing genetic syndrome.(15) Furthermore, not all BCCs occur in chronically sun-exposed sites.(15) Unusual sites for BCC, deemed unrelated to sun-exposure, occur at a rate of around 1%; and include sites such as the nipple-aerola complex.(23) Thus aetiological pathways likely differ between BCCs; highlighting that this is not a homogeneous tumour group.(24)

1.3. Molecular pathogenesis

BCCs have a higher burden of mutations than any other cancer.(24) Many of these mutations carry the UV signature of cytosine to thymine substitution, consistent with UVA- or UVB-induced DNA damage – as discussed under BCC risk factors. Mutations translate into a change of function of housekeeping genes, tumour suppressor genes, and proto-oncogenes; and eventual transformation of basal keratinocytes into BCC.(25) The high mutation burden may account for the slow progression of most BCCs, possibly by increasing tumour susceptibility to the host immune system.(24) Various established and novel pathways have been identified in the development of BCC; the most well-established of which is the upregulation of the Hedgehog (HH) pathway (Figure 1.1).(25)

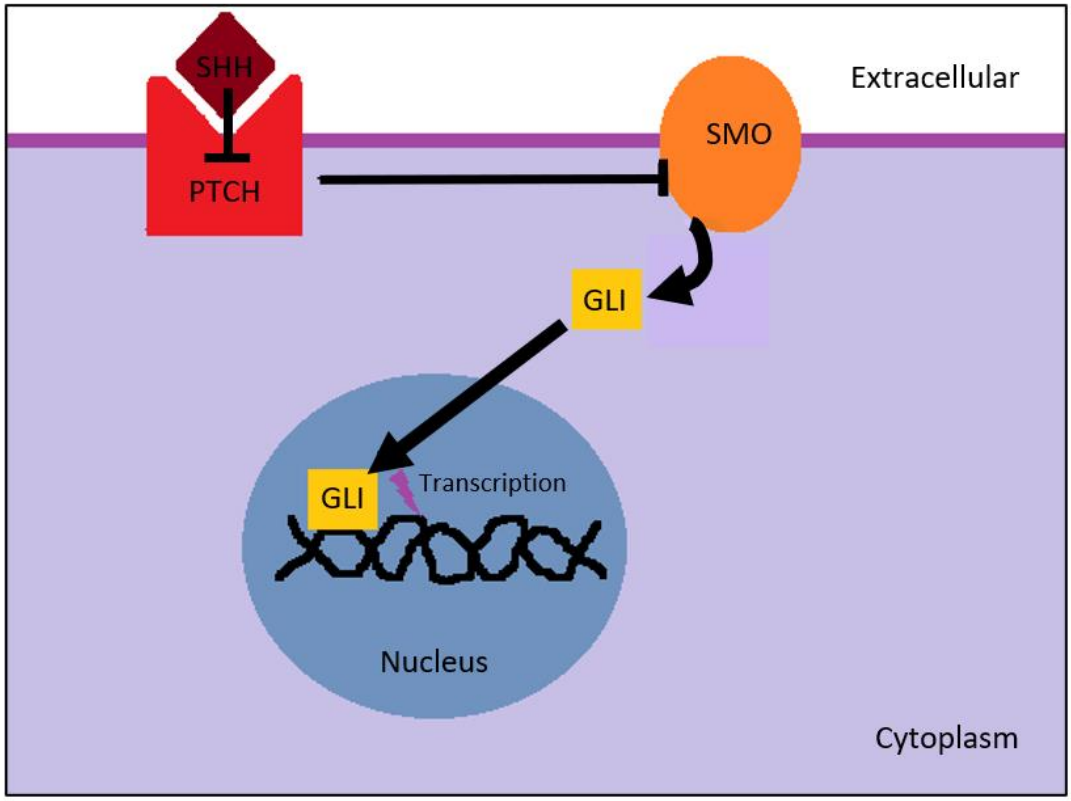

Figure 1.1 The Hedgehog Pathway. Adapted from Marzuka and Book.(26)

The Sonic Hedgehog (SHH) ligand binds the patched homolog 1 (PTCH) transmembrane protein and inhibits it. This releases suppression of smoothened (SMO) enabling GLI activation and translocation to the nucleus and subsequent gene transcription.

The HH pathway is a developmental pathway essential for the maintenance of the stem cell population of the skin, as well as for the development of hair follicles and sebaceous glands.

Activation of this pathway due to mutations in various components drives tumourigenesis; with approximately 90% of BCCs having a molecular aberration in one component of this pathway. Key proteins involved in this pathway include patched homolog 1 (PTCH-1), smoothened (SMO) and glioma-associated oncogene family member 1 (GLI-1).[24]

The second most common genetic event in BCC pathogenesis is *TP53* inactivation.[23] The *TP53* tumour suppressor gene encodes the p53 protein. Mutations in this gene are recorded in up to 70% of BCC, and are associated with an increase in SMO protein expression and subsequent HH pathway signalling.(24,25)

1.4 Classification and microscopy of BCC

The current classification of BCC has expanded since the first histologic descriptions by Sloane in the 1970s(27) and later by Sexton, who described some of the major histologic patterns still recognised today.(28) The WHO adopted the National Comprehensive Cancer Network (NCCN) classification; and divides BCC into low- and high-risk subtypes according to risk of recurrence. The low-risk subtypes include nodular, superficial, pigmented, infundibulocystic and fibroepithelial patterns. The high-risk subtypes include basosquamous, sclerosing/ morphoeic, infiltrating, micronodular and BCC with sarcomatoid differentiation.(1) Other classification systems also exist.(29) The most frequently and consistently reported patterns of BCC in the literature are nodular (78.7%) followed by superficial BCC (15.1%). Other patterns follow in variable, but consistently lower frequencies.(10,15,21,28) Nodular BCC are also the most frequent subtype (74%) in the South African context.(11)

All BCCs are characterised by a proliferation of variably arranged basaloid cells with scanty cytoplasm, hyperchromatic nuclei, and peripheral palisading of cells (Figure 1.2).(1,29) The surrounding stroma is often fibromucinous(29) and stromal retraction clefts as well as lichenoid inflammation may be present.(10,28) Unique features define the different subtypes (Table 1.1). Mixed patterns also occur,(10,28,29) in which case the most aggressive subtype dictates management.(10)

The different BCC subtypes are not simply architectural patterns, but are postulated to represent phenotypic variation due to a potential difference in underlying aetiopathogenesis.(21) As a result, studies have explored differences in various protein expression between the different subtypes by use of immunohistochemistry (IHC). The following section details the current literature on three of these proteins, namely B-cell lymphoma-2 (BCL-2), p53 and CD138.

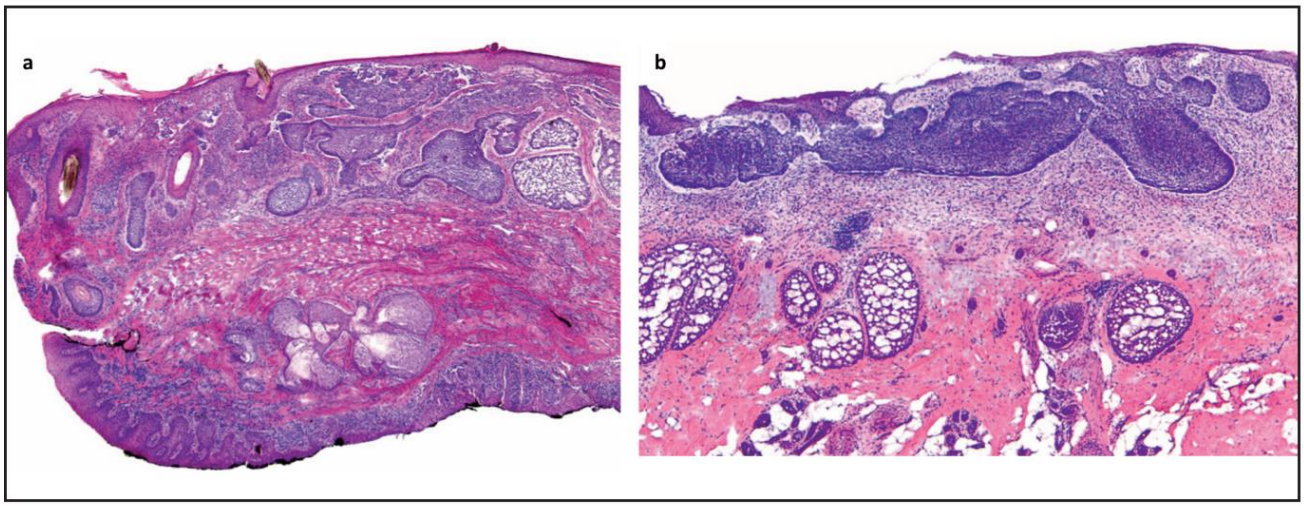

Figure 1.2. Histological features of basal cell carcinoma: two low-risk histological subtypes, nodular (a) and superficial (b) are displayed in the above figure and both demonstrate a proliferation of basaloid cells with peripheral palisading. Adapted from Marzuka and Book.(26)

Table 1.1 Main histological features of the basal cell carcinoma subtypes

Low risk	
Nodular (Variants: nodulocystic, adenoid and keratotic)	Well circumscribed. Large, variably sized and -shaped, basaloid lobules in the dermis. With or without amyloid deposition, keloid-stroma, central keratinisation, central cystic dilation, cribriform/ reticulate arrangement or ulceration.(1,30)
Superficial (multifocal)	Focal, small nests of basaloid cells connected to the inferior aspect of the epidermis, follicles or ducts. Lobules <1mm and confined to the papillary dermis.(1,30)
Fibro-epithelial (Fibro-epithelioma of pinkus)	Fenestrated arrangement of basaloid cells in 2-3 cell thick strands projecting downward into the dermis with a surrounding fibrotic stroma.(30)
BCC with adnexal differentiation (includes infundibulocystic)	Infundibulocystic: anastomosing cords and trabeculae of basaloid cells with peripheral palisading and scant stroma in the dermis; with interspersed small infundibular cysts.(1,30)
Pigmented	Different histological subtypes (nodular or superficial) with melanin in tumour cells, dendritic melanocytes or within stromal macrophages.(1,30)
High risk	
Infiltrative	Irregular and permeative jagged nests of basaloid cells (>5-8 cells thick), with little peripheral palisading and intervening loose, mucinous stroma.(1,30)
Sclerosing/ morphoeic (Morpheaform)	Irregular and comprising of thin, compressed cords (1-5 cells thick) of basaloid cells with no peripheral palisading; and a dense, sclerotic stroma.(1,30)
Micronodular	Multiple small (<0.15mm diameter), uniform, diffusely infiltrative basaloid nests with limited peripheral palisading in the dermis; comprising >50% of the tumour. Lacks retraction artifact.(1,30)
Basosquamous (metatypical)	Infiltrative architecture with areas of malignant squamous differentiation – focal or scattered throughout.(1,30)
BCC with sarcomatoid differentiation (metaplastic)	Contains malignant mesenchymal component of various differentiations e.g. leiomyosarcoma.(1,30)

1.5. Protein expression in BCC subtypes

1.5.1 BCL-2

1.5.1.1 Defining BCL-2 and its expression in human skin

BCL-2 is an intracellular transmembrane protein encoded by the *BCL-2* proto-oncogene on chromosome 18.(31) BCL-2 protein is expressed in many tissue types and localises to the nuclear membrane, mitochondria and endoplasmic reticula.(32) Expression in the skin was demonstrated in basal keratinocytes and epithelia of the outer root sheath of the hair isthmus and infundibulum. In contrast, differentiating suprabasilar keratinocytes are negative for BCL-2.(31,33) BCL-2 is also expressed in dermal lymphocytes, which serve as a useful internal control in immunohistochemical studies.(31) There is no staining difference observed between formalin fixed or fresh frozen specimens.(32)

1.5.1.2 BCL-2 expression in BCC

BCL-2 is frequently upregulated in BCCs; in keeping with its' cell of origin. Whilst rates of BCL-2 expression are reported to vary in the literature (Annexure 1.1), three papers showed positivity in 93.4 to 100% of BCC.(34–36) It is proposed that the increased expression of BCL-2 in BCC extends cell survival rather than driving proliferation; and thus tumoral growth is characteristically slow rather than rapid.(34) Earlier studies speculated that BCL-2 expression confers a growth advantage to slowly proliferative neoplastic cells through evasion of apoptosis; and promotes the development of BCC through the progressive acquisition of additional mutations.(31,37) However, this has been refuted by a mouse model which showed that increased BCL-2 expression in basal keratinocytes did not promote tumourigenesis and paradoxically delayed the onset as well as slowed the progression of subsequent UVB and chemically induced skin tumours.(38) This supports the observation that BCL-2 expression in BCC is likely attributed to the cell of origin(35) rather than being the equivalent of a driver mutation leading to tumourigenesis; and that preservation of BCL-2 expression may account for the indolent, slow growth of most BCC.(32,39) BCL-2 expression seems to be independent of aetiology; with expression shown in sporadic BCC, XP-associated BCC, and BCC induced by arsenical exposure.(40,41) As such, several studies have developed scoring systems for evaluating proportion with or without intensity of BCL-2 expression (Annexure 1.2).(34–37,39,42–47)

BCL-2 immunopositivity is not homogeneous in BCCs and some cells may be completely negative in the tumour. One study comparing BCC and trichoblastoma noted that BCC may show positive and negative nests within the same tumour and attributed the negative nests to areas of follicular differentiation.(48) In addition, there is no characteristic pattern of BCL-2 expression within the tumour nests, with the cells in the center and periphery staining equally.(33)

1.5.1.3 BCL-2 expression in histological subtypes of BCC

BCL-2 expression also shows variation between the histologic subtypes of BCC. This was observed in a study comparing low-risk (superficial and circumscribed) with high-risk (infiltrative, basosquamous and sclerosing/morphoeic) BCC subtypes. The proportion of tumoural cells showing BCL-2 expression was noted to be greater in low-risk BCC subtypes.(37) Subsequently, several additional studies showed a reduction in both the proportion of BCL-2 expression(33,35,36,49) and the intensity in high-risk BCC subtypes.(35) However, not all high-risk BCC subtypes show equal reduction in BCL-2 expression. Two studies noted that sclerosing/ morphoeic BCC showed the greatest reduction in BCL-2 expression,(39,42) whereas another study demonstrated that micronodular BCC have both low and high BCL-2 expression.(34) Furthermore, BCC with mixed histologic components showed heterogeneity of BCL-2 staining due to differential expression in the low- and high-risk histologic components.(34)

A local South African study further evaluated the differential expression of BCL-2 between aggressive and non-aggressive BCC stratified by defined clinical and pathological criteria. The study found that low BCL-2 expression was predictive of aggressive BCC, independent of the histologic subtype, with a statistically significant difference between aggressive (88%) and non-aggressive groups (10%).(34) In addition, low BCL-2 expression was observed in a small number of metastatic BCC. A study evaluating BCC at the primary and metastatic sites found that none of the metastatic BCC had high BCL-2 expression.(47) The reason for this apparent differential expression of BCL-2 between BCC is not clear. However, loss of heterozygosity of the *BCL-2* gene on chromosome 18q was observed in a small subset of BCC and could account for the reduced expression of BCL-2 in some cases.(42) In addition, the accumulation of additional genetic mutations in high-risk BCC subtypes may lead to down regulation of BCL-2 and increased aggressive behaviour.(49)

In contrast to the above, several studies have found no association between BCL-2 expression and high-risk histologic subtypes; with one study concluding that BCL-2 cannot reliably predict BCC behaviour.(47) In some of these studies, high BCL-2 expression was observed in high-risk BCC subtypes. One study found strong BCL-2 expression in 40% of sclerosing/ morphoeic and 80% of basosquamous BCC;(47) a second study could not account for strong BCL-2 expression in three infiltrating BCC;(35) and a third study found 80% of the sclerosing/ morphoeic BCC to have 4+ BCL-2 expression.(44) Conversely, other studies have observed low BCL-2 expression in low-risk BCC subtypes. One study found that one third of solid (low-risk) BCC showed low BCL-2 expression,(42) while another found just under two thirds of superficial BCC to be negative for BCL-2 – although the sample size was small.(44) A third study found that 38% of low-risk BCC showed an absence of BCL-2 expression altogether (Annexure 1.1).(43)

1.5.1.4 Clinical significance of BCL-2 expression in BCC

Regardless of these conflicting results, the difference in BCL-2 expression between BCC subtypes has been acknowledged and interpreted as confirmation that BCCs are a group of heterogeneous tumours despite their common cell of origin.(34) Importantly, functional BCL-2 in BCC can be inhibited to induce tumour regression. This is highlighted by a study showing that the application of topical imiquimod resulted in BCC cells becoming more susceptible to apoptosis through decreased BCL-2 expression alone. The mechanism of action of imiquimod is not well understood; however topical imiquimod has proven efficacy in the treatment of superficial BCCs, which often overexpress BCL-2. In addition, reduced BCL-2 expression in response to topical imiquimod was noted even in infiltrating BCC, a high-risk subtype.(50) We found no studies correlating immunohistochemical BCL-2 scores on biopsy with outcome after topical imiquimod therapy in the English literature.

1.5.2 p53

1.5.2.1 Defining p53

p53 is an intracellular DNA-binding protein encoded by the *TP53* gene on chromosome 17p and has six major domains required for transcriptional activation.(51,52) The protein is maintained at low intracellular levels under normal cell conditions and increases in response to cell stress signals via its' upregulation and stabilisation.(51) The subsequent downstream intracellular response is complex and interconnected with pleiotropic results. Some propose

the end result is regardless of cell-type and context, while others hypothesize that its' dependent not only on the cause for p53 activation but also the lineage, differentiation, and state of the cell; as well as the pattern of signalling, for example a steady or pulsed release of the p53 protein.(51,52)

Despite extensive publications on this topic, research is still ongoing to better understand the function of p53.(51) p53 function can be broadly categorised into cell autonomous and non-cell autonomous tumour suppression (Table 1.2);(52) relying on both nuclear and cytoplasmic p53 localisation.(53) The most well-established function of p53 is as the "Guardian of the genome" with the promotion of cell cycle arrest to assist in DNA repair; cellular senescence; and apoptosis. This enables the prevention of mutant cell survival, proliferation and/or promotes repair – thus preventing tumourigenesis.(51) More recently elucidated processes include embryonic development, tissue remodelling, cell metabolism, oxidative stress response, autophagy and ferroptosis.(51) In addition, p53 has also been shown to inhibit epithelial-to-mesenchymal transition.(52) Furthermore, p53 expression may result in opposing outcomes depending on the tissue type(51) and, contrary to its tumour suppressor function, may even promote tumour growth by modulating metabolism.(52)

Table 1.2 p53 tumour suppressor function categories

Cell autonomous tumour suppression		Non-cell autonomous tumour suppression
Transactivation - dependent	Transactivation - independent	E.g. tumour micro-environment
E.g. Cell cycle arrest	E.g. Apoptosis	

1.5.2.2 Mutant p53

TP53 is the most frequently mutated gene in human cancer; with many types of *TP53* mutations and complex combinations described. The resultant phenotype includes partial or complete loss of function; selection of function; and even gain of function. Overall, the most frequent mutation combination is a missense mutation of the DNA-binding domain of one allele and a segmental deletion of the second allele.(51)

NMSC harbours unique *TP53* mutations.(54) BCCs harbour *TP53* mutations at a frequency of up to 70%;(24,25) although lower rates are reported in Asian populations.(42,55) Regardless of ethnicity, when mutations do occur the majority are missense and carry a UV signature.(24,54–56) Mutational hotspots are noted in BCC, and are often located in the central DNA-binding core domain. These include codon 177, 196 and 245.(13,25,55) These mutations arise early during the development of NMSC and are usually isolated, although several tumours harboured multiple mutations.(54) Other mutation types include transitions at non-dipyrimidine sites, transversions and less frequently silent and frameshifts mutations.(54) In addition, *TP53* mutations also occur in non-UV related BCC.(57,58) One study found that arsenic-related BCC carried *TP53* mutations; one silent and one transition.(58) The resultant loss of p53 function due to these mutations has been shown to accelerate both the initiation of microscopic BCCs and progression of microscopic BCCs to macroscopic BCCs.(59)

1.5.2.3 p53 upregulation

p53 protein expression is increased in a proportion of BCCs, with one study demonstrating an increase in messenger ribonucleic acid (mRNA) in 40% of cases studied.(60) This increase in protein does not equate to an underlying mutation; and may represent upregulation of wild-type (WT) p53 due to oncogenic stressors or activation of other upstream pathways.(61) Signalling of the HH pathway, discussed earlier, leads to p53 stabilisation.(59)

1.5.2.4 p53 IHC

IHC can be used to evaluate both wild-type and mutant p53 protein expression in formalin-fixed, paraffin embedded tissue with the use of commercially available polyclonal and monoclonal antibodies.(61)

IHC directed against wild-type p53 protein is negative in normal tissue, including keratinocytes, due to the short half-life.(62) However, in neoplasms, WT p53 immunoreactivity is often increased in neoplastic compared with non-neoplastic tissues because of stabilisation. Although increased overall in the neoplastic cohort, WT p53 immunohistochemistry is still heterogenous and expression may even overlap with mutant p53 patterns, discussed below, and show absent or very strong immunoreactivity. This is due to superimposed influencing

factors such as increased proliferation, other genetic mutations, cellular stressors or therapy.(61)

Similarly to upregulated WT p53, mutant p53 is often more stable than WT p53 with resultant immunoreactivity.(23,63) However, the type of *TP53* mutation along with other factors - such as cellular differentiation or the effect of the mutant protein on residual WT p53 - determine the quantity and quality of p53 protein expressed. Mutant p53 protein expression is thus also heterogenous;(61) although the majority of mutant proteins are expressed at high levels.(51) Despite being overly simplistic, increased immunohistochemical staining is therefore often interpreted as representing mutant p53.(23)

Studies have attempted to correlate *TP53* mutations with immunohistochemical patterns. For example, The International Society of Gynecological Pathologists (ISGYP) describes four patterns for p53 IHC interpretation in high-grade tubo-ovarian serous carcinoma; namely diffuse nuclear overexpression, diffuse cytoplasmic overexpression and complete absence of staining. The fourth pattern represents WT p53, described as variable proportions of tumour cell nuclei showing an admixture of negative, weak, and strong p53 immunoreactivities. This categorisation was found to predict p53 mutations with > 94% accuracy as well as to identify the type of underlying mutation in this setting.(61)

Current antibodies are available for the detection of both WT and/or mutant p53. Clone D07 is a “pan-p53” antibody used to detect both forms of the protein(64) and has been used in multiple studies examining the expression of p53 in BCC; with one study finding the staining intensity comparably higher when this clone was used.(23,44,45,55,63,65–79)

1.5.2.5 p53 expression in BCC

Multiple articles in both the English and non-English literature have evaluated p53 IHC in BCC.(23,39,42–45,47,63,65–89). The findings range, although 70% of studies demonstrate p53 immunoreactivity in greater than 50% of BCCs (Annexure 1.3).(77) p53 staining is reported as intense and diffuse by some(72) and heterogeneous by others with prominent peripheral staining.(71,76,77) The staining intensity of p53 increased along with the proportion of staining(69); and most studies apply a scoring system combining the proportion and intensity

of p53 staining. There are various cut off values for determining positivity, ranging from no minimum up to a minimum of 25%.(66,89) Interpretation is most frequently done manually using a light microscope, however digital interpretation is not uncommon either.(66,71,74,79,83)

In addition to the above, p53 staining can show different sites of subcellular localisation. Nuclear p53 staining is most frequent, with one study demonstrating a nuclear positivity rate of 82.1% compared with a combined nuclear and cytoplasmic localisation rate of only 17.9% and no cases with cytoplasmic staining alone.(81) In fact, many studies only evaluated nuclear p53 in their interpretations of positive staining; one outlier only evaluated cytoplasmic and membranous p53.(83)

In BCC, a difference between mutation status and IHC has been observed(56) with immunoreactivity rates exceeding *TP53* mutation rates.(42) This may be accounted for by the upregulation of WT p53 in BCC. On the other hand, p53 mutations may not confer immunoreactivity if there is no change in the half-life of the protein, for example when a silent mutation occurs(56,58) and therefore a negative p53 immunohistochemical stain does not imply WT functioning p53.(59) Furthermore, one study found that the mutation type did not correlate with immunohistochemical staining proportion or intensity; (56) although data such as that used by ISGYP is lacking for BCC.(61) Overall, this highlights the limitation of IHC in determining the presence or absence of *TP53* mutations.(42,45,68)

1.5.2.6 p53 expression in histological subtypes of BCC

The above variation in p53 immunoreactivity may further be accounted for by a host of other variables; often not described or accounted for by many of the studies (Annexure 1.3).(23,39,45,47,66,68,69,71,73,74,76,77,80,81,85,86) These variables have been studied to a degree, and include tumour site, patient age, UV exposure, tumour necrosis, histological subtypes, and clinically aggressive BCCs as defined by set criteria etc. For example, p53 protein expression has been correlated with clinically aggressive BCC.(39,90)

The expression of p53 IHC in different BCC histological subtypes has been evaluated by at least 17 studies between 10 countries in the English literature over the past 30 years (Annexure 1.4)

– none of which have taken place in Africa.(39,45,47,63,66,68,69,71,73,74,76,77,80,81,84–86) The results are conflicting, and a small sample size is a limiting factor of a number of these studies;(23) however, three studies with larger sample sizes also published conflicting results.(74,77,86) Nine of the studies found no statistically significant difference between the histological subtypes studied;(47,68,69,73,74,76,77,80,85) while others found that p53 immunoreactivity correlated with dedifferentiation, infiltrative growth pattern, and other high risk histological subtypes such as micronodular BCC.(39,66,71,84,86)

There are even fewer studies correlating molecular data in BCC with the above variables. One study found that *TP53* mutations were present in 66% of clinically aggressive BCCs, compared with only 38% of clinically non-aggressive BCCs. In addition, they observed that transversions were the more common mutation type among aggressive BCCs when compared with nonaggressive BCCs; that there were differences in mutation hotspots; and that aggressive BCCs more frequently had multiple mutations than nonaggressive BCCs.(54) To our knowledge, there is no data evaluating differences in *TP53* mutations between histological subtypes of BCC. This is in spite of recommendations for molecular techniques for the accurate detection of *TP53* mutation in BCC.(88)

The impact of imiquimod on p53 has also been evaluated. Imiquimod was found to induce p53 mRNA expression and p53 nuclear accumulation with resultant apoptosis of BCC tumour cells.(91) This is in contrast to a previous study which found an insignificant reduction in p53 immunopositivity after topical imiquimod application, although *TP53* mutation status was not accounted for in this small study.(50) It has also been shown that mutant *TP53* cells are more resistant to imiquimod-induced apoptosis than WT-*TP53* cells.(91) This raises the question of whether there is a relationship between *TP53* mutations and IHC expression in BCC, such as that published by the ISGYP in ovarian cancer; and if so whether p53 immunohistochemical scoring in BCC biopsies has a role in guiding treatment with imiquimod, for example.(61)

1.5.2.7 p53 and BCL-2 expression in BCC

Several studies have evaluated both BCL-2 and p53 in the same cohort of BCC(39,42–45,47,68,82), although only limited studies have correlated p53 with BCL-2 expression. These studies found that BCL-2 expression decreased with increasing p53 in BCC.(42,92) To our

knowledge, there are no studies in the English literature comparing and/or combining BCL-2 and p53 scores between histological subtypes of BCC.

1.5.3 CD138

1.5.3.1 Defining CD138

CD138, also known as Syndecan-1, is a cell surface proteoglycan which binds various extracellular matrix (ECM) components via heparan sulphate.(93) In addition, CD138 interacts with mediators of cell proliferation, adhesion and migration.(94) In humans, CD138 is predominantly expressed in epithelial tissues and plasma cells.(93) Our understanding of CD138 is still evolving and is of particular interest given frequent changes in both the expression and distribution of CD138 in neoplastic cells as well as the potential for therapeutic targeting, e.g. anti-CD138 immunotherapy.(94,95)

In the skin, CD138 is expressed by epithelia and is absent in the mesenchyme under normal circumstances; although expression may be induced in mesenchymal cells during organogenesis.(96) In a large multitumour tissue microarray study, CD138 expression was present in 88% of the 85 tumour categories examined: with epithelial tumours ranking highest overall. In addition, CD138 expression differed between the types of epithelial tumours; and SCCs showed the greatest expression overall.(95)

1.5.3.2 C138 expression in BCC

CD138 expression is also present in most BCC; and is often strongly expressed by the tumour cells. One study found that 82.9% of BCCs strongly expressed CD138.(95) CD138 expression is predominantly membranous and occasionally cytoplasmic. Nuclear staining was not observed.(95,97) However CD138 expression in BCC tumour cells was weaker in comparison to adjacent non-neoplastic epidermis; although this was not quantified.(96,97) This decrease in CD138 expression may be due to tumoral protease activity and/or transcriptional- or posttranscriptional regulation in BCC.(96) Loss of CD138 expression in malignancy has been associated with an increase in tumour aggression, grade, invasion and worse patient outcome.(94,95) In addition, stromal CD138 expression is a poor prognostic indicator in most tumour types.(94)

1.5.3.3 C138 expression in histological subtypes of BCC

Two studies in the English literature have evaluated the expression of CD138 in BCC subtypes to determine whether these changes in CD138 expression could also be observed in high-risk BCC.(96,97) These studies noted differences in both tumoural and stromal CD138 expression between low- and high-risk BCC subtypes.(96,97) CD138 expression by the tumour cells was more frequently reduced or absent in high-risk BCC subtypes compared with low-risk BCC subtypes (55.6 versus 41.4%), although this finding was not significant.(97) The greatest reduction was noted in sclerosing/ morphoeic followed by infiltrative BCC; with preserved expression in both nodular and superficial BCC. However, a reduction in CD138 expression within the center of tumour nests was noted in low-risk BCC; and was found to be more marked in nodular compared with superficial BCC. CD138 expression was further noted to be disordered in high-risk subtypes, with island-to-island staining variability.(96)

CD138 expression in the peritumoral stroma was also observed in BCC; with both studies finding significant differences between the BCC subtypes. The one study observed that 72.2% of 18 infiltrative BCC showed peritumoral CD138 positivity compared with 0% of 29 low-risk BCC subtypes (superficial, nodular, or mixed) – a significant finding ($p < 0.001$).(97) This was corroborated by the second study which confirmed that high-risk BCC subtypes (15 infiltrative and 19 sclerosing/ morphoeic) more frequently expressed CD138 in the peritumoral stroma than low-risk BCC subtypes (14 nodular and 16 superficial); 73.53% versus 10% ($p = 0.002$). In addition, BCC with mixed low and high-risk histological components showed differential CD138 in each component. Furthermore, CD138 peritumoral stromal expression was more prominent at the leading edge of the tumour; and all subtypes showed reduced peritumoral staining in the areas of stromal clefting. The reduction in tumoral CD138 expression and accompanying peritumoral stromal expression in high risk BCC subtypes may be due to CD138 shedding or induction of stromal expression by tumour cells.(96)

Studies correlating CD138 expression with tumoral BCL-2 and p53 expression are lacking.

1.6. Image analysis

The interpretation of immunohistochemistry by conventional light microscopy (LM) can be subjective. This has led to the increased use of image analysis – defined as "computer-aided quantitative analysis of digital images" - in place of LM to extract numerical data and produce an objective measurement.(98)

Digital scanning and whole slide imaging (WSI) of glass slides has aided the acceleration of image analysis in pathology;(98) and WSI was approved for clinical use by the Food and Drug Administration (FDA) in 2017.(99) WSI is becoming more affordable and accepted in the field of Pathology. Whole slide scanning is an increasingly utilised method of digital scanning; and generates high resolution images of the original glass slides which can then be examined remotely. In addition, the magnification at which the slide is scanned can be adjusted and an area can be selected for subsequent image analysis.(98) Computers are then used to extract numerical data on the density and distribution of immunohistochemical staining from the digital images. This requires the application and/or development of image analysis algorithms; available through a number of different platforms.(98)

One such platform is QuPath, which provides open-source software for the analysis of WSI data. QuPath has been applied to interpret the immunohistochemical staining of p53, amongst others, in WSI to demonstrate its capabilities. QuPath's software is a cross-platform Java application.(100)

1.7. Rationale for this study

As histopathologists working in South Africa, we frequently encounter BCC specimens in our laboratories and, given recent data, are even more likely to encounter them daily in the future. Recognising the histological subtype is important for patient management and prognosis.

Whilst BCL-2, p53, and CD138 immunoreactivity have been studied to various degrees in the histological subtypes; no study to our knowledge has correlated the expression of tumoural BCL-2, p53, CD138 and stromal CD138 nor combined the data. In addition, excluding two studies from more than 15 years ago,(34,41) there has been no recent data published in the English literature from the African continent. Furthermore, the number of studies using reproducible digital analysis to interpret immunoreactivity in this field are limited.(66,71,74,79,83)

1.7. Aims and objectives

i) Determine the expression of BCL-2, p53 and CD138 in BCC in our setting by using immunohistochemistry.

ii) Observe if there is a difference in the immunohistochemical expression of BCL-2, p53 and CD138 between low and high-risk BCC subtypes by performing statistical analysis.

iii) Observe if there is a correlation between BCL-2, p53 and CD138 expression in low and high-risk BCC subtypes through statistical analysis.

iv) Generate a standardised, reproducible method of scoring using image analysis to enable accurate comparison of data in future research.

Chapter 2: Research method and materials

2.1 Ethics approval

Scientific approval for the study was obtained from the Department of Pathology Research Committee, Faculty of Health Sciences, University of Cape Town (UCT). The protocol was subsequently approved by the Human Research Ethics Committee (HREC) of the Faculty of Health Sciences, UCT (Annexure 2.1). Thereafter annual renewal was obtained (Annexure 2.2).

2.2 Study design

A retrospective, laboratory-based, observational study design was used in this research.

The specific type of observational design was cross-sectional; with the collection of multiple categorical and numerical variables (Table 2.1) applied to a defined population at a single point in time. This cross-sectional design allowed both the analytical and descriptive research aims to be answered.

Table 2.1 Study variables

Numerical	Categorical		
Continuous	*Binary*	*Ordinal*	*Nominal*
Age in years	Sex	p53 expression	Site of lesion
p53 expression		BCL-2 expression	Histological subtype
BCL-2 expression		CD138 expression	Subcellular localisation of CD138
CD138 expression			Peritumoral localisation of CD138

2.3 Sample selection

2.3.1 Sample size calculation

The sample size was calculated with the assistance of a statistician, Dr Michelle Henry, based on published literature evaluating BCL-2, p53 and CD138 expression in BCC (Annexure 2.3). The final desired sample size (n = 124) was based on the results of Demirkan et al (2000) to maintain a reasonable power (Power of 0.71 for n = 125) while utilising limited financial resources and working under considerable time constraints.

2.3.2 Sample sourcing

A computer-generated list of all BCCs diagnosed at the National Health Laboratory Services (NHLS) Anatomical Pathology Laboratory, Groote Schuur Hospital (GSH), Cape Town between January 2016 to December 2019 was obtained. These patients were seen at various health facilities within the Western Cape. After applying the inclusion/ exclusion criteria (Table 2.2), a shorter list of BCCs was created and all relevant demographic and clinical data pertaining to this initial cohort was extracted from TrakCare and recorded on an Excel spreadsheet. The Haematoxylin and Eosin (H&E) slides were then retrieved from the laboratory archive and reviewed by Drs R Roberts and J de Stadler to confirm the diagnosis, sampling method, and BCC histological subtype. The histological subtyping allowed the cases to be divided into low and high-risk groups for BCC recurrence as defined by the WHO. Thereafter, the final study sample was selected by applying simple random sampling of equal numbers to each group, using the function in an Excel spreadsheet. Finally, the formalin fixed paraffin embedded (FFPE) tissue blocks were obtained from the laboratory archive and the inclusion/ exclusion criteria re-applied to obtain the final study cohort.

The immunohistochemical staining and digital analysis of the study took place in the Division of Anatomical Pathology Research Laboratory, Faculty of Health Sciences, UCT from 2019 to 2022.

Table 2.2 Inclusion and exclusion criteria applied to study participants

Inclusion criteria	Exclusion criteria
Date	
01/01/2016 until 31/12/2019	Prior to 2016 or beyond 2019
Sampling method	
Excision	Biopsy
Excision biopsy	Punch biopsy
Local excision	Incomplete excision
Elliptical excision	Curettage
Wedge resection	Partial excision
Surgical excision	Incisional biopsy
Amputation	Surgical biopsy
Complete excision of organ	Re-excision
Unspecified method	
Other	
More than a single diagnosis, so long as one diagnosis is a BCC	Duplicate entries
Slides & tissue blocks	
	Insufficient tissue on tissue block(s)
	Slide and/or block(s) missing
	Incorrect diagnosis i.e., not a basal cell carcinoma

2.3.3 Standard case definition

"A skin excision with a confirmed diagnosis of BCC and sufficient, available tissue from the Division of Anatomical Pathology, GSH, NHLS for the period January 2016 to December 2019".

2.3.4 Sample inclusion/ exclusion criteria

The inclusion and exclusion criteria (Table 2.2) were applied on multiple occasions in the sample selection process. Firstly, after the initial TrakCare search, duplicate entries and unwanted methods of tumour sampling were excluded. Secondly, upon review of the H&E slides, cases with insufficient tissue, incorrectly documented and unwanted methods of tumour sampling, as well as incorrect diagnoses (i.e., not a BCC) were excluded. Thirdly, upon acquisition of FFPE tissue blocks, cases with missing blocks or insufficient remaining tissue for subsequent immunohistochemical staining were excluded.

Flow diagram summarising the sample selection process:

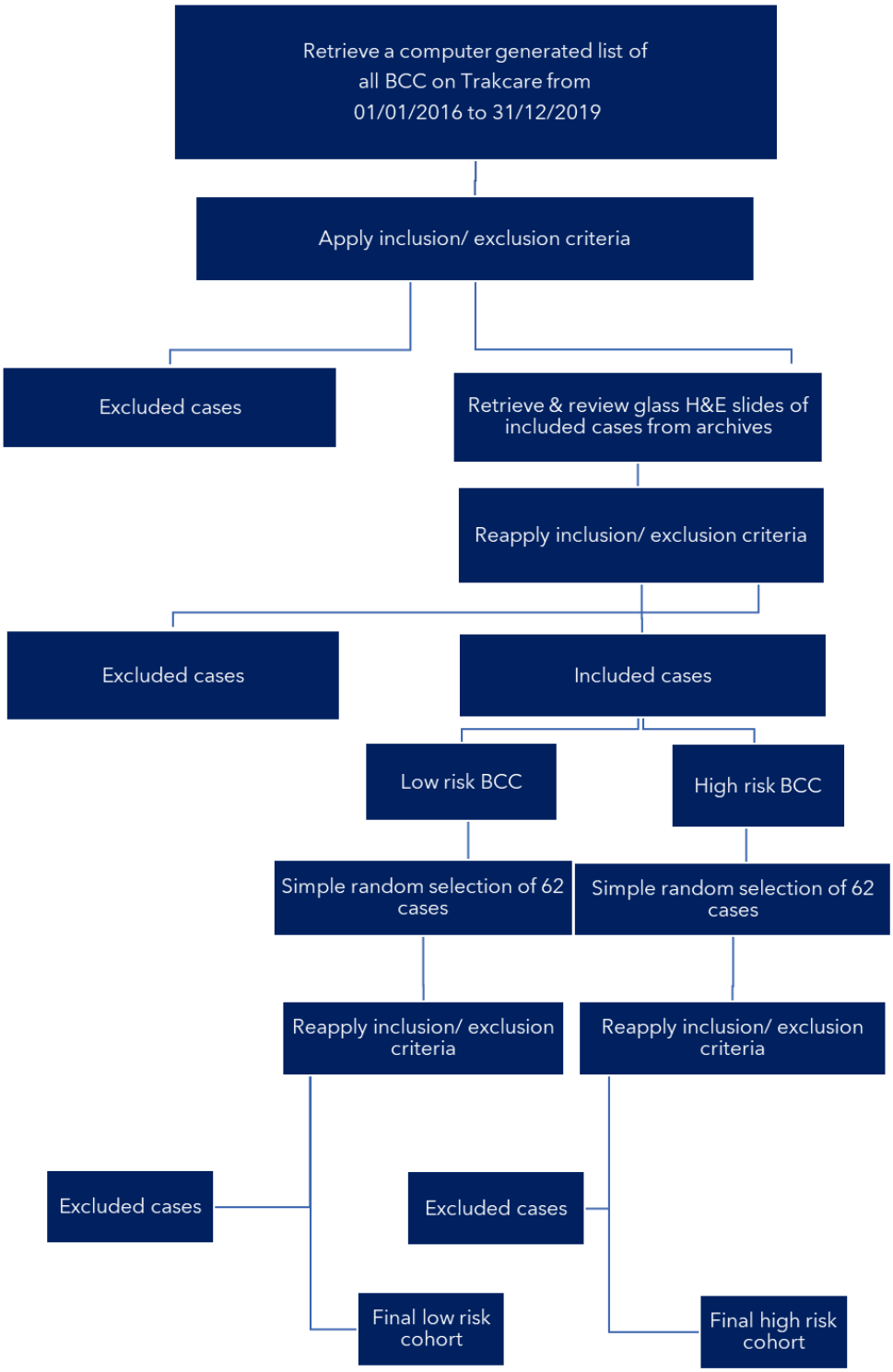

2.4 Immunohistochemistry (IHC) technique

2.4.1 Microtomy procedure of test specimens and controls

A single H&E-stained slide was selected for each case and the corresponding FFPE block used to cut three tissue sections for application of the BCL-2, p53 and CD138 antibodies (Table 2.3)

Table 2.3 Primary antibodies

Primary Antibody	Antibody type	Clone (Manufacturer)	Dilution factor
BCL-2	Monoclonal mouse anti-human	124 (DAKO, Denmark)	1:20
p53	Monoclonal mouse anti-human	DO-7 (DAKO, Denmark)	1:75
CD138	Monoclonal mouse anti-human	MI15 (DAKO, Denmark)	1:20

The tissue sections were cut at a thickness of four microns (4 um). All sections were then floated on a waterbath and picked up on silanised slides (Histobond). The slides were labelled according to the case number. Next, the sections were evaluated to ensure that the tissue was perfectly flat and that no creases or bubbles were present to later entrap reagents. Thereafter, the sections were blotted, and heat fixed at 37 degrees Celsius in an incubator overnight.

The control tissue was chosen for each antibody (Table 2.4) and tissue sampled from appropriate cases available within the NHLS laboratory. The control blocks were sectioned and fixed the same as the test cases.

Table 2.4 Control tissues

Antibody	Control tissue	Cell-type assessed	Localisation of staining
BCL-2	Appendix	Lymphocytes	Nuclear & cytoplasmic
p53	Colorectal adenocarcinoma	Tumour cells	Nuclear
CD138	Appendix	Epithelium	Membranous & cytoplasmic

2.4.2 Automated IHC staining

The Ventana XT auto-stainer platform (Ventana Medical Systems, United States of America) was used to perform the IHC staining according to the Divisional Standard Operating Procedure (Annexure 2.4). Prior to running, protocols were created for each IHC stain and optimised. The auto-stainer had a capacity for thirty slides at a time: comprising of twenty-nine case slides and one control slide. A single antibody was applied at a time and five batches completed prior to commencement of the next antibody. After automated IHC staining, the slides were rinsed with water, the sections dehydrated, and the cover slips mounted.

2.4.3 Interpretation of IHC stains

The original H&E slides as well as the IHC stained slides were scanned as whole slide images at 20x magnification using an Olympus VS120 Digital Slide Scanner (Olympus Corporation, Japan) in the Pathology Learning centre. Thereafter, each IHC stain was digitally interpreted with the assistance of Mr J. Geitner using the free opensource bioimage analysis software QuPath (Version 0.2.3).(101)

The BCL-2, p53 and CD138 staining within the tumour itself were evaluated by selecting a set area of 4000 representative tumour cells from each case and evaluating each case for both the intensity and proportion of staining. The value of 4000 cells was chosen to better standardise the cases whilst minimising the exclusion of cases with fewer cells.

The cellular localisation of staining was selected based on the specific IHC stain being interpreted. In addition, CD138 was evaluated within the peritumoral stroma.
The QuPath scripts for the above can be found in Annexure 2.5.

2.4.3.1 IHC evaluation within the tumour

After manually selecting the areas of interest, analysis was performed using QuPath's *Positive cell detection* command. This command detects cells and can calculate several measurements of intensity and morphology. Intensity thresholds were set to classify tumour cells as being negative (0), weak (+1), moderate (+2) or strongly positive (+3) for staining based upon mean DAB optical densities.(100) Annexure 2.6 shows the values used for QuPath's *Positive cell detection* command in this analysis.

2.4.3.2 IHC evaluation within the peritumoral stroma

CD138 was also evaluated within the peritumoral stroma. This included manual review of each case to classify the type of staining into a) peritumoral stroma or b) peritumoral cells or c) both. Thereafter an area of 400 000µm^2 was selected and the proportion and intensity of staining was determined using the QuPath Pixel classifier command. Thresholds were set to the same optical density values as used in CD138 Tumour analysis.

The stromal area selected included both mesenchymal and inflammatory cells; and excluded peritumoral clefts, artefactual tissue loss, and blood vessels to avoid falsely lower scores. Where possible, large inflammatory aggregates were avoided to better standardise cases.

2.4.3.3 Summary scores

Summary scores were generated as the total number of cells classified as negative, weak, moderate, or strongly positive, as well as the overall percentage of cells classified as positive. For cases with tumour cells fewer than 4000 or a stromal area of less than 400 000µm^2, the entire available area was selected, and the total number (tumour cells or area) documented. The numerical data generated by QuPath was displayed in an Excel spreadsheet and the desired values transferred into the Redcap database for each case.

The data was collected as both continuous numerical variables and ordinal categorical variables; the latter to allow comparison with the existing scoring systems in the current literature (Annexure 2.7).

2.5 Data collection, safety, and monitoring

2.5.1 Data collection

The data collected on each sample included demographic variables (age, sex), site of the lesion, immunohistochemical scores for BCL-2, p53 and CD138 expression in the tumour and the immunohistochemical expression of CD138 in the peritumoral stroma. The former data was obtained from TrakCare, while the latter was obtained by applying the immunohistochemical technique described in paragraph 2.4.

2.5.2 Data safety and monitoring

The numerical and categorical variables of the final study cohort were captured into a Redcap database generated by Dr JL de Stadler to maintain privacy & confidentiality of participants (Annexure 2.8). All samples were assigned a number starting from 1; to anonymise them. The data was continuously updated and monitored throughout the study process.

As there was neither inherent risk nor direct interaction with participants, informed consent was not required for this research. Similarly, the benefits of this study pertain to the contribution of research and knowledge to the medical field, rather than to the individual participants.

2.6 Data analyses

Statistical analyses were performed using STATA version 17.0 (Stata Corporation, College Station, Texas, USA) and R (version 4.2.1; R Core Team, Vienna, Austria). The analyses focused on the expression of p53, BCL-2, tumoural CD138 and stromal CD138 stratified by BCC risk category. The proportions described in the study were reported as median percentages with interquartile ranges. The differences between the risk groups were compared using Chi-squared/Fisher's exact test and Wilcoxon rank-sum tests. The associations between protein expression in each tumour were assessed using simple linear regression and statistical analysis was performed using the Spearman rank test. A p value <0.05 was considered statistically significant.

Chapter 3: Results

3.1 Demographics

The study participants (n = 104) comprised 65.38% males (n = 68) and 34.62% females (n = 36). The mean age of was 70.05 years, while the median age was 72 years (Figure 3.1). The interquartile range (IQR) was 20 years, with 50% of participants aged between 60 and 80 years old. The youngest participant was 32 years old and the oldest 96 years old.

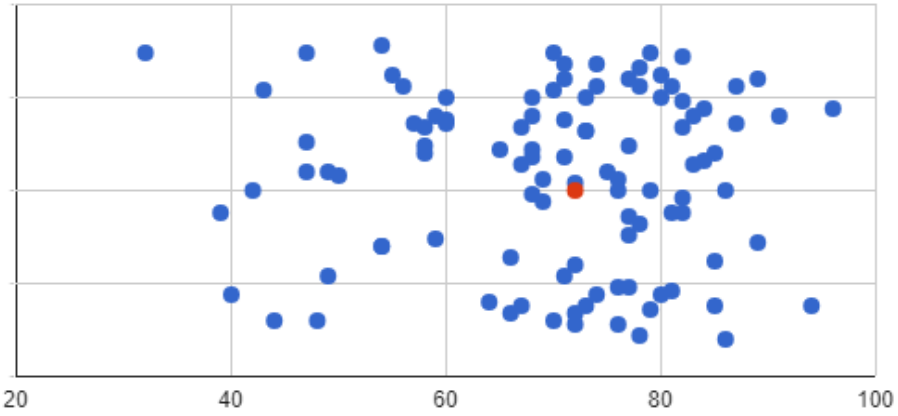

Figure 3.1 Scatter plot of age distribution of basal cell carcinoma in years. The red dot represents the median.

3.2 Anatomical distribution

The anatomical site of BCC occurrence was documented for 98.07% (n = 102) of the participants. Of these 62.5% (n= 65) were documented as from the head and neck region, 18.27% (n = 19) from the trunk, 16.35% (n = 17) from the limbs, and 0.96% (n = 1) from the upper body.

Of those in the head and neck region 35.4% (n = 23) were broadly from the face, 20% (n = 13) from the nose, 16.9% (n = 11) from the ear, and 15.4% (n = 10) from the neck (Figure 3.2). Lastly 8,32% (n = 8) were from other sites. Overall, at least 43.08% (n ≥ 28) arose in the high-risk mask area of the face.(11) When excluding those labelled only as 'face', the percentage of remaining cases in the high-risk mask area increased to 66.67% (n = 28).

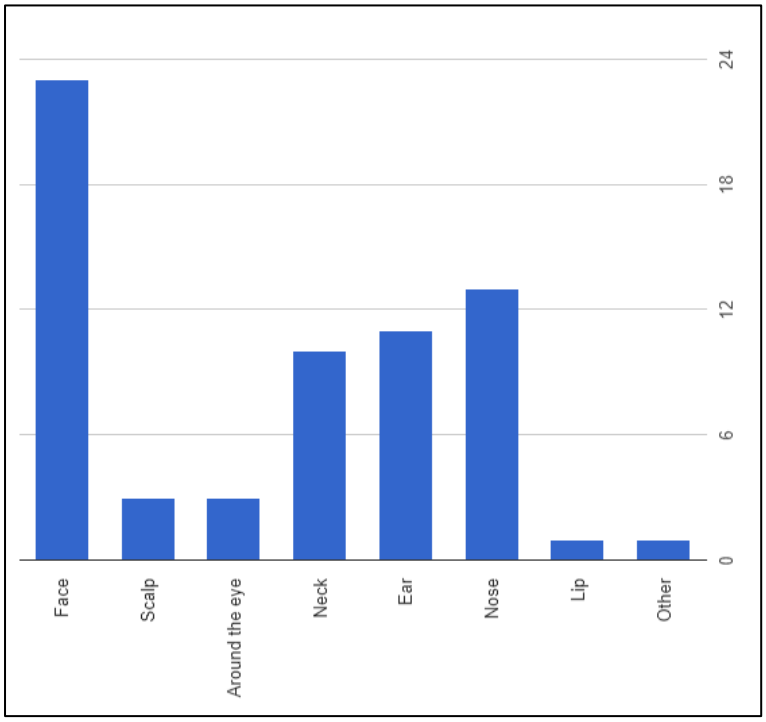

Figure 3.2 Anatomical distribution of basal cell carcinoma in the head and neck region.

3.3 WHO histological subtypes

Of the cases, 82.69% (n = 86) had a single histological component. The remaining 17.3% (n = 18) had two histological components and were therefore classified as mixed BCC (example in Figure 3.3). In addition to the mixed BCC subtype 42.3% (n = 44) were nodular, 21.2% (n = 22) infiltrating, 14.4% (n = 15) superficial, 1.9% (n = 2) micronodular, 1.9% (n = 2) basosquamous, and 1% (n = 1) sclerosing/ morphoeic (Figure 3.4). There was no BCC with sarcomatoid or adnexal differentiation, pigmented BCC nor fibroepithelial BCC subtype (n = 0).

Of the 18 mixed BCCs, 1 case (superficial and infiltrating) did not have representation of both components on a single H&E slide and only the low-risk (superficial) component was assessed further. Of the remaining 17 mixed BCCs, 1 comprised of two low-risk components (nodular and superficial) and 16 comprised of both a low- and high-risk component. Of these 16 BCCs 13 comprised of a nodular and infiltrating component, 2 comprised of a nodular and sclerosing/ morphoeic component, and 1 of a superficial and infiltrating component. Of the high-risk mixed BCCs 88.24% (n = 15) had nodular low-risk component and 11.76% (n = 2) had a superficial low-risk component.

Of the total 104 cases 57.69% (n = 60) were categorised as low-risk BCCs and 42.31% (n = 44) as high-risk BCCs.

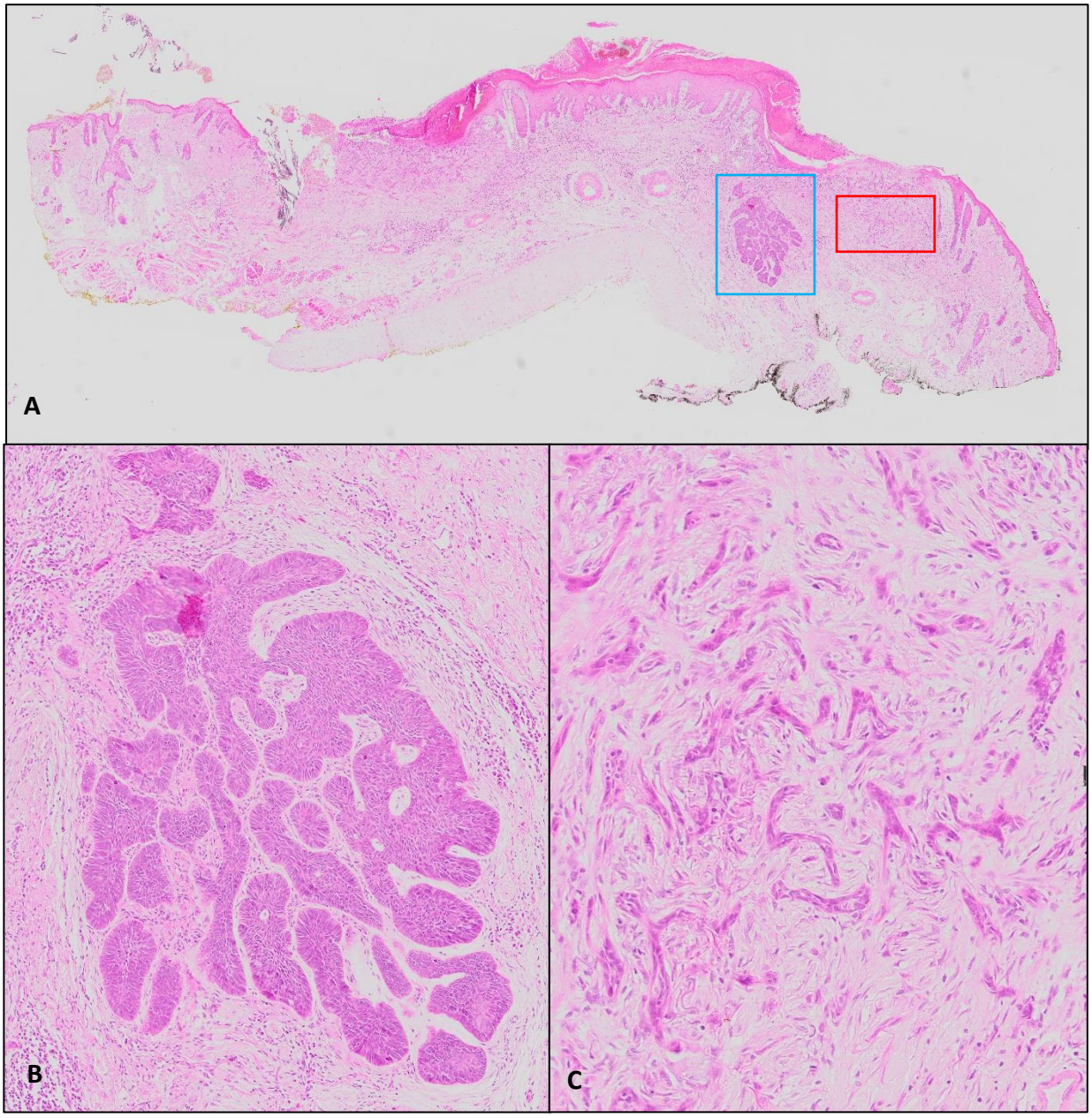

Figure 3.3 Histology of a mixed basal cell carcinoma. A. Low power view of a WSI taken of an H&E section from an excision of a mixed cutaneous BCC arising on the nose. The blue box denotes the low-risk component and the red box the high-risk component. B. The low-risk nodular component (5 x magnification). C. The high-risk sclerosing/morphoeic component (10 x magnification). *All images generated from WSI originally taken at 20x magnification using an Olympus VS120 Digital Slide Scanner (Olympus Corporation, Japan).*

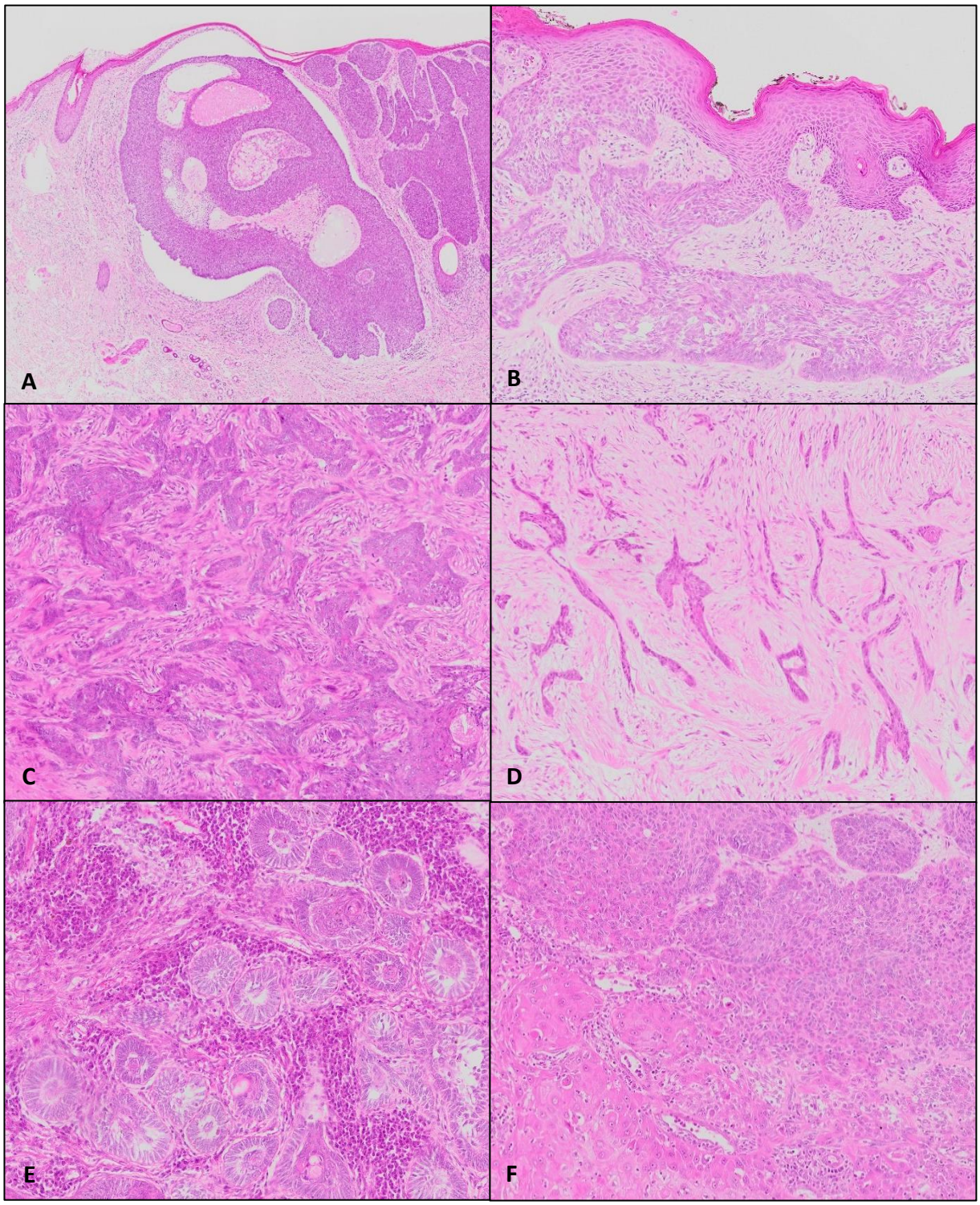

Figure 3.4 H&E images of the histological subtypes of basal cell carcinoma. A. Nodular BCC (1.25 x magnification). B. Superficial BCC (5 x magnification). C. Infiltrating BCC (5 x magnification). D. Sclerosing/ morphoeic BCC (5 x magnification). E. Micronodular BCC with a plasma cell rich stromal infiltrate (7.5 x magnification). F. Basosquamous BCC with the squamous component at the lower left (5 x magnification). *All images generated from WSI originally taken at 20x magnification using an Olympus VS120 Digital Slide Scanner (Olympus Corporation, Japan).*

3.3.1 Sex and risk category

There was no significant difference in sex between low- and high-risk BCC (p = 0.25). Males predominated in both the low- and high-risk categories (Table 3.1).

Table 3.1 Descriptive variables in low- and high-risk basal cell carcinomas.

	Total N=104 (100%)	High Risk N=44 (42.31%)	Low Risk N=60 (57.69%)	p Value
Sex				*0.25*
Female	36 (34.62)	18 (40.91)	18 (30)	
Male	68 (65.38)	26 (59.09)	42 (70)	
Age (Years)				*0.24*
Min	32	32	40	
Max	96	96	91	
Mean (SD)	70.06 (13.45)	68.75 (14.16)	71.02 (12.94)	
Median (IQR)	72 (60 - 80)	71 (64.5 – 77.5)	73.5 (60 – 81.5)	
Categories				
30-39	2 (1.92)	2 (4.55)	0 (0)	
40-49	10 (9.62)	4 (9.09)	6 (10)	
50-59	12 (11.54)	4 (9.09)	8 (13.33)	
60-69	17 (16.35)	9 (20.45)	8 (13.33)	
70-79	36 (34.62)	17 (38.64)	19 (31.67)	
80-89	24 (23.08)	6 (13.64)	18 (30.00)	
≥90	3 (2.88)	2 (4.55)	1 (1.67)	
Site				*0.30*
Head and neck	65 (62.50)	31 (70.45)	34 (56.67)	
Limbs	17 (16.35)	6 (13.64)	11 (18.33)	
Trunk	19 (18.27)	6 (13.64)	13 (21.67)	
Other	1 (0.96)	1 (2.27)	0 (0)	
Missing	*2 (1.92)*	*0 (0)*	*2 (3.33)*	

3.3.2 Age and risk category

There was no significant difference in the age of participants between low- and high-risk BCC (p = 0.24). The mean age in the low-risk category was 71.02 years (standard deviation (SD) of 12.94) compared to a mean age of 68.75 years (SD of 14.16) in the high-risk category (Table 3.1).

3.3.3 Site and risk category

BCCs occurred most frequently in the head and neck region across both the low- and high- risk categories (Table 3.1). There was no significant difference in site between the two categories ($p = 0.3$).

3.4 BCL-2, p53 and CD138 immunohistochemical expression

For the immunohistochemical analysis, the mixed BCCs were divided into their two components and each component was assessed as a single case (Figure 3.5). Of the 104 cases, 86 were non-mixed BCC and comprised 59 low-risk BCC and 27 high-risk BCC. In addition, 18 cases were mixed BCC. Of these, 1 had only a single low-risk component available for further analysis. The remaining 17 cases each had two components which were individually assessed: thus contributing 16 high-risk and 18 low-risk BCCs to the total number of cases. Therefore, a total of 78 low-risk BCC and 43 high-risk BCC ($n = 121$) were evaluated for BCL-2, p53 and CD138 immunoreactivity (Annexure 3.1).

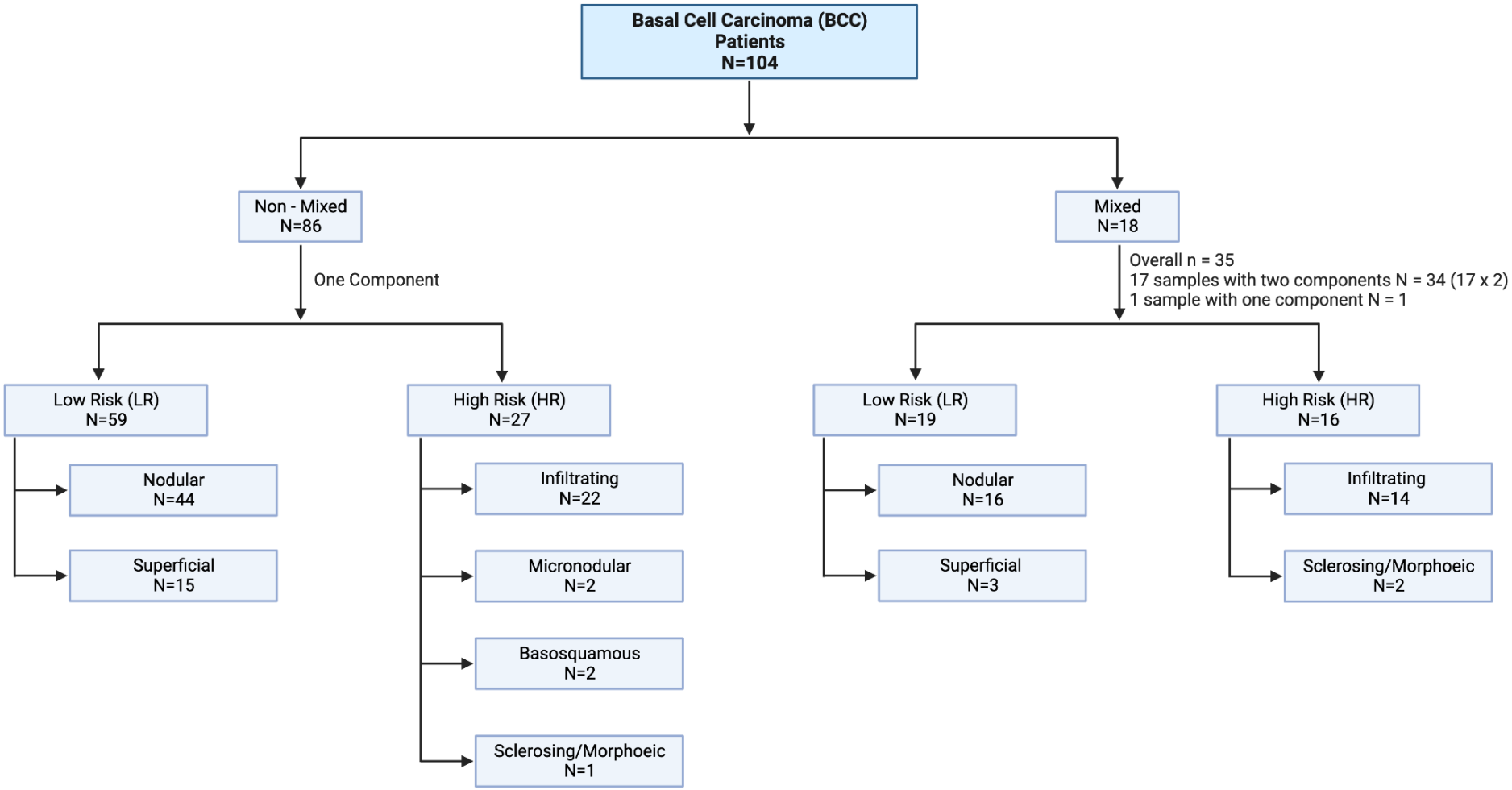

Figure 3.5 The composition of the final cohort of high- and low-risk basal cell carcinoma for analysis of immunohistochemistry.

3.4.1 BCL-2

BCL-2 expression within the tumour cells was assessed in 120 cases (78 low- and 42 high-risk BCC) and 78.33% (n = 94; score ≥ 1) of BCCs were found to be positive for BCL-2. BCL-2 intensity ranged from 0 to 3+ (Figure 3.6) and the proportion of BCL-2 positive tumour cells ranged from 0 to 99.75%. The mean proportion of any intensity of BCL-2 expression in tumour cells (1+, 2+, 3+) was 34% (SD of 31.3%). BCL-2 expression by tumour cells was most frequently negative (mean 66.02%; SD 31.33%) followed by 1+ intensity of expression (mean 31.26%; SD 27.60) and less often 2+ intensity (mean 2.71%) or 3+ intensity (mean 0.0098). Lastly, the mean BCL-2 score overall was 1.67 (SD of 1.35).

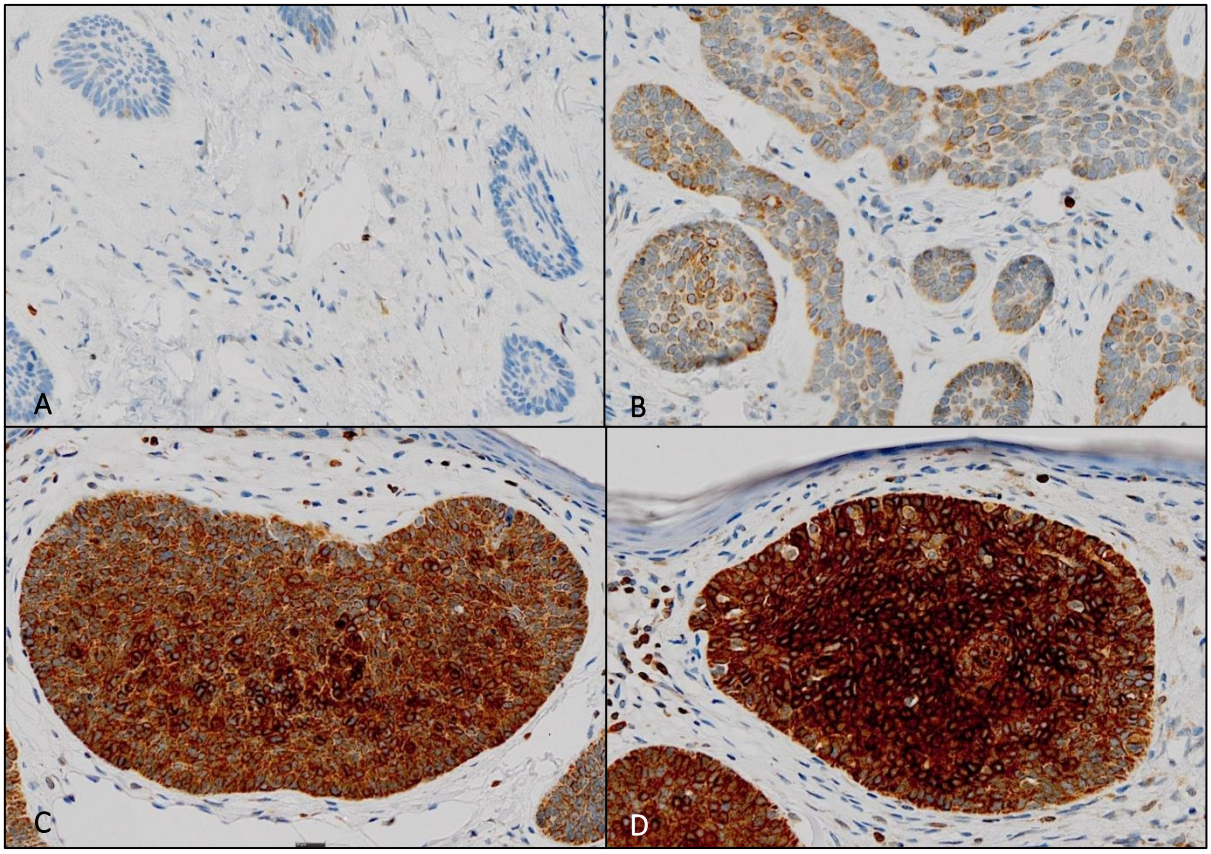

Figure 3.6 BCL-2 intensity from 0 to 3+. A. Case 90 (micronodular BCC) displaying an absence of BCL-2 staining at 10x magnification. Stromal lymphocytes show nuclear positivity serving as an internal control. B. Case 62 (infiltrating BCC) displaying areas of 1+ intensity (weak cytoplasmic staining) at 20x magnification. C. Case 16 (nodular BCC) displaying areas of 2+ intensity (moderate cytoplasmic staining) at 20x magnification. D. Case 16 (nodular BCC) displaying other areas of 3+ intensity (strong cytoplasmic staining) at 20x magnification.

The mean expression of BCL-2 by tumour cells in the low-risk category was 37.81% (SD of 32.74%) compared to a mean of 26.84% (SD of 27.48%) in the high-risk category (p = 0.14). In addition, the mean expression of BCL-2 in the 1+ and 2+ categories was higher in the low-risk category compared to the high-risk category (Figure 3.7), although these differences were not statistically significant. The intensity category 1+ contributed the most to BCL-2 tumoural expression in both categories with a mean of 34.29% and 25.6% in the low- and high-risk categories respectively (p = 0.17). Furthermore, there was no significant difference when comparing mean BCL-2 scores between the low-risk (1.84) and high-risk (1.36) BCC categories (Figure 3.8), although there was a trend to higher BCL-2 scores in the low-risk category (p = 0.074). Lastly, we found no significant difference between the BCC categories when we combined BCL-2 scores 1 and 2 (low labelling) to BCL-2 scores 3 and 4 (high labelling)(p = 0.059).(34) However, we did find that high-risk BCCs had significantly lower BCL-2 labelling compared to low-risk BCCs when we combined a BCL-2 score of 0 with scores of 1 and 2 into the low labelling category (p = 0.04).(35)

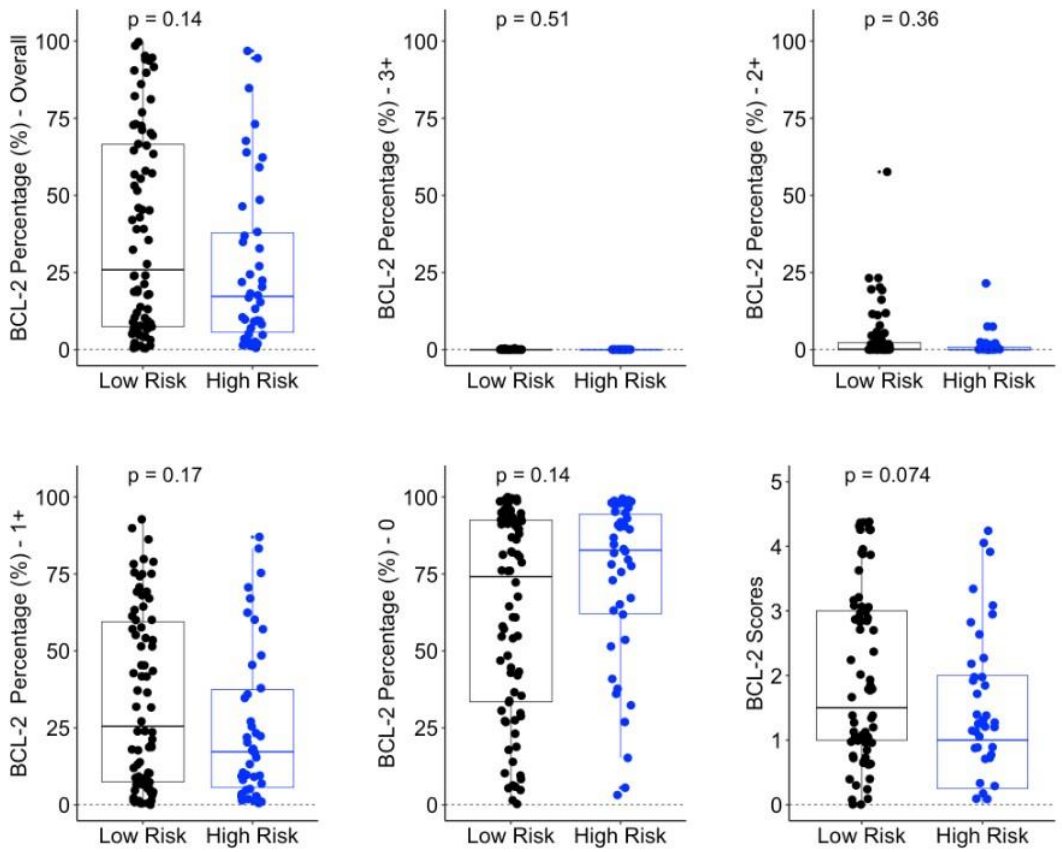

Figure 3.7 BCL-2 expression stratification by risk category.

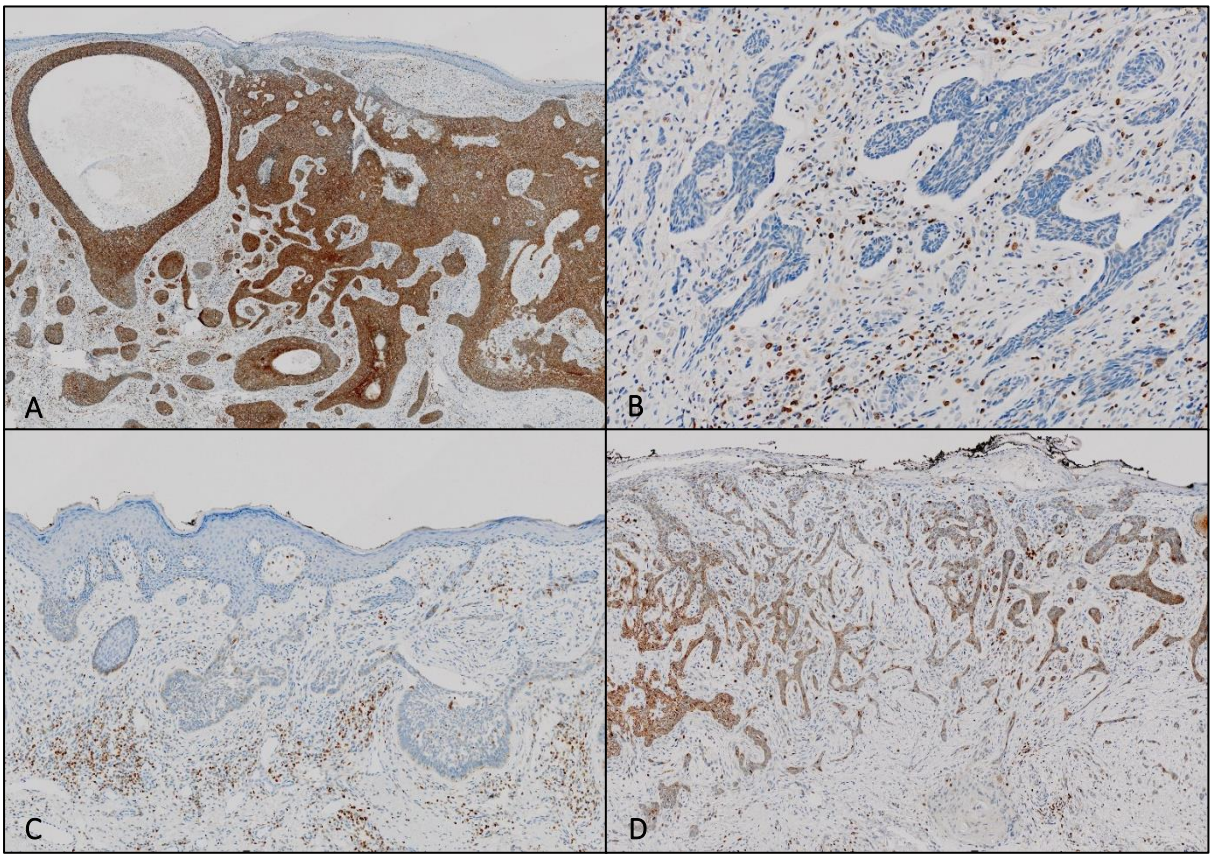

Figure 3.8 Staining outcomes for BCL-2 in low- and high-risk patterns. A. Case 8 (low-risk: nodular BCC) with a score of 4 at 1.25 x magnification. B. Case 56 (high-risk: infiltrating BCC) with a score of 0 at 10 x magnification. C. Case 5 (low-risk: superficial BCC) with a score of 1 at 2.5 x magnification. D. Case 53 (high-risk: infiltrating BCC) with a score of 3 at 2.5 x magnification.

3.4.2 p53

p53 expression within the tumour cells was assessed in 120 cases (78 low- and 42 high-risk BCC) and 90.83% (n = 109; score ≥ 1) were positive for p53. The intensity of p53 expression ranged from 0 to 3+ (Figure 3.9) and the proportion ranged from 0.28 to 99.98% of tumour cells. The mean proportion of any intensity of p53 expression in tumour cells across both categories was 77.89% (SD of 31.8%). p53 expression by tumour cells was most frequently of 3+ intensity (mean 36.09%; SD 33.04%) followed by 2+ (mean 22.54%; SD 14.62) and 1+ intensity (mean 19.27%; SD 19.74%). The mean absence of p53 staining by tumour cells was 22.11% (SD 31.79%). In addition, the mean p53 score overall was 3.32 (SD 1.28).

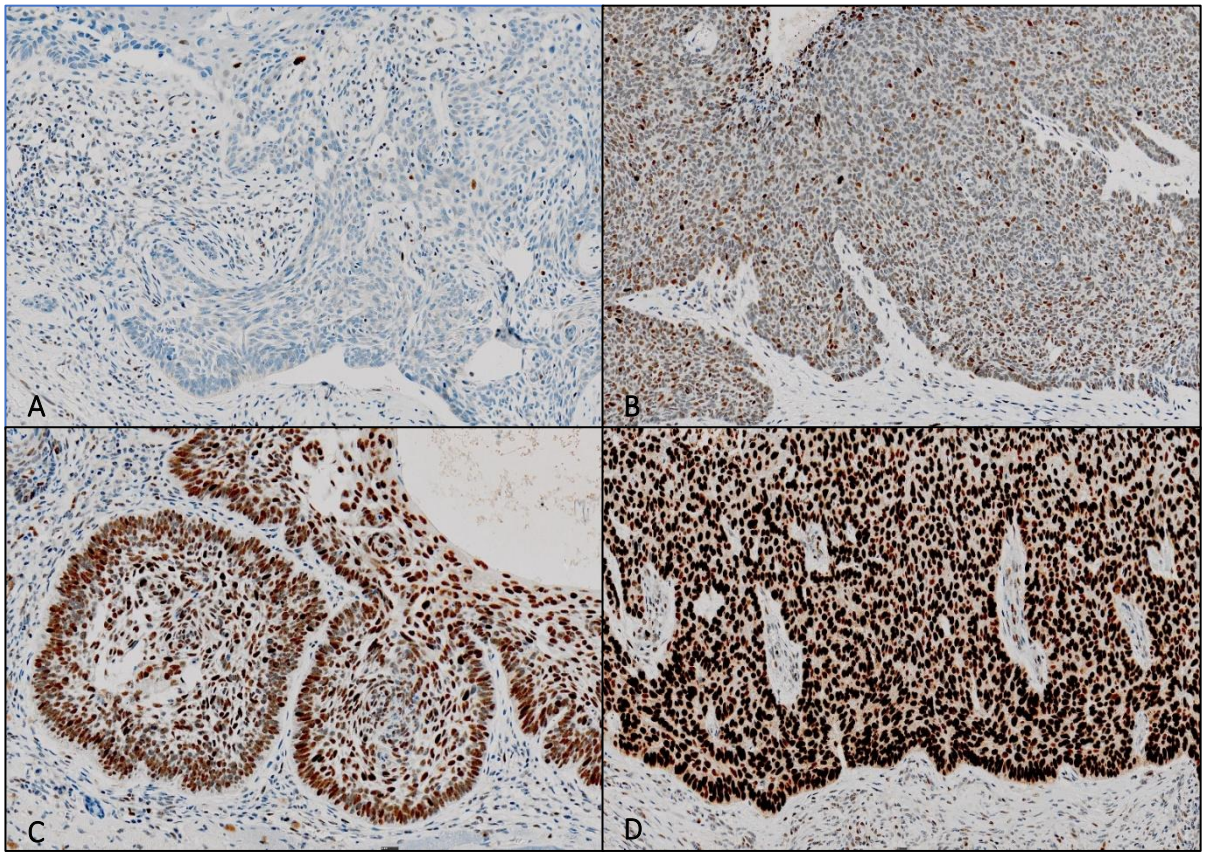

Figure 3.9 p53 intensity from 0 to 3+ at 10x magnification. A. Case 5 (superficial BCC) displaying a near absence of p53 staining. B. Case 31 (nodular BCC) displaying a predominance of 1+ intensity (weak nuclear staining). C. Case 95 (nodular BCC) displaying a predominance of 2+ intensity (moderate nuclear staining). D. Case 3 (nodular BCC) displaying diffuse 3+ intensity (strong nuclear staining).

The mean expression of p53 by tumour cells in the low-risk category was 77.54% (SD of 31.32%) compared to a mean of 78.55% (SD of 33.02%) in the high-risk category – an insignificant difference ($p = 0.64$; Figure 3.10). In addition, there was no significant difference when comparing the individual intensity categories (0, 1+, 2+, 3+) between low-risk and high-risk BCC (Figure 3.11). The intensity category 3+ contributed the most to p53 tumoural expression in both categories with a mean of 32.48% and 42.80% in the low- and high-risk categories respectively. Furthermore, there was no significant difference when comparing mean p53 scores between the low-risk (3.34) and high-risk (3.28) BCC categories ($p = 0.82$).

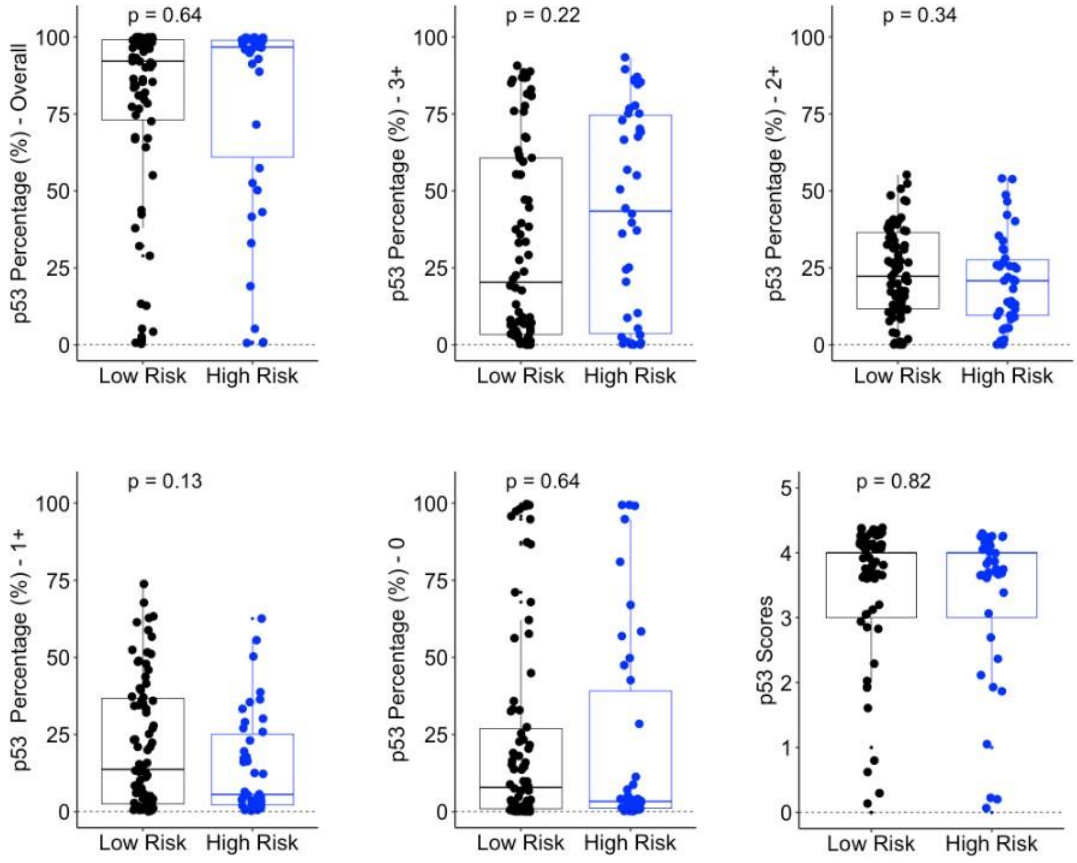

Figure 3.10 p53 expression stratification by risk category.

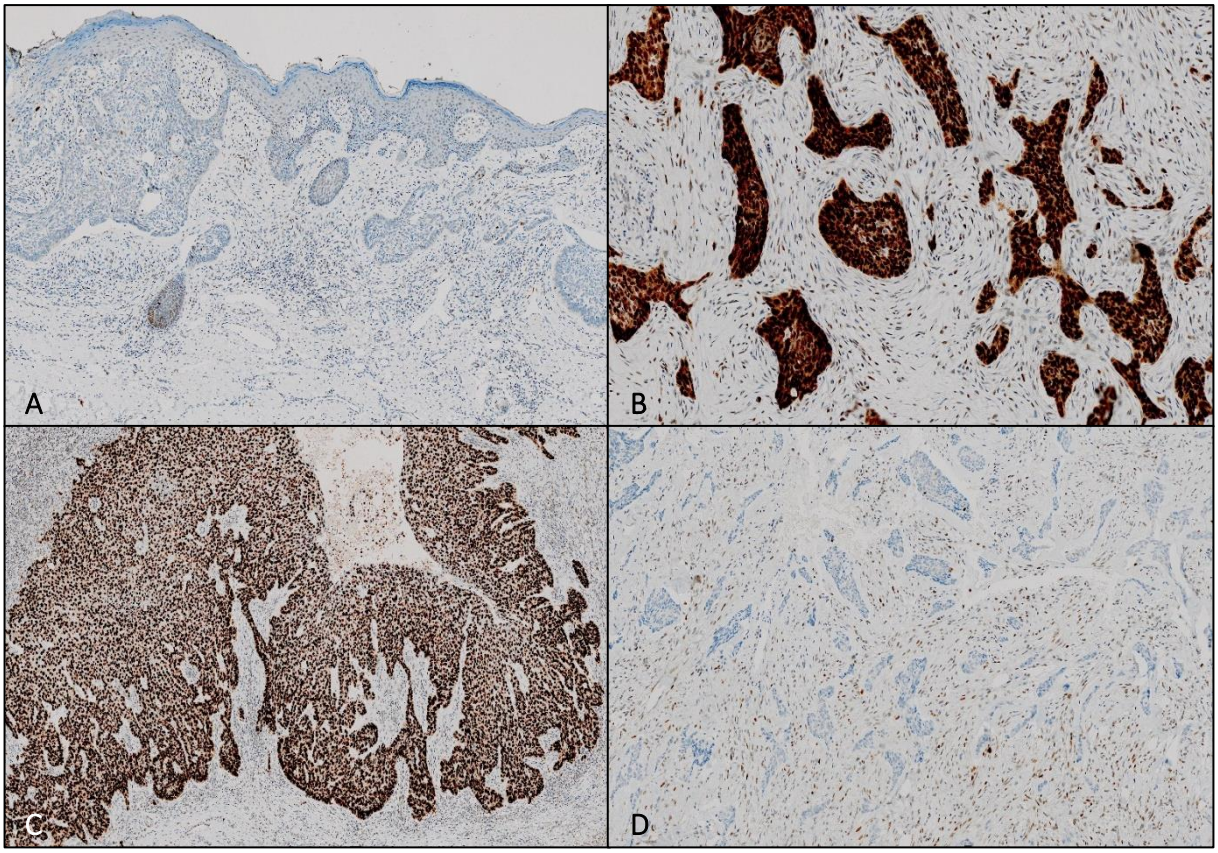

Figure 3.11 Staining outcomes for p53 in low- and high-risk patterns. A. Case 5 (low-risk: superficial BCC) with a score of 0 at 2.5 x magnification. B. Case 59 (high-risk: mixed BCC, infiltrating component) with a score of 4 at 5 x magnification. C. Case 3 (low-risk: nodular BCC) with a score of 4 at 2.5 x magnification. D. Case 58 (high-risk: mixed BCC, infiltrating component) with a score of 0 at 5 x magnification.

3.4.3 CD138 in the tumour

CD138 expression within the tumour cells was assessed in 118 cases (76 low- and 42 high-risk BCC) and all cases were positive for CD138. The intensity of CD138 tumoural expression ranged from 0 to 3+ (Figure 3.12) and the proportion ranged from 95.54 to 100% of tumour cells. The mean proportion of any intensity of CD138 expression in the tumour cells across both categories was 99.81% (SD of 0.71%). The most frequent intensity category was 2+ intensity and the mean percentage of CD138 expression by tumour cells for 0, 1+, 2+ and 3+ intensity was 0.19 (SD 0.7), 6.71 (SD 13.61), 76.52 SD (22.07) and 16.58 (SD 22.04) respectively. In addition, 100% of cases had a CD138 score of moderately or strongly positive. Of these, 93.22% (n = 110) were strongly positive and 6.78% (n = 8) were moderately positive.

The subcellular localisation of CD138 was predominantly membranous (n = 97) with less than 18% of cases displaying cytoplasmic and/or nuclear positivity. There was no difference in subcellular localization of CD138 between the low- and high-risk BCC categories.

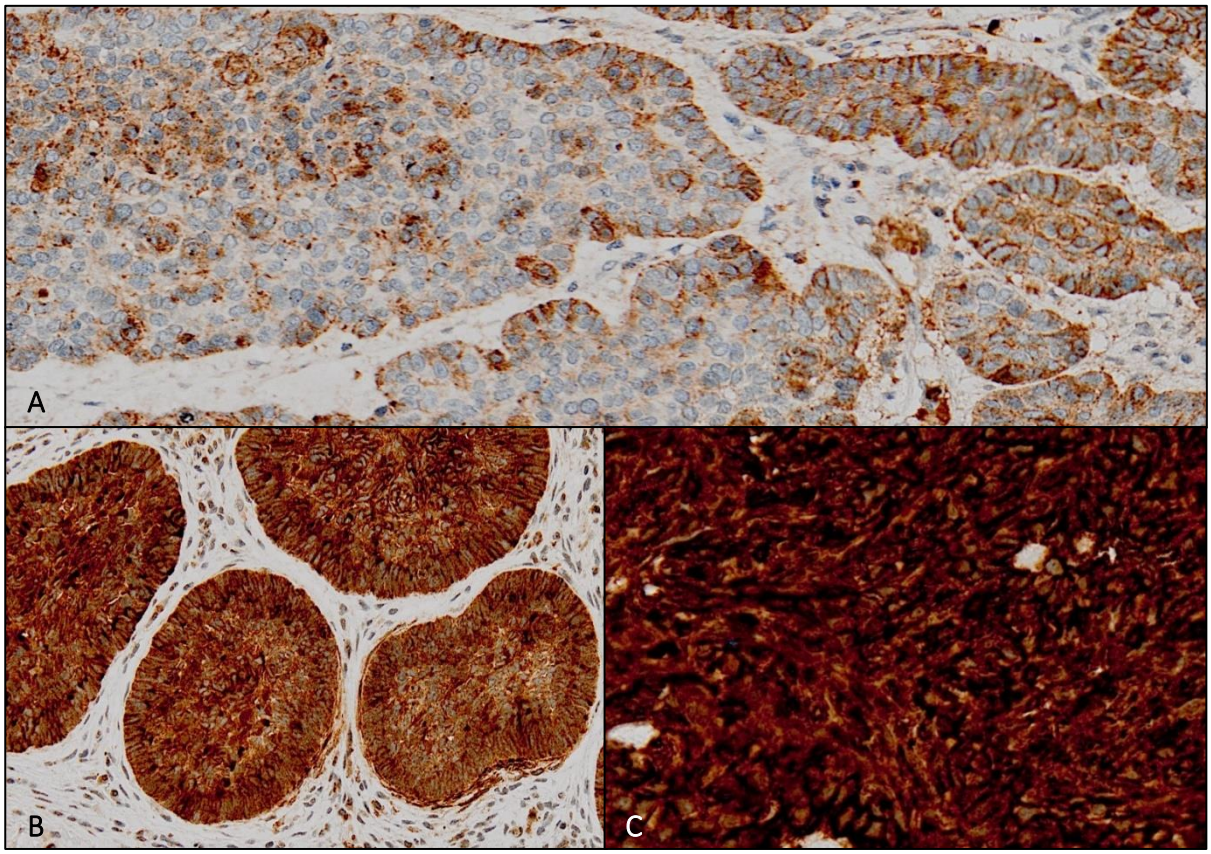

Figure 3.12 Tumoural CD138 intensity from 1 to 3+ at 20x magnification. A. Case 67 (basosquamous BCC) displaying the highest number of 1+ intensity (weak membranous and cytoplasmic) in the areas without squamous differentiation. B. Case 22 (nodular BCC) displaying diffuse 2+ intensity (moderate membranous and cytoplasmic). C. Case 85 (mixed nodular and infiltrating BCC) displaying a diffuse 3+ intensity (strong membranous and cytoplasmic) in the nodular component.

There were statistically significant findings in tumoural CD138 expression between the two risk categories (Figure 3.13). The mean expression of tumoural CD138 in the low-risk category was slightly higher (mean 99.86%; SD 0.62) compared to the high-risk category (mean 99.71%; SD 0.83%) ($p = 0.0035$). The mean expression of tumour CD138 in intensity categories 1+ and 2+ was lower in the low-risk category (4.44% and 75.22%) compared to the high-risk category (10.81% and 78.87%), however this difference was only significant for the 1+ category ($p =$

0.00086; Figure 3.14). In addition, low-risk BCC had a greater expression of 3+ intensity (20.21%) compared with high-risk BCC (10.03%), although this was not statistically significant (p = 0.041). Of the low-risk BCC, 97.37% had a strongly positive CD138 score compared to 85.71% of high-risk BCC (p = 0.016) and univariate analysis confirmed that high-risk BCCs were significantly less likely to have strong positive CD138 scores (p=0.001; risk ratio 0.44; confidence interval 0.27 - 0.71). Furthermore, on multivariate analysis, high-risk BCCs were significantly less likely to have a strong positive CD138 score (p<0.0001; risk ratio 0.33; confidence interval 0.21 - 0.52) even after adjusting for the p53 and BCL-2 scores.

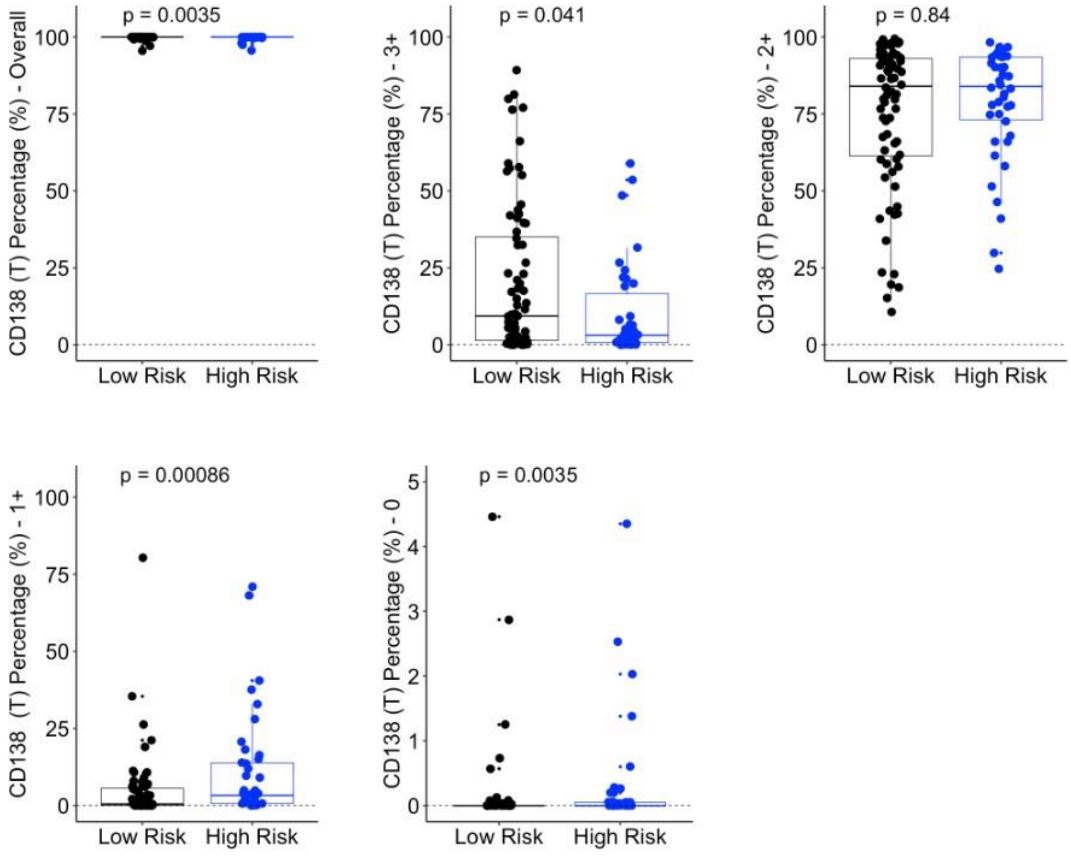

Figure 3.13 Tumoural CD138 expression stratification by risk category.

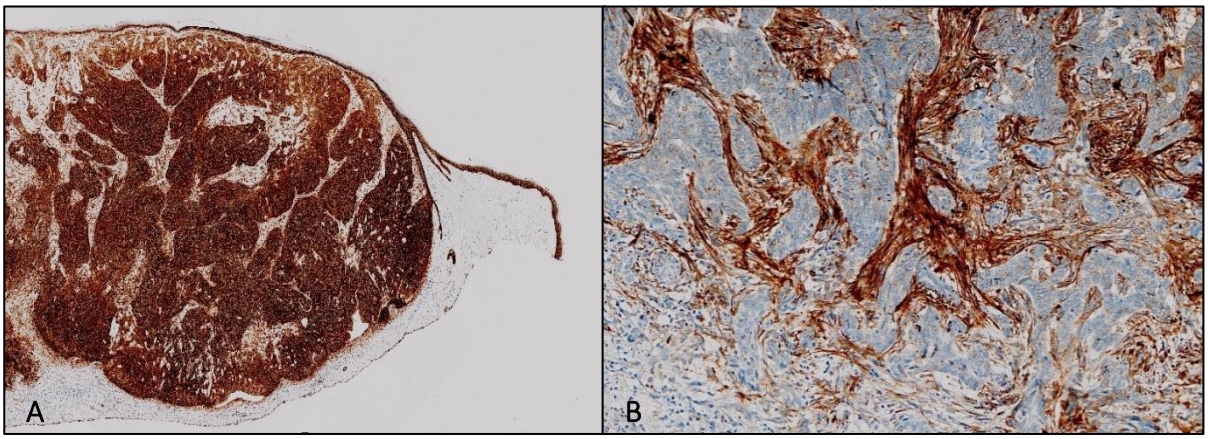

Figure 3.14 Staining outcomes for CD138 in the tumour of low- and high-risks. A. Case 4 (low-risk: nodular BCC) with a score of 'strongly positive' at 2 x magnification. B. Case 65 (high-risk: infiltrating BCC) with a score of 'moderately positive' overall with a focal area (31.03%) of 0 to 1+ intensity depicted here at 10x magnification.

3.4.4 CD138 in the peritumoural stroma

CD138 expression within the peritumoral stroma was assessed in 118 cases (76 low- and 42 high-risk BCC). Of these, 83.05% (n = 98) showed CD138 expression in both the stromal cells and matrix, 11.86% (n = 14) in the stromal cells only, and 5.09% (n = 6) in the stromal matrix only. The intensity of stromal CD138 expression ranged from 0 to 3+ and the proportion of staining ranged from 6.86% to 99.81% (Figure 3.15). The mean proportion of any intensity of CD138 expression in the peritumoural stroma in BCC overall was 73.11% (SD of 22.18%). The intensity was most frequently of 1+ intensity. The mean percentage of CD138 expression by peritumoral stroma for 0, 1+, 2+ and 3+ intensity categories was 26.9 (22.18), 30.89 (9.74), 25.59 (11.68) and 16.62 (10.57) respectively.

There were also statistically significant findings within peritumoural stromal CD138 expression between the two risk categories (Figure 3.16). The overall expression of stromal CD138 in low-risk BCCs was lower (mean 66.71%; SD 23.65) than high-risk BCCs (mean 84.70%; SD 12.91%) ($p < 0.0001$). This reduction was mostly caused by the lower frequency of the intensity categories 2+ and 3+ for low-risk BCCs (mean 21.77% and 13.30%) compared to high-risk BCCs in the same categories (mean 32.52% and 22.65%). In addition, there was a greater absence of stromal CD138 expression in low risk BCCs (mean 33.29%; SD of 23.65) compared to high-risk BCCs (mean 15.30%; SD of 12.91) ($p = <0.0001$).

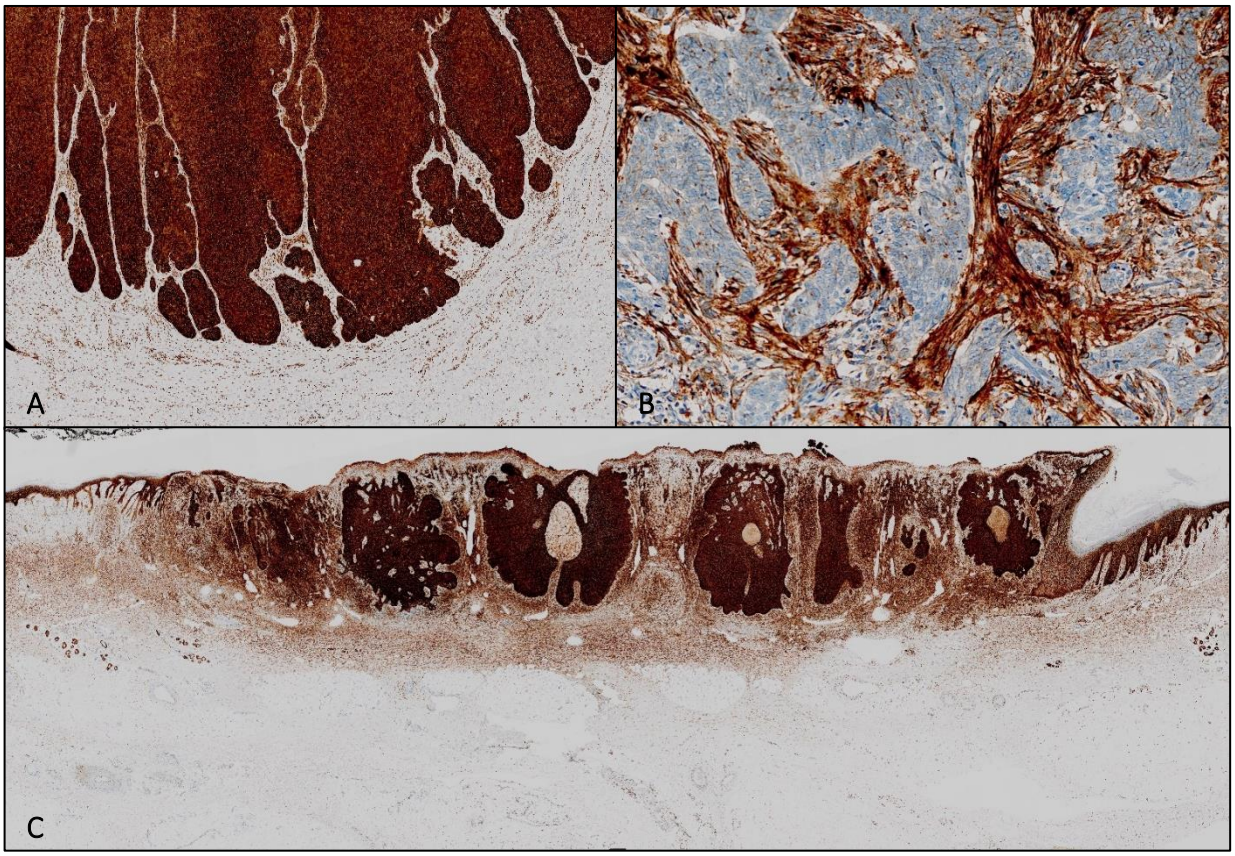

Figure 3.15 Staining outcomes for CD138 in the peritumoural stroma of low- and high-risk patterns. A. Case 99 (low-risk: nodular BCC) with a predominance of 1+ staining of stromal cells without stromal matrix staining (overall expression 51.97%) at 2.5 x magnification. B. Case 65 (high-risk: infiltrating BCC) with a predominance of 2 + staining of stromal cells and stromal matrix (overall expression 94.06%) at 10x magnification. C. Case 26 (low-risk: nodular BCC) with a predominance of 2+ and 3+ staining of stromal cells and stromal matrix (overall expression 95.21%) at 0.74 x magnification.

The expression of CD138 in the peritumoural stromal cells and stromal matrix was individually assessed between the low- and high-risk BCC categories. There was no significant difference in stromal cell positivity for CD138 between the two categories. However, high-risk BCCs were significantly more likely to display peritumoural stromal matrix positivity for CD138 compared to low-risk BCC ($p = 0.018$).

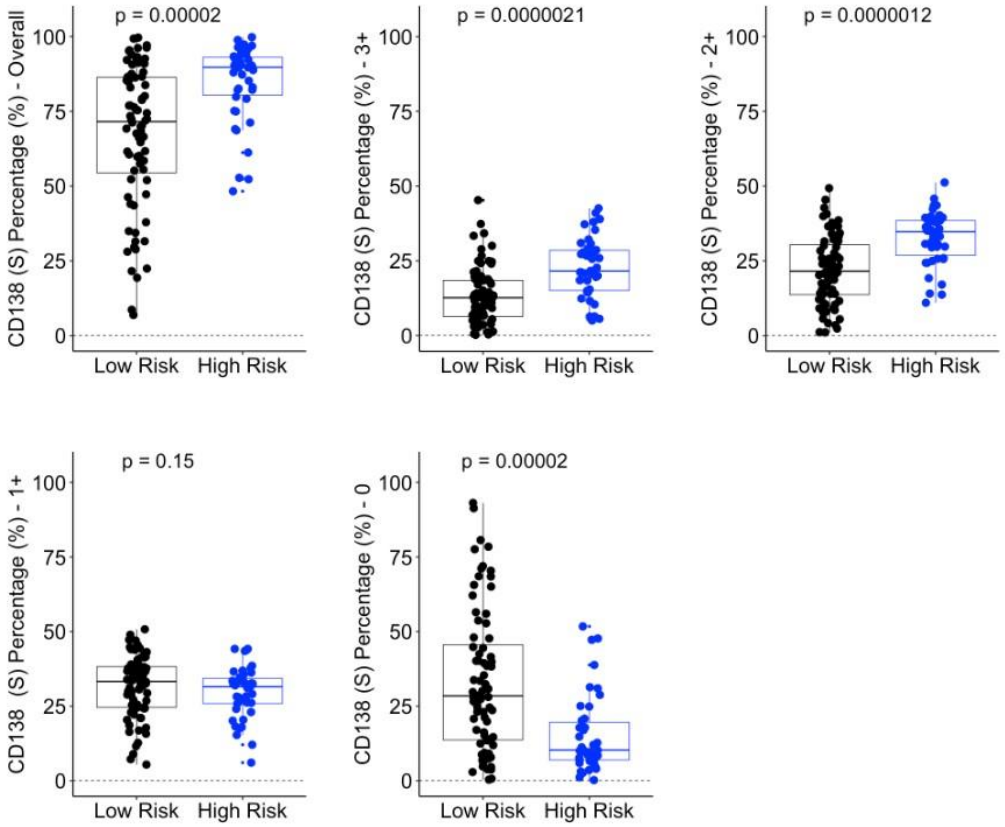

Figure 3.16 Peritumoural CD138 expression stratification by risk category.

3.5 Correlation of BCL-2, p53, CD138 immunohistochemical expression

The overall IHC expression (1+, 2+, 3+ intensities) of BCL-2, p53, tumoural CD138 and stromal CD138 in low-risk and high-risk categories was compared (Figure 3.17). A statistically significant correlation was found in the low-risk category when comparing CD138 expression in the tumour and stroma ($R = 0.31$, $p = 0.0072$). An increase in the expression of tumoural CD138 was positively correlated with an increase in the expression of stromal CD138. The high-risk category had a similar trajectory on the scatter plot; however, it did not have a statistically significant correlation. In addition, there was no statistically significant correlation between p53 and BCL-2 in both the low-risk and high-risk categories. In the low-risk category, the scatter plot shows a statistically insignificant decrease in p53 expression with increasing BCL-2 expression ($p = 0.87$). Furthermore, there was no statistically significant correlation between p53 and tumoural CD138, p53 and stromal CD138, BCL-2 and tumoural CD138, and BCL-2 and stromal CD138.

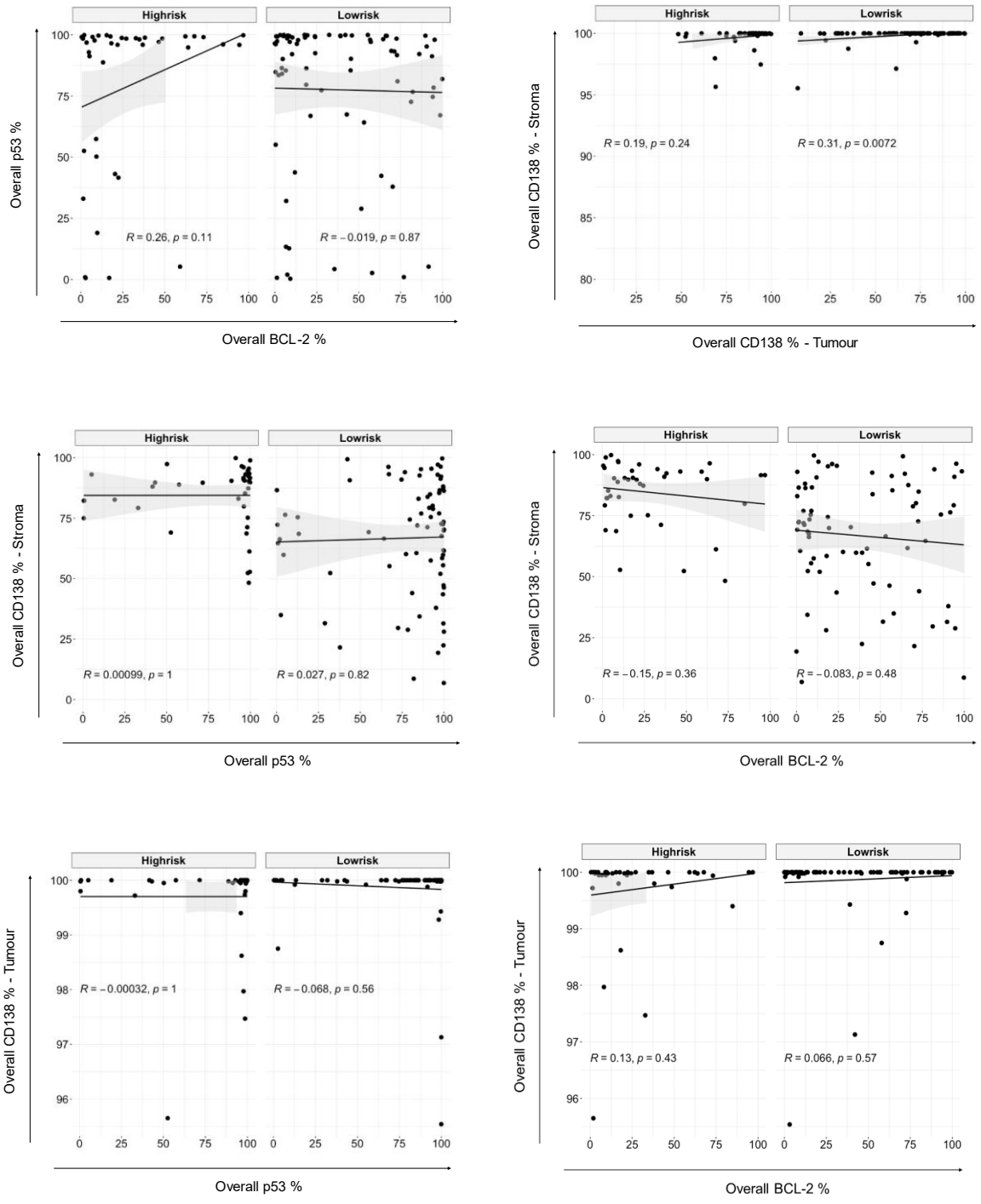

Figure 3.17 Correlation of immunohistochemical expression of BCL-2, p53, tumoural CD138 and stromal CD138.

Chapter 4: Discussion and recommendations

4.1 Key findings of our research and the interpretation thereof

4.1.1 Descriptive variables

Older age and male sex are established phenotypic risk factors for BCC, with international data reporting that males are 1.5 to 2 times as likely to develop BCC than females.(10,14) We found that BCCs occurred 1.5 times more frequently in males compared to females and predominantly in older adults (median age of 72 years). Our findings are also in keeping with local demographic data on BCC from TAH in Cape Town, South Africa where participants were more frequently male (55.7%) and older (median age of 70 years).(11)

The head and neck region is the most commonly documented site for BCC occurrence in both local and international literature, with published rates ranging from 53.5% to 95.9%.(4,6,11,15,17) This is ascribed to the higher UVR exposure from the sun in this region of the body.(17) We found that 62.5% of BCCs in our cohort arose in the skin of the head and neck region followed, in order of frequency, by the skin of the trunk, limbs, and other sites. When excluding cases labelled only as 'face' we found that 66.67% of BCC in the head and neck region arose within the high-risk mask area. This is similar to the findings from TAH where 69.05% of head and neck BCCs arose in the high-risk mask area.(11)

We found that the sex, age, and site distribution were similar in both low- and high-risk BCC categories. However, our study was limited by combining distinct histological subtypes to simplify our analysis. Superficial BCCs have been reported to occur more frequently in younger patients and more frequently on the trunk compared to other histological BCC subtypes.(39,102) The low number of superficial BCC (14.4%) in our study may explain why the data was not significantly skewed in the low-risk BCC category, although other published data does dispute the unequal distribution of superficial BCC arising on the trunk.(103)

4.1.2 BCC histological subtypes

In accordance with local and international data, we found that nodular BCCs were the most common histological BCC subtype.(10,11,15,21,28) Although superficial BCCs in our cohort comprised a similar percentage of BCC to published data, it was not the second most common

histological subtype.(10) Instead, infiltrating and mixed BCCs occurred more commonly than superficial BCCs, and the proportion of infiltrating BCCs was higher than that reported in the literature.(103) This apparent elevated prevalence can be explained by selection bias, as the aim of our method was to select an equal number of high-risk and low-risk BCCs for our study. When looking at each cohort separately, nodular and infiltrating BCCs were the most frequent histological subtype in the low- and high-risk categories respectively which is in keeping with published data.(103)

Mixed BCCs comprised 17.3% of our cohort and, although lower than the prevalence reported in many studies,(104,105) was similar to the prevalence of 17.8% reported by one other study.(106) This result may also have been affected by selection bias, as most of the mixed BCCs had a high-risk histological component and therefore a selection advantage. Similar to another study, we found that the mixed BCCs most frequently comprised of nodular and infiltrative components.(104)

4.1.3 IHC expression

4.1.3.1 BCL-2

Of all the assessed BCC, 78.33% expressed BCL-2 based on a ≥ 6% cut off proportion (score of 1). This proportion is comparable to most publications, including a local South African study, with BCL-2 expression in BCCs ranging from 62 to 100%.(31–37,39–41,43–47,49,50,82) A single study has reported a lower BCL-2 positivity rate of 39% despite the use of a similar scoring system to many other studies; however, they acknowledged that this may have been due to the use of a different BCL-2 antibody clone - which they did not name.(42) This high expression of BCL-2 can be relied upon to support the diagnosis of BCC in clinical practice when other differential diagnoses, e.g. squamous cell carcinoma, are being considered; and BCL-2 expression is attributed to the origin from basal keratinocytes.(35,46) Our results affirm the use of BCL-2 to assist in the diagnosis of BCC in clinical practice.

We found the mean proportion of BCL-2 staining to be approximately one third of tumour cells. This is comparable to the proportion of 31.76% previously reported in non-XP related BCCs.(41) However, this proportion is lower than elsewhere reported (65.6 to 93.5%)(35,50) and despite one study cohort with a large proportion of high-risk BCCs (83%) which could be expected to

lower the BCL-2 score.(50) Nevertheless, comparable data is limited as many studies do not report on the mean proportion of BCL-2 staining and our data may well be within normal limits. For example, two such studies not reporting a mean proportion of BCL-2 staining both showed a predominance of low BCL-2 scores (60.3 to 66.1%) and would therefore likely have had a mean BCL-2 proportion of less than 50%.(36,43) Interestingly, despite similar BCL-2 proportions, the one study had a predominance of high-risk BCCs (77%)(36) while the other had a predominance of low-risk BCC (100%)(43) – explored later.

This low mean proportion is further reflected by the finding of a mean BCL-2 score of 1.67 in our study. This is regarded as low 'BCL-2 labelling' by some scoring systems.(34) This mean BCL-2 score is comparably lower than the mean BCL-2 score of 2.95 in first BCC occurrences reported by another local study evaluating aggressive and non-aggressive BCCs. This study found that low BCL-2 expression was predictive of aggressive BCCs and collected data on both patient clinical presentation and follow-up.(34) Our study did not collect this data; and therefore is limited by the inability to further contextualise this low mean BCL-2 score fully. However, our cohort did have a higher proportion of high-risk BCCs compared to the previous study (42.31% versus 36%) which could account for this lower mean BCL-2 score - as discussed later.

We also found that the composition of BCL-2 intensity was predominantly weak (1+) as opposed to moderate (2+) or strong (3+) in a single tumour. Although there is data qualifying BCL-2 intensity in BCC(35), to our knowledge the composition of different BCL-2 intensities in BCC has not been objectively quantified before in the English literature. Together with the low proportion, the predominance of weak BCL-2 staining highlights the potential limitation of BCL-2 immunohistochemistry to corroborate the diagnosis of BCC in small biopsies, as weak and focal expression may be missed or not represented in the tumour sample.

When comparing low- and high-risk BCCs, we found that high-risk BCCs tended to have lower mean BCL-2 scores than low-risk BCCs. This data aligns with published literature, including several studies which have reported significantly lower BCL-2 expression in high-risk BCCs.(34–37,39,49) The lack of statistical significance in our above finding may be due to our small sample size. Although reporting statistical significance, several studies evaluating BCL-2 are

limited by: the lack of clarity of the specific BCL-2 variable they measured statistically e.g. BCL-2 score versus BCL-2 labelling,(37,49) how BCL-2 expression was quantified,(39) a lack of statistical analysis to support their interpretation,(68) or not being published in English.(44,82) In fact, when we aligned our analysis to reflect those studies with transparent statistical analysis using 'BCL-2 labelling', we found we achieved a statistically significant finding between high- and low-risk BCC. 'BCL-2 labelling' combines BCL-2 scores 1 and 2 into 'low labelling' and scores 3 and 4 into 'high labelling'. Two studies comparing BCL-2 low versus BCL-2 high labelling(34,36) found significantly lower BCL-2 expression in aggressive and high-risk BCCs respectively. We did not find significantly lower BCL-2 expression in high-risk BCC when we grouped our BCL-2 scores in a similar manner. Again, this may be due to our small sample size. However, similar to a third study,(35) our results achieved statistical significance when we combined BCL-2 negative scores into the 'low labelling' cohort; with high-risk BCC showing significantly lower BCL-2 expression compared to low-risk BCC. A plausible reason for this reduction in BCL-2 expression is that high-risk BCCs may have more frequent mutations resulting in loss of heterozygosity of the *BCL-2* gene, with a resultant loss of protein expression,(42)or additional genetic mutations leading to the down regulation of BCL-2.(49) Perhaps it is these underlying mutations which drives the aggressive phenotype reportedly associated with low BCL-2 expression.(34) Although low BCL-2 expression may be a surrogate predictor of aggressive behaviour in BCCs,(34) the inconsistent expression in individual cases means the utility of BCL-2 immunohistochemistry on a case-by-case basis in clinical practice is unlikely to add useful prognostic information to existing histologic features such as histological subtype and perineural invasion, for example.

4.1.3.2 p53

Of all the assessed BCC, 90.83% expressed p53 based on a ≥ 6% cut off proportion (score of 1). This high proportion of p53 staining in BCC is comparable to four other studies,(68,81,87,88) one of which used a similar cut off proportion.(68) The staining of p53 has been reported as strong and diffuse by some authors(72) and our findings were similar: the average proportion of staining was greater than three quarters of the tumour cells and the intensity of staining was mostly strong, resulting in a mean score of 3.32 overall. This increased expression of p53 may reflect either underlying *TP53* mutations(24,25) or an upregulation of WT p53 due to oncogenic stressors.(61) We did not assess p53 subcellular localisation.

Like many other studies published in the English literature(47,68,69,73,74,76,77,80,85), we found no statistically significant differences in the proportion, intensity, or scores of p53 immunoreactivity between low and high-risk BCCs. While some studies have found differential p53 expression in some high-risk histological BCC subtypes,(39,66,71,86) it is difficult to interpret these results accurately without knowing the proportion of underlying *TP53* mutations and WT p53 upregulation in these cohorts. For example, *TP53* mutations have been observed more frequently in aggressive BCC(54) and yet existing data suggests that p53 immunohistochemistry and *TP53* mutations do not correlate in BCCs.(56) Additionally, unlike in high-grade tubo-ovarian serous carcinoma;(61) p53 immunohistochemical expression patterns have not been correlated with mutation status in BCC.

4.1.3.3 Tumoural CD138

We found that all the assessed BCCs expressed CD138; an anticipated finding as BCCs are epithelial in origin.(93) In addition, the vast majority were scored as 'strongly positive' - in keeping with existing data.(95) Furthermore, we found significantly lower CD138 scores in high-risk BCCs compared to low-risk BCCs, thus confirming a previously published similar finding which lacked statistical significance.(97) This difference was a result of a significantly lower proportion of '3+' and significantly higher proportions of '1+' and '0' intensity of CD138 tumour cell immunoreactivity in high-risk BCCs. This is also in keeping with research into CD138 expression in other malignancies, which has found reduced CD138 tumoral expression to be associated with an increase in tumour aggression, grade, invasion and worse patient outcome.(94,95) (96,97) This decrease is thought to be due to tumoral protease activity and/or transcriptional- or posttranscriptional regulation.(96)

4.1.3.4 Stromal CD138

All the assessed BCCs expressed CD138 within the peritumoural stroma and most showed a combination of immunoreactivity of the stromal matrix and cells. This was higher than previously described,(96,97) possibly because we included both matrix and cells for assessment.

CD138 expression in the peritumoral stroma was most frequently of weak intensity. Low-risk BCCs had a significantly lower proportion of peritumoural stromal CD138 immunoreactivity;

including a significantly lower proportion of '0+' and significantly higher proportions of '2+' and '3+' intensity of CD138 stromal immunoreactivity compared to high-risk BCCs. This significant difference was maintained when comparing the stromal matrix between risk categories, however not when only stromal cells were compared. These stromal cells included plasma cells; and it is likely that the inflammatory infiltrate does not differ between different BCC subtypes. The increased expression of CD138 in the stromal matrix of high-risk BCCs is not unexpected given the significant results of two previous studies(96,97) and may be either due to CD138 shedding or induction of stromal expression by tumour cells.(96) CD138 expression is a poor prognostic indicator in most tumour types(94) and the increased expression in high-risk histological subtypes confirms this finding for BCCs too.

4.1.3.5 Correlation between IHC proportions

Two studies found that p53 staining increases as BCL-2 staining decreases(42,92) and a third found p53 and BCL-2 staining to be mutually exclusive with the exception of one patient.(41) We failed to find a similar correlation between p53 and BCL-2 staining. This may be because, unlike some studies, we found no significant increase in p53 in our high-risk cohort. Alternatively, because we correlated the results separately for high- and low-risk BCCs rather than overall.

An increase in the expression of tumoural CD138 in low-risk BCCs was significantly correlated with an increase in the expression of stromal CD138. This finding was not present in high-risk BCCs. This is an unexpected finding, as tumoural CD138 expression was marginally reduced in high-risk BCCs and stromal CD138 staining was increased. Therefore, we anticipated a negative rather than positive correlation. Perhaps the inclusion of stromal cells to the stromal matrix altered this correlation; and we should have excluded the former from the analysis.

4.2 Study strengths and limitations

A retrospective, cross-sectional study design was chosen due to its simplicity and feasibility; to align with the short time frame in which to complete a Masters of Medicine (MMed.) This design also enabled the use of readily available material in our division's archives to measure and compare multiple variables. It was also relatively inexpensive and therefore fell within the budget allowed by the NHLS Research Trust grant. Additionally, the analytical design allowed

us to collect data to which statistical analysis could be applied to compare our study groups and variables. The design further eliminated potential bias due to loss to follow-up or a change in desired outcome such as an alternative diagnosis or sample type. The observational nature of the design made the study feasible, as the low risk to participants meant we did not require informed consent which can be time consuming and result in selection bias.

Another strength was that our results added to the pool of existing data on protein expression in BCC, contributing to our understanding of BCCs and the high- and low-risk BCC subtypes. We were able to confirm previously published findings in a unique African setting. This is an important area of research, as BCCs are common cancers globally as well as in our setting; and have also been noted to be increasing in frequency. In addition, they are costly to the health sector and new treatment modalities are emerging to combat recurrences.

Furthermore, we made use of digital analysis to provide objectivity to our data interpretation and thus ensure the validity of our results. Our methods are transparent and the scripts for the QuPath digital analysis platform are available for use by future researchers to replicate, enabling reproducibility of future data. Lastly, the capturing of our results onto the secure Redcap database means we can potentially contribute this preserved data to future research by ourselves or other researchers globally. Redcap also has an advantage over programs such as Excel in that data cannot be erroneously deleted or incorrectly captured in an undesired format.

One limitation of our study design was that we were unable to study a rare occurrence, namely UV-unexposed BCCs. We identified only a single case over a 5-year period and therefore had to exclude the comparison of UV- exposed and UV-unexposed BCCs from our study. A case-control study would have been better suited to this aim. Another limitation was that we were required to reduce the optimal sample size to make the study more cost- and time-effective. However, we still managed to achieve statistical significance in several of our aims despite this. A further limitation of the cross-sectional design is that we were unable to explain the differences we observed in our cohorts based purely on our own data and without extrapolation from the literature. We could also not exclude confounders, such as underlying genetic mutations, from our study. Additionally, we had no follow-up data to assess for disease

recurrence and patient outcome in relation to the differences we noted between high- and low-risk BCCs. The conventional drawbacks of a cross-sectional study, e.g., inability to measure incidence, duration of disease and temporality etc. were not applicable to this research.

A limitation in our study method was to include mixed BCCs. Mixed BCCs were more time consuming to study as we had to ensure that both components were adequately represented on one H&E slide, the tissue block, and the three subsequent immunohistochemical stains. It also made the data analysis, data capturing and statistical analysis more complex than necessary with duplicate entries, mislabelling of components and putting poorly planned databases to the test. This was resolved with meticulous rechecking and redesigning of the parent spreadsheet for statistical analysis; a time consuming yet valuable lesion that was learnt! In hindsight, excluding mixed BCCs would have saved both time and effort.

As briefly mentioned above, our results were limited to an observed difference in BCL-2 and CD138 staining between high- and low-risk BCCs. We were unable to provide an explanation for this difference based on our own research and had to use existing data to theorise about why this difference exists. Nevertheless, it remains useful that we have confirmed this difference and future research with experimental designs may further elucidate the “why” for us.

Lastly, the limitations of the digital analysis were overcome by interdisciplinary collaboration. The use of the Olympus VS120 Digital Slide Scanner and QuPath digital analysis platform required expertise in technology and an individual well-versed in the software, while the interpretation of tumour cells versus stroma, for example, requires expertise in histopathology. We were fortunate to have this expertise available to us and it required good communication and frequent meetings to identify the areas of interest for analysis and subsequently apply the software to generate the output of interest. Although this is a limitation in terms of time and potential cost, it is outweighed by the benefit of obtaining a more objective and reproducible data set. Digital analysis is also limited by the need for a constant energy supply and potentially expensive virtual storage of data. Our equipment is based on UCT medical school campus and is therefore subject to Eskom power outages.

4.3 Implications of results and recommendations for future research

The implications of our results are that BCCs in our setting emulate BCCs globally and thus our data can be compared with international literature. Conversely, we can safely apply outcomes and recommendations of international data to our clinical practice. We have also shown that the expression of select proteins differs between high- and low-risk BCCs. This knowledge is useful to better understand BCCs and direct future experimental research to potentially improve treatment options for recurrent and clinically aggressive BCCs.

Our recommendations for future research into immunohistochemistry include examining the differences in BCL-2 and CD138 in high- and low-risk BCCs in UV- exposed and UV-unexposed sites. In addition, to compare p53 immunoexpression and subcellular localisation with *TP53* mutations in BCCs overall; and to compare the frequency of *TP53* mutations between high- and low-risk BCCs. Furthermore, to assess the histological subtypes of BCL-2 negative BCCs and to further subject them to molecular analysis to assess for chromosome 18q loss of heterozygosity and/ or other genetic alterations. Lastly, to compare CD138 expression in the stromal matrix of ulcerated versus non-ulcerated BCCs as well as between BCCs with severe solar elastosis and those with little to no solar elastosis.

Other recommendations for future research include a meta-analysis of the large pool of existing data relating to BCL-2 and p53 immunohistochemistry in BCC. To aid this, we would recommend the use of standardised terminology based on the WHO Classification of Skin Tumours(1) and clear definitions of “aggressive” versus “high-risk BCC”. In addition, to make available a transparent and complete study method including information such as the antibody clone used, the scoring system applied for interpretation of positive and negative staining, as well as manual versus digital analysis. Further, to consider the worthwhile investment into digital pathology of both human- and non-human resources and to share software scripts across institutions to make data as comparable as possible.

4.4 Conclusion

BCCs are common cutaneous cancers of older adults, with a slight male predominance. They are frequently associated with UV-exposure and as such typically arise in the head and neck region. BCL-2 is a marker of basal keratinocyte differentiation and is frequently expressed by

BCC, thus forming a useful adjunct in the diagnosis when considering histological mimickers. Importantly, BCL-2 expression may be weak and focal in BCCs and even reduced in both clinically aggressive and high-risk histological patterns. This limitation should be borne in mind when interpreting a negative BCL-2 stain. Although a reduction in BCL-2 may be associated with aggressive behaviour in BCCs, we would recommend against the use of BCL-2 in clinical practice to add prognostic or predictive value until further research indicates otherwise. In addition, *TP53* mutations are common in BCCs and may even predominate in high-risk BCCs. However, p53 immunohistochemistry is not a useful surrogate for these mutations as the majority of BCCs are positive with no difference in expression between high- and low-risk BCCs. Although several studies with opposing data do exist, we believe that there is currently no advantage to the use of p53 immunohistochemistry in evaluating BCCs in the clinical setting. Lastly, the cell membrane protein CD138 is moderately to strongly expressed by the tumour cells of BCCs. This immunohistochemical expression is reduced, although not absent, in high-risk BCCs which also show an increase in stromal matrix expression compared to low-risk BCCs. This transition from tumour to stroma may aid in tumour growth and recurrence.

Chapter 5: References

1. Messina J, Epstein EJ, Kossard S, McKenzie C, Patel R, Patterson J, et al. Basal cell carcinoma. In: Elder D, Massi D, Scolyer R, Willemze R, editors. WHO Clasification of Skin Tumours. Fourth. Lyon: IARC; 2018. p. 26–34.
2. Jacob A. Observations respecting an ulcer of peculiar character, which attacks the eyelids and other parts of the face. 7;4. In: Dublin Hospital Rep Commun Med Surg. 1827. p. 232–9.
3. Lomas A, Leonardi-Bee J, Bath-Hextall F. A systematic review of worldwide incidence of nonmelanoma skin cancer. Br J Dermatol. 2012;166(5):1069–80.
4. Kappelin J, Green AC, Ingvar Å, Ahnlide I, Nielsen K. Incidence and trends of basal cell carcinoma in Sweden: a population-based registry study*. Br J Dermatol. 2022;186(6):963–9.
5. National Cancer Registry data [Internet]. 2014 [cited 2020 Mar 27]. Available from: http://www.nicd.ac.za/wp-content/uploads/2019/12/2014-NCR-tables.pdf
6. Norval M, Kellett P, Wright CY. The incidence and body site of skin cancers in the population groups of south africa. Photodermatol Photoimmunol Photomed. 2014;30(5):262–5.
7. De Wet J, Steyn M, Jordaan HF, Smith R, Claasens S, Visser WI. An Analysis of Biopsies for Suspected Skin Cancer at a Tertiary Care Dermatology Clinic in the Western Cape Province of South Africa. J Skin Cancer. 2020;2020.
8. York K, Dlova NC, Wright CY, Khumalo NP, Kellett PE, Kassanjee R, et al. Primary cutaneous malignancies in the Northern Cape Province of South Africa: A retrospective histopathological review. South African Med J. 2017;107(1):83–8.
9. Gordon LG, Elliott TM, Wright CY, Deghaye N, Visser W. Modelling the healthcare costs of skin cancer in South Africa. BMC Health Serv Res [Internet]. 2016;16(1):1–9.
10. Cameron MC, Lee E, Hibler BP, Barker CA, Mori S, Cordova M, et al. Basal cell carcinoma: Epidemiology; pathophysiology; clinical and histological subtypes; and disease associations. J Am Acad Dermatol [Internet]. 2019;80(2):303–17.
11. Gallo JC, Schneider JW, De Wet J, Moxley K, Jordaan HF, Visser WI, et al. A Profile and Three-Year Follow-Up of Patients with Basal Cell Carcinoma in the Western Cape, South Africa. J Skin Cancer. 2022;2022.

12. Hoorens I, Vossaert K, Ongenae K, Brochez L. Is early detection of basal cell carcinoma worthwhile? Systematic review based on the WHO criteria for screening. Br J Dermatol. 2016;174(6):1258–65.
13. Kilgour JM, Jia JL, Sarin KY. Review of the molecular genetics of basal cell carcinoma; inherited susceptibility, somatic mutations, and targeted therapeutics. Cancers (Basel). 2021;13(15).
14. Verkouteren JAC, Ramdas KHR, Wakkee M, Nijsten T. Epidemiology of basal cell carcinoma: scholarly review. Br J Dermatol. 2017;177(2):359–72.
15. Kasumagic-Halilovic E, Hasic M, Ovcina-Kurtovic N. A Clinical Study of Basal Cell Carcinoma. Med Arch (Sarajevo, Bosnia Herzegovina). 2019;73(6):394–8.
16. Kopf AW. Basal-cell carcinomas of the skin. J Dermatol. 1979;6(5):267–81.
17. Chinem, Valquiria P. Miot H. Epidemiology of basal cell carcinoma Epidemiologia do carcinoma basocelular. An Bras Dermatolog [Internet]. 2011;86(2):292–305.
18. Goon P, Banfield C, Bello O, Levell NJ. Skin cancers in skin types IV–VI: Does the Fitzpatrick scale give a false sense of security? Ski Heal Dis. 2021;1(3):1–5.
19. Ferreira FR, Pevide B da C, Rodrigues RF, Nascimento LFC, Lira ML de A. Differences in age and topographic distribution of the different histological subtypes of basal cell carcinoma, Taubaté (SP), Brazil. An Bras Dermatol. 2013;88(5):726–30.
20. Rosso S, Zanettil R, Martinez C, Tormo MJ, Schraub S, Franceschi S, et al. The multicentre south European study ' Helios ' II : different sun exposure patterns in the aetiology of basal cell and squamous cell carcinomas of the skin. Br J Cancer. 1996;73(11):1447–54.
21. Scrivener Y, Grosshans E, Cribier B. Variations of basal cell carcinomas according to gender, age, location and histopathological subtype. Br J Dermatol. 2002;147(1):41–7.
22. Lam C, Ou JC, Billingsley EM. "pTCH"-ing it together: A basal cell nevus syndrome review. Dermatologic Surg. 2013;39(11):1557–72.
23. Süngü N, Kiran MM, Tatli Doğan H, Kiliçarslan A, Karakök E, Akyol M. Evaluation of p53 and Ki67 expression profiles in basal cell carcinomas in a usual and an unusual location. Turk Patoloji Derg. 2018;34(2):165–70.
24. Jayaraman SS, Rayhan DJ, Hazany S, Kolodney MS. Mutational landscape of basal cell carcinomas by whole-exome sequencing. J Invest Dermatol [Internet]. 2014;134(1):213–20.

25. Pellegrini C, Maturo MG, Di Nardo L, Ciciarelli V, Gutiérrez García-Rodrigo C, Fargnoli MC. Understanding the molecular genetics of basal cell carcinoma. Int J Mol Sci. 2017;18(11).
26. Marzuka AG, Book SE. Basal cell carcinoma: Pathogenesis, epidemiology, clinical features, diagnosis, histopathology, and management. Yale J Biol Med. 2015;88(2):167–79.
27. Sloane JP. The value of typing basal cell carcinomas in predicting recurrence after surgical excision. Br J Dermatol. 1977;96(2):127–32.
28. Sexton M, Jones DB, Maloney ME. Histologic pattern analysis of basal cell carcinoma: Study of a series of 1039 consecutive neoplasms. J Am Acad Dermatol [Internet]. 1990;23(6):1118–26.
29. Correia De Sá TR, Silva R, Lopes JM. Basal cell carcinoma of the skin (part 2): Diagnosis, prognosis and management. Futur Oncol. 2015;11(22):3023–38.
30. Costache M, Georgescu TA, Oproiu AM, Costache D, Naie A, Sajin M, et al. Emerging concepts and latest advances regarding the etiopathogenesis, morphology and immunophenotype of basal cell carcinoma. Rom J Morphol Embryol. 2018;59(2):427–33.
31. Cerroni L, Kerl H. Aberrant bcl-2 protein expression provides a possible mechanism of neoplastic cell growth in cutaneous basal-cell carcinoma. J Cutan Pathol. 1994;21(5):398–403.
32. Verhaegh MEJM, Sanders CJG, Arends JW, Neumann HAM. Expression of the apoptosis-suppressing protein Bcl-2 in non-melanoma skin cancer. Br J Dermatol. 1995;132(5):740–4.
33. Rodriguez-Villanueva J, Colome MI, Brisbay S, McDonnell TJ. The Expression and Localization of bcl-2 Protein in Normal Skin and in Non-Melanoma Skin Cancers. Pathol Res Pract [Internet]. 1995;191(5):391–8.
34. Ramdial PK, Madaree A, Reddy R, Chetty R. Bcl-2 protein expression in aggressive and non-aggressive basal cell carcinomas. J Cutan Pathol. 2000;27(6):283–91.
35. Bartoš V, Kullová M. Expression of Anti-Apoptotic Protein Bcl-2 in Cutaneous Basal Cell Carcinoma. J Cancer Allied Spec. 2018;4(4).
36. Sivrikoz O, Kandiloğlu G. The Effects of Cyclin D1 and Bcl-2 Expressıon on Aggressive Behavior in Basal Cell and Basosquamous Carcinoma. Iran J Pathol. 2016;42(1):9–14.

37. Crowson AN, Magro CM, Kadin ME, Stranc M. Differential expression of the bcl-2 oncogene in human basal cell carcinoma. Hum Pathol. 1996;27(4):355–9.
38. Rossiter H, Beissert S, Mayer C, Schön MP, Wienrich BG, Tschachler E, et al. Targeted expression of bcl-2 to murine basal epidermal keratinocytes results in paradoxical retardation of ultraviolet- and chemical-induced tumorigenesis. Cancer Res. 2001;61(9):3619–26.
39. Zagrodnik B, Kempf W, Seifert B, Müller B, Burg G, Urosevic M, et al. Superficial Radiotherapy for Patients with Basal Cell Carcinoma: Recurrence Rates, Histologic Subtypes, and Expression of p53 and Bcl-2. Cancer. 2003;98(12):2708–14.
40. Chang CH, Tsai RK, Chen GS, Yu HS, Chai CY. Expression of bcl-2, p53 and Ki-67 in arsenical skin cancers. J Cutan Pathol. 1998;25(9):457–62.
41. Abid K, Fazaa B, Hadouchi C, El Mezni F, Kamoun MR, Hamzaoui K. Differential expression of Bcl-2, Bax, and CD95 in DNA repair-proficient and DNA repair-deficient basal cell carcinoma patients [32]. Int J Dermatol. 2006;45(12):1482–5.
42. Cho S, Hahm JH, Hong YS. Analysis of p53 and BAX mutations, loss of heterozygosity, p53 and BCL2 expression and apoptosis in basal cell carcinoma in Korean patients. Br J Dermatol. 2001;144(4):841–8.
43. Wang WJ, Huang JY, Wong CK, Chang YT. A study of secondary cutaneous amyloidosis in basal cell carcinoma in Chinese patients: Lack of correlation with bcl-2 or p53 protein expression. Arch Dermatol Res. 2000;292(8):379–83.
44. Corrêa MDPD, Ferreira AP, Gollner ÂM, Rodrigues MF, Guerra MCDS. Expressão de marcadores de proliferação celular e apoptose em carcinoma basocelular. An Bras Dermatol. 2009;84(6):606–14.
45. Abu Juba B, Şovrea A, Crişan D, Melincovici C, Coneac A, Badea M, et al. Apoptotic markers in photoinduced cutaneous carcinoma. Rom J Morphol Embryol. 2013;54(3):741–7.
46. Ramezani M, Mohamadzaheri E, Khazaei S, Najafi F, Vaisi-Raygani A, Rahbar M, et al. Comparison of EMA, CEA, CD10 and Bcl-2 biomarkers by immunohistochemistry in squamous cell carcinoma and basal cell carcinoma of the skin. Asian Pacific J Cancer Prev. 2016;17(3):1379–83.
47. Ionescu DN, Arida M, Jukic DM. Metastatic basal cell carcinoma: Four case reports, review of literature, and immunohistochemical evaluation. Arch Pathol Lab Med.

2006;130(1):45–51.

48. Córdoba A, Guerrero D, Larrinaga B, Iglesias ME, Arrechea MA, Yanguas JI. Bcl-2 and CD10 expression in the differential diagnosis of trichoblastoma, basal cell carcinoma, and basal cell carcinoma with follicular differentiation. Int J Dermatol. 2009;48(7):713–7.
49. Bozdogan Ö, Erkek E, Atasoy P, Koçak M, Birol A, Çaydere M. Bcl-2-related proteins, α-smooth muscle actin and amyloid deposits in aggressive and non-aggressive basal cell carcinomas. Acta Derm Venereol. 2002;82(6):423–7.
50. Vidal D, Matías-Guiu X, Alomar A. Efficacy of imiquimod for the expression of Bcl-2, Ki67, p53 and basal cell carcinoma apoptosis. Br J Dermatol. 2004;151(3):656–62.
51. Kastenhuber ER, Lowe SW. Putting p53 in Context. Cell [Internet]. 2017;170(6):1062–78.
52. Boutelle AM, Attardi LD. p53 and Tumor Suppression: It Takes a Network. Trends Cell Biol [Internet]. 2021;31(4):298–310.
53. Green DR, Kroemer G. Cytoplasmic functions of the tumour suppressor p53. Nature. 2009;458(7242):1127–30.
54. Bolshakov S, Walker CM, Strom SS, Selvan MS, Clayman GL, El-Naggar A, et al. P53 Mutations in Human Aggressive and Nonaggressive Basal and Squamous Cell Carcinomas. Clin Cancer Res. 2003;9(1 I):228–34.
55. Wang YM, Huang YS, Ma ZH, Bu DF, Wang Y, Tu P, et al. Frequency and features of TP53 mutation in 30 Chinese patients with sporadic basal cell carcinoma. Clin Exp Dermatol. 2014;39(7):829–34.
56. Weihrauch M, Bader M, Lehnert G, Wittekind C, Tannapfel A, Wrbitzky R. Carcinogen-specific mutation pattern in the p53 tumour suppressor gene in UV radiation-induced basal cell carcinoma. Int Arch Occup Environ Health. 2002;75(4):272–6.
57. Mizuno T, Tokuoka S, Kishikawa M, Nakashima E, Mabuchi K, Iwamoto KS. Molecular basis of basal cell carcinogenesis in the atomic-bomb survivor population: p53 and PTCH gene alterations. Carcinogenesis. 2006;27(11):2286–94.
58. Hsu CH, Yang SA, Wang JY, Yu HS, Lin SR. Mutational spectrum of p53 gene in arsenic-related skin cancers from the blackfoot disease endemic area of Taiwan. Br J Cancer. 1999;80(7):1080–6.
59. Wang GY, Wood CN, Dolorito JA, Libove E, Epstein EH. Differing tumor-suppressor

functions of Arf and p53 in murine basal cell carcinoma initiation and progression. Oncogene [Internet]. 2017;36(26):3772–80.

60. Kanellou P, Zaravinos A, Zioga M, Spandidos DA. Deregulation of the tumour suppressor genes p14ARF, p15 INK4b, p16INK4a and p53 in basal cell carcinoma. Br J Dermatol. 2009;160(6):1215–21.
61. Xue Y, San Luis B, Lane DP. Intratumour heterogeneity of p53 expression; causes and consequences. J Pathol. 2019;249(3):274–85.
62. Evke E, Minbay FZ, Temel SG, Kahveci Z. Immunohistochemical detection of p53 protein in basal cell skin cancer after microwave-assisted antigen retrieval. J Mol Histol. 2009;40(1):13–21.
63. Barrett TL, Smith KJ, Hodge JJ, Butler R, Hall FW, Skelton HG. Immunohistochemical nuclear staining for p53, PCNA, and Ki-67 in different histologic variants of basal cell carcinoma. J Am Acad Dermatol [Internet]. 1997 Sep;37(3):430–7.
64. Hwang LA, Phang BH, Liew OW, Iqbal J, Koh XH, Koh XY, et al. Monoclonal Antibodies against Specific p53 Hotspot Mutants as Potential Tools for Precision Medicine. Cell Rep [Internet]. 2018;22(1):299–312.
65. Gorji H, Shahbazi N, Habibollahi P, Tavangar SM, Firooz A, Ghahremani MH. The glutathione-S-transferase P1 polymorphisms correlates with changes in expression of TP53 tumor suppressor in cutaneous basal cell carcinoma. J Dermatol Sci [Internet]. 2009 Dec;56(3):207–9.
66. Koseoglu RD, Sezer E, Eyibilen A, Aladag I, Etikan I. Expressions of p53, cyclinD1 and histopathological features in basal cell carcinomas. J Cutan Pathol. 2009;36(9):958–65.
67. Stamatelli A, Saetta AA, Bei T, Kavantzas N, Michalopoulos N V., Patsouris E, et al. B-Raf mutations, microsatellite instability and p53 protein expression in sporadic basal cell carcinomas. Pathol Oncol Res. 2011;17(3):633–7.
68. Mateoiu C, Pirici A, Bogdan FL. Immunohistochemical nuclear staining for p53, PCNA, ki-67 and bcl-2 in different histologic variants of basal cell carcinoma. Rom J Morphol Embryol. 2011;52(1):315–9.
69. Karagece Yalçin Ü, SeçkIn S. The expression of p53 and Cox-2 in basal cell carcinoma, squamous cell carcinoma and actinic keratosis cases. Turk Patoloji Dergisi/Turkish J Pathol. 2012;28(2):119–27.
70. Khodaeiani E, Fakhrjou A, Amirnia M, Babaei-Nezhad S, Taghvamanesh F, Razzagh-

Karimi E, et al. Immunohistochemical evaluation of p53 and Ki67 expression in skin epithelial tumors. Indian J Dermatol [Internet]. 2013 May;58(3):181–7.

71. Mercuţ R, Ciurea ME, Mărgăritescu C, Popescu SM, Cràiţoiu MM, Cotoi OS, et al. Expression of p53, D2-40 and α-smooth muscle actin in different histological subtypes of facial basal cell carcinoma. Rom J Morphol Embryol. 2014;55(2):263–72.
72. Esmaeili R, Khorasani MS, Monsef A. Immunohistochemical expression of p53 and Ki-67 in different histopathological variants of basal cell carcinoma. Middle East Journal of Cancer. 2015. 6(1): 29-34.
73. Enache AO, Stepan AE, Mărgăritescu C, Pătraşcu V, Ciurea RN, Simionescu CE, et al. Immunoexpression of p53 and COX-2 in basal cell carcinoma. Rom J Morphol Embryol. 2018;59(4):1115–20.
74. Castanheira A, Vieira MJ, Pinto M, Dias C, Prada L, Macedo S, et al. TERTp mutations and p53 expression in head and neck cutaneous basal cell carcinomas with different aggressive features. Sci Rep [Internet]. 2021;11(1):1–10.
75. Barbareschi M, Girlando S, Cristofolini P, Togni R, Boi S. P53 Protein Expression in Basal Cell Carcinomas. Histopathology. 1992;21(6):579–81.
76. Demirkan NC, Colakoglu N, Düzcan E. Value of p53 protein in biological behavior of basal cell carcinoma and in normal epithelia adjacent to carcinomas. Pathol Oncol Res [Internet]. 2000 Dec;6(4):272–4.
77. Boonchai W, Walsh M, Cummings M, Chenevix-Trench G. Expression of p53 in arsenic-related and sporadic basal cell carcinoma. Arch Dermatol. 2000;136(2):195–8.
78. Ghaderi R, Haghighi F. Immunohistochemistry assessment of P53 protein in basal cell carcinoma. Iran J Allergy, Asthma Immunol. 2005;4(4):167–71.
79. Stratigos AJ, Kapranos N, Petrakou E, Anastasiadou A, Pagouni A, Christofidou E, et al. Immunophenotypic analysis of the p53 gene in non-melanoma skin cancer and correlation with apoptosis and cell proliferation. J Eur Acad Dermatology Venereol. 2005;19(2):180–6.
80. Khalesi M, Waterhouse M, Whiteman DC, Johns R, Rosendahl C, Hackett T, et al. Comparison of PTCH1, COX-2, p53, and Ki-67 protein expression in basal cell carcinomas of nodular and superficial subtypes arising on the head and trunk. Int J Dermatol. 2016;55(10):1096–105.
81. Adamkov M, Halasova E, Rajcani J, Bencat M, Vybohova D, Rybarova S, et al. Relation

between expression pattern of p53 and Survivin in cutaneous basal cell carcinomas. Med Sci Monit. 2011;17(3):3.

82. Ortiz B DM, Masi RM, Knopfelmacher O, Bolla L. Comunicación corta Expresión de p53 , proteína bcl-2 y ki-67 en carcinomas basocelulares . Expression of p53 , bcl-2 protein and Ki67 in basal cell tumours . 2010;(May 2017):47–50.
83. Chen Z, Yang J, Huang Q. Correlation and expression of COX-2 and P53 protein in basal cell carcinoma of eyelid. J Huazhong Univ Sci Technol - Med Sci. 2009;29(3):383–6.
84. De Rosa G, Staibano S, Barra E, Donofrio V, Salvatore G, Vessecchia G, et al. P53 Protein in Aggressive and Non-Aggressive Basal Cell Carcinoma. J Cutan Pathol. 1993;20(5):429–34.
85. Javeed S, Kumar A, Asrar I, Fawad R, Waqar M, Nabi N. Immunohistochemical expression of P53 in basal cell carcinoma of skin. Prof Med J. 2019;26(09):1500–5.
86. Auepemkiate S, Boonyaphiphat P, Thongsuksai P. P53 Expression Related To the Aggressive Infiltrative Histopathological Feature of Basal Cell Carcinoma. Histopathology. 2002;40(6):568–73.
87. Shea CR, McNutt NS, Volkenandt M, Lugo J, Prioleau PG, Albino AP. Overexpression of p53 protein in basal cell carcinomas of human skin. Am J Pathol. 1992;141(1):25–9.
88. Rajabi MA, Rajabi P, Afshar-Moghaddam N. Determination of P53 expression in basal cell carcinoma tissues and adjacent nontumoral epidermis from sun-exposed areas of the head and neck. Arch Iran Med. 2006;9(1):46–8.
89. Oh ST, Stark A, Reichrath J. The p53 signalling pathway in cutaneous basal cell carcinoma: An immunohistochemical description. Acta Derm Venereol. 2020;100(6):1–2.
90. Shamsi Meymandi S, Dabiri S, Zeynadini Meymand A, Iranpour M, Khalili M, Alijani S, et al. Evaluation of immunohistochemical findings and clinical features associated with local aggressiveness in basal cell carcinoma. Iran J Pathol. 2019;14(3):193–6.
91. Huang SW, Chang SH, Mu SW, Jiang HY, Wang ST, Kao JK, et al. Imiquimod activates p53-dependent apoptosis in a human basal cell carcinoma cell line. J Dermatol Sci [Internet]. 2016;81(3):182–91.
92. Wikonkal NM. bcl-2 vs p53 Protein Expression and Apoptotic Rate in Human Nonmelanoma Skin Cancers. Arch Dermatol [Internet]. 1997 May 1;133(5):599.
93. Palaiologou M, Delladetsima I, Tiniakos D. CD138 (syndecan-1) expression in health

and disease. Histol Histopathol. 2014;29(2):177–89.

94. Couchman JR. Syndecan-1 (Cd138), carcinomas and emt. Int J Mol Sci. 2021;22(8).

95. Kind S, Merenkow C, Büscheck F, Möller K, Dum D, Chirico V, et al. Prevalence of Syndecan-1 (CD138) Expression in Different Kinds of Human Tumors and Normal Tissues. Dis Markers. 2019;2019.

96. Bayer-Garner IB, Dilday B, Sanderson RD, Smoller BR. Syndecan-1 Expression Is Decreased With Increasing Aggressiveness of Basal Cell Carcinoma. Am J Dermatopathol [Internet]. 2000;22(2):119–22.

97. Bartos V, Kullov M. Epithelial and Stromal Expression of Syndecan-1 (CD138) in Cutaneous Basal Cell Carcinoma. J Res Med Dent Sci. 2017;5(2):21.

98. Hamilton PW, Bankhead P, Wang Y, Hutchinson R, Kieran D, McArt DG, et al. Digital pathology and image analysis in tissue biomarker research. Methods [Internet]. 2014;70(1):59–73.

99. Rodriguez JPM, Rodriguez R, Silva VWK, Kitamura FC, Corradi GCA, de Marchi ACB, et al. Artificial intelligence as a tool for diagnosis in digital pathology whole slide images: A systematic review. J Pathol Inform [Internet]. 2022;13(September):100138.

100. Bankhead P, Loughrey MB, Fernández JA, Dombrowski Y, McArt DG, Dunne PD, et al. QuPath: Open source software for digital pathology image analysis. Sci Rep. 2017;7(1):1–7.

101. Bankhead, P., Gelbard, M., Inglis, F., & Lamb M. QuPath [Internet]. University of Edinburgh; 2021.

102. Arits AHMM, Schlangen MHJ, Nelemans PJ, Kelleners-Smeets NWJ. Trends in the incidence of basal cell carcinoma by histopathological subtype. J Eur Acad Dermatology Venereol. 2011;25(5):565–9.

103. Raasch BA, Buettner PG, Garbe C. Basal cell carcinoma: Histological classification and body-site distribution. Br J Dermatol. 2006;155(2):401–7.

104. Bartoš V, Kullová M. Basal cell carcinoma of the skin with mixed histomorphology: acomparative study. Cesk Patol. 2016;52(4):222–6.

105. Roozeboom MH, Mosterd K, Winnepenninckx VJL, Nelemans PJ, Kelleners-Smeets NWJ. Agreement between histological subtype on punch biopsy and surgical excision in primary basal cell carcinoma. J Eur Acad Dermatology Venereol. 2013;27(7):894–8.

106. Betti R, Radaelli G, Crosti C, Ghiozzi S, Moneghini L, Menni S. Margin involvement and

clinical pattern of basal cell carcinoma with mixed histology. J Eur Acad Dermatology Venereol. 2012;26(4):483–7.

Annexure 0.1 MMED Research Methods Course Certificate

University of Cape Town

Clinical Research Centre

Certificate of Attendance

Janet De Stadler

MP No: 0783650

has successfully completed the

MMED Research Methods Course

On 11th and 14th June 2021

At

Clinical Research Centre, Groote Schuur Hospital, Observatory

CRC Director: A/Prof Delva Shamley

Date of Issue: 14 June 2021

UCT CLINICAL RESEARCH CENTRE
every step of the study

Annexure 1.1: Studies of BCL-2 immunohistochemical expression in basal cell carcinoma

First Author	Year	Country	Number of cases	Scoring system	Percentage expression	Antibody used for immunohistochemistry	Tissue
Cerroni	1994	Austria	20	None	100	Monoclonal antibody, Dakopatts, Denmark	FFPE
Rodriguez-Villanueva	1995	USA	17	None	100	Monoclonal antibody rabbit-antimouse, DAKO	FFPE
Verhaegh	1995	Netherlands	20	None	100	Monoclonal antibody clone 124, DAKO, Denmark	Frozen and FFPE
Crowson	1996	USA and Canada	30	P + I	93	Monoclonal antibody clone 124, DAKO, Dimension Laboratories, Mississauga, Ontario	FFPE
Chang	1998	Taiwan	10	None	100	Monoclonal antibody clone 124, DAKO, Denmark	FFPE
Wang	2000	Taiwan	53	P	62	DAKO, Glostrup, Denmark	FFPE
Ramdial*	2000	South Africa	75	P	100	Monoclonal antibody clone 124, DAKO, Denmark	FFPE
Cho	2001	Korea	33	P	39	Anti-BCL2 antibody, Santa Cruz Biotechnology, Santa Cruz, California, USA	PE
Bozdogan	2002	Turkey	50	None	68	DAKO-N 1587, prediluted	FFPE
Zagrodnik	2003	Switzerland	60	I	90	Monoclonal antibody, DAKO, Zug, Switzerland	Not stated
Vidal	2004	Spain	30	None	83	Monoclonal antibody clone 124, DAKO, Denmark	FFPE
Abid*	2006	Tunisia	17	None	94.18%**	Monoclonal antibody clone 124, DAKO, Denmark	FFPE
Ionescu	2006	USA	18	P	86	DAKO, Denmark	Not stated
Corrêa	2009	Brasil	15	P	80	Clone D5, Novocastra Laboratories	FFPE
Di Martino Ortiz	2010	Paraguay	20	P	70	DAKO	FFPE
Mateoiu	2011	Romania	21	P + I	"Significant"	Clone D5, DAKO	FFPE
Juba	2013	Romania	14	P + I	86	Monoclonal antibody clone 124	FFPE
Sivrikoz	2015	Turkey	109	P	100	Monoclonal antibody clone 124, DAKO	FFPE
Ramezani	2016	Iran	29	P	100	Monoclonal antibody clone 124, DAKO, N1587	FFPE
Bartoš	2018	Slovakia	45	P + I	93	Monoclonal antibody clone 124, DAKO	Not stated

P = proportion, *I* = intensity, *FFPE* = formalin fixed paraffin embedded, * African countries, ** calculated based on proportion cut-off ≥6%

Annexure 1.2: Scoring applied to BCL-2 immunohistochemical interpretation

First author	Year	Country	Number of cases	Percentage BCL-2 expression	Scoring system
Intensity only					
Zagrodnik	2003	Switzerland	60	90.00	0 No staining + Weak staining ++ Intermediate staining +++ Strong staining
Proportion only					
Wang	2000	Taiwan	53	62.30	Positive staining in whole tumour: Negative: < 5.0 % Positive: + 5.0 – 25 % ++ 25 – 50 % +++ > 50 %
Ramdial	2000	South Africa	75	100.00	Positive staining in whole tumour and division into low (+/ ++) versus high labelling (+++/ ++++) Negative: 0 – 5.0 % Positive: + 6.0 – 25 % ++ 26 – 50 % +++ 51 – 75 % ++++ > 75 %
Cho	2001	Korea	33	39.00	Positive staining in whole tumour: Negative: < 5.0 % Positive: + 5.0 – 25 % ++ 25 – 50 % +++ > 50 %
Ionescu	2006	USA	22	86.36	Positive staining in whole tumour: *25 – 50 % not stated* Negative: 0 % Positive: + < 25 % ++ 50 – 75 % +++ > 75 %

Corrêa	2009	Brazil	15	80.00	Positive staining in whole tumour at 200x magnification: Negative: 0 % Positive: + Few cells positive ++ Many cells positive but < 50 % +++ Few cells negative ++++ All cells positive
Ramezani	2016	Iran	29	100.00	Positive staining in whole tumour: Negative: <5.0 % Positive: + 5.0 – 25 % ++ 26 – 50 % +++ 51 – 75 % ++++ > 75 %
Sivrikoz	2016	Turkey	109	100.00	Count >1000 cells, evaluate the + proportion, divide into low (+/++) versus high (+++/++++) + 0 – 25 % ++ 26 – 50 % +++ 51 – 75 % ++++ >75 %
Di Martino Ortiz	2017	Paraguay	20	70.00	Positive staining in whole tumour and division into low (+/++) versus high positivity (+++/++++) Negative: < 5.0 % Positive: + 6.0 - 25% ++ 26 – 50% +++ 51 – 75% ++++ > 75 %
<u>Proportion and Intensity</u>					
Crowson	1996	USA/ Canada	30	93.33	**Proportion** Negative: 0 % Positive: + 1.0 – 25 % ++ 26 – 50 % +++ 51 – 75 % ++++ 76 – 100 % **Intensity** A) Slight B) Moderate C) Intense

Juba	2013	Romania	14	85.71	**Proportion** Negative: 0 % Positive: + 1.0 – 25 % ++ 25 – 50 % +++ > 50 % **Intensity** Grade 0) No colour Grade 1) Low Grade 2) Moderate Grade 3) Intense **Immunohistochemical index (IHI)** = Proportion x intensity Interpretation: Negative: 0 Low: 1 – 3 Moderate: >3 – 6 High: 9
Bartoš	2018	Slovakia	45	93.40	**Proportion** Negative ≤ 5.0 % Low expression: +/ ++ High expression: +++/ ++++ Positive + 6.0 – 25 % ++ 26 – 50 % +++ 51 – 75 % ++++ ≥ 76 % **Intensity** Weak: majority of tumour cells weaker than stromal lymphocytes Strong: majority of tumour cells stained with same intensity as stromal lymphocytes

Annexure 1.3: Studies evaluating p53 immunohistochemical expression in basal cell carcinoma

Primary author (Year)	City, Country	Sample size	Percentage Expression	Scoring system	P53 primary antibody	Concentration
Barbareschi, 1992	Trento, Italy	27	48.15	Proportion (P) and intensity (I) of nuclear staining scored with a semiquantitative scale. [P: 1 = 10%; 2 = 10-50%; 3 = > 50%/ I: 1 = low; 2 = moderate; 3 = strong]. Value = P X I. Low-score (< 3) = negative/ high-score (> 4) = positive.	Monoclonal PAb 1801 (Oncogene Science, Manhassett, NY. USA)	1:200
					Monoclonal DO7 (Novocastra Laboratories, Newcastle upon Tyne. UK)	1:400
Shea, 1992	New York, USA	36	83.00	Proportion (P) of strong nuclear staining scored with a semiquantitative scale. [P: 0 = < 1 %; + = 1-25%; ++ = 26-50%; +++ = 51-75%; ++++ = 76-100%].	Monoclonal murine PAb 1801	1:25
			58.00		Monoclonal murine PAb 240	1:10
De Rosa, 1993	Naples, Italy	38	52.63	Proportion (P) of nuclear staining scored with a semiquantitative scale. [P: 0 = 0%; + = <40%; ++ = 40–69%; +++ = >70%]. Pattern = focal or diffuse	Polyclonal NCLp53-CMl (YLEM)	1:100
Barrett, 1997	Multiple sites, USA	30	76.66	Proportion < 5%, 5% to 10%, 10% to 20%, 20% to 30%, 30% to 40%, 40% to 50%, > 50%). Quality: diffuse/ intense/ moderate/ peripheral accentuation of / scattered nuclear staining. Intensity = light nuclear staining discounted.	D07 (DAKO)	1:100
Wang, 2000	Taipei, Taiwan	53	64.20	Proportion (P) of tumour mass staining scored with a semiquantitative scale. [P: 0 = < 5%; + = 5–25%; ++ = 25–50%; +++ = > 50%].	DO7; Dako	No information
Demirkan, 2000	Izmir, Turkey	42	42.90	Proportion (P) of nuclear staining scored with a semiquantitative scale. [P: 0 = 0%; + = <10%; ++ = 10–50%; +++ = 50-70%; ++++ >70%].	Monoclonal DO7; Dako	No information
Boonchai, 2000	Brisbane, Australia	213	43.19	Proportion (P) and intensity (I) of nuclear staining scored with a semiquantitative scale [P: + = 0-25%; ++ = 26-50%; +++ = 51-75%; ++++ = 76-100% / I: 0 to 4. 4 = greatest intensity]. Positive = >25%.	Monoclonal mouse D0-7, Dako, Carpinteria, CA	1:100

Cho, 2001	Seoul, Korea	33	27.00	Proportion (P) of nuclear staining scored. Negative: < 5%. Positive (+ to +++): + 5% - 25%/ ++ 25% - 50%/ +++ > 50%	Monoclonal mouse anti-p53 antibody (DAKO, Carpinteria, CA, U.S.A.)	1:50
Auepemkiate, 2002	Songkhla Province, Thailand	158	48.70	Proportion (P) of nuclear staining scored as either positive or negative. [P: Negative = ≤24%; Positive = >24%]. Intensity (I) scored as faint (+), moderate (++) and strong (+++). Strong = darkest brown.	Polyclonal rabbit anti-p53-CM1 (Novocastra Laboratories, Newcastle, UK)	1:700
Zagrodnik, 2003	Zurich, Switzerland	58	15.52	No staining (-), weak (+), intermediate (++), strong (+++)	Mouse p53 antibody (DAKO)	1:2
Ghaderi, 2005	Birjand, Iran	41	68.29	Proportion (P) of nuclear staining scored as either positive or negative. [P: Negative = ≤10%; Positive = >10%].	DO7; Dako	No information
Stratigos, 2005	Athens, Greece	19	54.40	Any proportion of dark nuclear staining interpreted as positive	Monoclonal mouse DO7 (Biogenex, San Ramon, CA, USA)	1:200
Rajabi, 2006	Isfahan, Iran	150	82.00	No information	Mouse	No information
Ionescu, 2006	Pittsburg, USA	18	77.78	Positive or negative - not defined	No information	No information
de Pádua Dornelas Corrêa, 2009	Juiz de Fora, Brasil	Non-English	66.70	Non-English	Monoclonal DO7 (Novocastra Laboratories, Newcastle upon Tyne. UK)	1:100
Chen, 2009	Wuhan, China	40	n/a	Any proportion of brown-yellow cell membrane and cytoplasmic staining interpreted as positive	Polyclonal rabbit Zhongshan Biotechnology Co. Ltd., China.	
Gorji, 2009	Tehran, Iran	61	54.10	Proportion (P) of staining: negative (0) and positive (1–100)	Monoclonal DO-7 (DAKO, Denmark)	No information
Koseoglu, 2009	Tokat, Turkey	50	30.00	Proportion (P) of nuclear staining scored as either positive or negative. [P: Negative = ≤24%; Positive = >24%].	Clone DO7, Biogenex Laboratories, San Ramon, CA, USA	1 : 200
Di Martino Ortiz,	Paraguay	20	35.00	Non-English	Non-English	Non-English

2010						
Stamatelli, 2011	Athens, Greece	83	44.58	Proportion and intensity assessed. Positive = > 10% nuclear staining with moderate to strong intensity. Negative = < 10% proportion OR weakly stained tumour cells	Monoclonal DO-7 (DAKO, Glostrup, Denmark)	No information
Adamkov, 2011	Martin, Slovak Republic	31	90.30	No formal scoring system: assessed proportion, intensity, and subcellular localisation of staining	Monoclonal mouse DAKO, Carpinteria, CA	No information
Mateoiu, 2011	Ramnicu-Valcea, Romania	21	85.71	Proportion (P) of nuclear staining with a semiquantitative scale. Negative <6%. Positive: 6–25% = 1+, 26–50% = 2+, 51–75% = 3+, >75% = 4+. "High" labeling = 3+ or 4+/ "low" = 1 + or 2 + labeling. The intensity = intensity of staining of majority of the + cells. Cells with light nuclear staining were not counted. To be judged as moderately intense staining, the staining had to be clearly more intense than any background staining on the slide with sharp demarcation of the nucleus.	Clone D0-7 (DAKO)	1:100
Karagece Yalçın, 2012	Yozgat, Turkey	50	98.00	Proportion (P) and intensity (I) of nuclear staining scored with a semiquantitative scale. [P: 0 = 0%; + = 1-25%; ++ = 26-50%; +++ 51-75%; ++++ 76-100%/ I: 0 = no staining; 1 = weak staining; 2 = strong staining].	DO7, neomarkers	No information
Juba, 2013	Cluj-Napoca, Romania	14	100.00	Proportion (P) and intensity (I) of nuclear staining scored with a semiquantitative scale. [P: 0 = 0%; 1 = 1-25%; 2 = 25-50%; 3 = >50%/I: 0 = no color; 1 = low; 2 = moderate; 3 = intense]. Immunohistochemical index (IHI) = P X I. Negative (0 points), low (1–3 points), moderate (>3–6 points), high (9 points)	Monoclonal mouse DO-7 (DAKO, Glostrup, Denmark)	1:50
Khodaeiani, 2013	Tabriz, Iran	30	67.77	Score 1 = absent to weak staining; score 2 = <5%; score 3 = 5-50%; score 4 = >50%.	Monoclonal mouse DO7	No information
Mercut, 2014	Craiova, Romania	25	84.00	Proportion (P) and intensity (I) of nuclear staining scored with a semiquantitative scale [P: 0 = 1-10%; 1 = 10-25%; 2 = 25-50%; 3 = 50-75%; 4 = 75-100% / I: 0 =	Monoclonal mouse DO-7 (Dako, Redox, Romania, code M7001)	1:50

				negative; 1 = weak; 2 = moderate; 3 = strong]. Immunoreactive score (IRS) = P X I. Range 0 -12.		
Esmaeili, 2015	Hamadan, Iran	100	76.00	Proportion (P) and intensity (I) of nuclear staining scored with a semiquantitative scale [P: 0 = 0%; 1 = 1-25%; 2 = 26-50%; 3 = 51-75%; 4 = 76-100% / I: 0 = negative; 1 = weak; 2 = strong].	Monoclonal mouse DO7 (Novocastra Laboratories, Newcastle upon Tyne. UK)	No information
Enache, 2018	Craiova, Romania	51	74.50	Proportion (P) and intensity (I) of nuclear staining scored with a semiquantitative scale [P: 0 = <5%; 1 = 6-25%; 2 = 26-50%; 3 = 51-75%; 4 = >75% / I: 0 = negative; 1 = low; 2 = moderate; 3 = high]. Final staining score (FSS) = P X I. 0 (negative), low (1–4) and high (6–12).	DO7 clone, DAKO	1:50
Sungu, 2018	Ankara, Turkey	33	81.82	Proportion (P) of staining with a semiquantitative scale. 0-5% =negative. Positive 1+ to 4+: 6-25%=1+, 26-50%=2+, 51-75%:3+, >75%=4+. Low positive = 1–2+ and high positive = 3-4+	Clone DO7-L-CE	1:100
Javeed, 2019	Islamabad, Pakistan	50	84.00	Proportion (P) of nucelar staining. Score 1: No staining (Negative). Scores 2-4 (Positive) Score 2: 1-4% 3. Score 3: 5-50% 4. Score 4: 51-100	No information	No information
Oh, 2020	Seoul, Korea	10	**	Proportion (P) and intensity (I) of nuclear staining scored with a semiquantitative scale [P: 0 = 0%; 1 = 0-25%; 2 = 25-50%; 3 = 50-75%; 4 = 75-100% / I: 0 = negative; 1 = weak; 2 = moderate; 3 = strong]. Immunoreactive score (IRS) = P X I. Range 0 -12.	Polyclonal SAF (SP 6874, recombinant human wild type, Sigma, Darmstadt, Germany)	1:4000
Castanheira, 2021	Porto, Portugal	157	60.50	Proportion (P) of nuclear staining scored as either positive or negative. [P: Negative = ≤10%; Positive = >10%].	Monoclonal Clone DO-7 NCL-L-p53, Leica	1:550

Annexure 1.4: Major findings in studies evaluating p53 immunohistochemistry in the basal cell carcinoma subtypes

Author, Year	City, Country	Sample size	Interpretation of staining	Tumour selection	Subtypes	Findings	Interpretation
De Rosa, G 1993	Naples, Italy	38	Negative = 0%	Not described	19 non-aggressive (BCC1) 19 aggressive (BCC2) *Aggressive defined as an irregular spiky pattern of invasion by small groups of cells; loss of peripheral palisading, hyalinized fibrous stroma, pleomorphic nuclei with irregularly clumped chromatin, high mitotic index*	17 (89.47%) BCC1 negative for p53 - The 2 cases of BCC1 positive for p53 protein exhibited low positivity 18 (**94.73%) BCC2 positive for p53**, with a focal or diffuse pattern of distribution. - 57.89% BCC2 exhibited high positivity	p53 protein correlated well with a dedifferentiation process in BCC2 BCC1 may have a mutated cellular phenotype, with loss of proliferative control even if the morphological parameters are not yet indicative of dedifferentiation. p53 protein may be indicator of increased aggressiveness
Barrett, T 1997	Multiple sites, USA	30	Only strong nuclear staining counted	Five high-power (x400) fields of the tumour with the highest density of stained nuclei	14 low-risk (7 nodular and 7 superficial) 13 high-risk (5 infiltrative, 4 morphaeic, 4 basosquamous)	The **high-risk BCC showed more intense and higher numbers of positive cells** for p53. The morphaeic & infiltrative BCCs showed peripheral accentuation in most cases; and more diffuse staining in the basosquamous BCC	Almost all BCCs showed increased nuclear immunostaining for p53, except for superficial BCC, in which half the tumours were p53-negative
Demirkan, NC 2000	Izmir, Turkey	42	Negative = 0%	Not described	24 low-risk (non-infiltrative)	P53 positive cases: 44.44% = NIBCC 44.44% = IBCC 11.11% = BSCC	Infiltrative BCC have higher p53 positivity and basosquamous the strongest positivity

					18 high-risk (12 infiltrative and 6 basosquamous) *NIBCC = non-infiltrative BCC* *IBCC = infiltrative BCC* *BSCC = basosquamous*	NIBCC = 33.33% + BSCC = 33% + **IBCC = 66.66% +** Strong (3+) p53: 2 NIBCC (8.33%) 2 IBCC (16.67%) **2 BSCC (33.33%)**	There was no significant correlation between the degree of positivity of p53 protein in all the three groups of BCC (p>0.05)
Boonchai, W 2000	Brisbane, Australia	212	Negative ≤ 25%	Non-English	176 low-risk (Superficial, solid, cystic) 36 high-risk (Infiltrative, metatypical)	**High-risk: 58.33% >25% p53 expression** Low-risk: 40.34% >25% p53 expression	High-risk BCCs have a higher number of positive p53 cells (p 0.4 not significant)
Auepemkiate, S 2002	Songkhla Province, Thailand	158	Negative ≤ 24%	Nuclear staining counted per 1000 tumour cells	107 low-risk (99 nodular and 8 superficial) 45 high-risk (Infiltrative) 6 mixed	P53 positive cases: 58.44% nodular 35.06% infiltrative 2.60% superficial 3.90% mixed Proportion +: Nodular= 45.5% **Infiltrative= 60.0%** Superficial= 25.0% Mixed= 50.0%	An infiltrative growth pattern was independently associated with p53 expression p53 may be a useful tool for prediction of tumour progression
Zagrodnik, B 2003	Zurich, Switzerland	58	Negative = 0%	Tissue microarrays	29 low-risk (17 nodular and 12 superficial) 29 high-risk (morphoeic)	Proportion +: Superficial = 0 Nodular = 0 Morphaeic = 9/29 (weak to strong intensity)	A significant correlation was found between high-risk tumours and p53 expression (p= 0.0049)

Ionescu, D 2006	Pittsburg, USA	18	Not defined	Not described	14 non-metastasizing: - 10 high-risk (5 basosquamous & 5 morphaeic) - 4 low-risk (nodular) 4 metastasizing: - All high-risk (2 mixed with a high risk component, 1 morphaeic, 1 metatypical)	Metastatic: 75% p53 + Non-metastatic: 78.57% p53+ High risk BCC = 70% positive. Low risk BCC = 100% positive	p53 do not distinguish BCCs with metastatic potential and no significant difference was noted between the different subtypes of BCC
Koseoglu, RD 2009	Tokat, Turkey	50	Negative ≤ 24%	Most evenly, heavily labelled areas identified at low-power magnification & image software used to count positive cells/ 1000 tumour cells	33 low-risk (32 nodular and 1 superficial) 17 high-risk (10 infiltrative and 7 mixed with an infiltrative component)	Proportion +: Nodular = 18.8% Infiltrative = 40% Superficial = 0% Mixed = 71.4% P53 positive cases: Nodular 40%, infiltrative 26.67%, mixed 33.33%	There was a significant correlation between p53 expression and histological growth pattern (p = 0.036). Nodular were mostly negative while 40% of infiltrative were positive. We suggest that the infiltrative growth pattern was related to a higher p53 expression
Adamkov, M 2011	Martin, Slovak Republic	31	No formal scoring system	Not described	27 low-risk (6 solid, 9 cystic, 1 pigmented, 10 multicentric, 1 adenoid cystic) 1 high-risk (micronodular) 3 unknown	90% positive: - Only 3/9 cystic cases negative - Others positive: 2 BCC <25% P 26 BCC >25% P	Did not interpret but shows low risk groups do express p53 strong and diffusely Underrepresent high risk groups
Mateoiu, C 2011	Ramnicu-Valcea, Romania	21	Negative = moderate to strong nuclear	Five high-power (×400) fields of the	14 low-risk (7 nodular and 7 superficial)	Proportion + (%): Nodular= 100 Superficial= 57.14	Almost all BCCs showed increased nuclear p53.

			staining in ≤ 5% or a > 5% but with light nuclear staining	tumor with the highest density of stained nuclei were chosen	7 high-risk (morphaeic)	Morphaeic= 100 Morphaeic: diffuse & intense	? p53 mutations less common in superficial BCC or mutation with a decrease in function or genomic area not detected by antibody or null type product production
Karagece Yalçın, U 2012	Yozgat, Turkey	50	Negative < 1%	Not described	33 low-risk (29 nodular, 2 keratotic, 2 superficial) 17 high-risk (10 infiltrative, 5 metatypical, 2 morphaeic	Not supplied	We did not find a statistically significant difference in p53 staining between BCC groups
Juba, BA 2013	Cluj-Napoca, Romania	14	Negative = 0 points on the immunohistochemical index (IHI = P X I)	The entire tumour was assessed at high magnification (400x objective)	7 low-risk (superficial) 2 high-risk (infiltrative) 5 unaccounted for	Superficial BCC = high p53 Deep infiltrating = low to medium expression for p53	P53 positive in all BCC
Mercut, R 2014	Craiova, Romania	25	Cut off not described	Not described	5 low-risk (superficial) 20 high-risk (6 basosquamous, 8 infiltrative- morphaeic, 6 micronodular)	85% high-risk + 80% low-risk + Micronodular: 100%, diffuse & the highest IRS score Morphaeic-infiltrative: 75% & > at invasive front Basosquamous: 83.33% with less p53 in squamous areas. Superficial: 90% & > at invasive front	Variable p53 staining pattern: highest reactivity in the peripheral palisading zone and in the deeper advancing parts Micronodular subtype most reactive Morphaeic least reactive

Khalesi, M 2016	Brisbane, Australia	80	Cut off not described	3 random non-overlapping fields of tumour at 20x objective	80 low-risk (41 nodular and 39 superficial)	Low score: - 75.61% nodular - 58.97% superficial High score: - 24.39% nodular - 41.03% superficial	No significant difference (p = 0.11) Higher proportion of positive cells in the superficial than in the nodular subtype
Enache, AO 2018	Craiova, Romania	51	Negative = 0 on the final staining score (FSS = P X I)	Not described	40 low-risk (nodular) 11 high-risk (infiltrative)	67.5% of nodular positive 100% of infiltrative positive	High percentage of tumour positivity regardless of the histological pattern or the depth of the invasion
Javeed, S 2019	Islamabad, Pakistan	50	Negative = no staining	Not described	32 low-risk (5 nodular and 27 superficial) 18 high-risk (9 infiltrative, 1 morphaeic, 7 basosquamous, 1 micronodular)	Proportion +: Superficial =85% Infiltrative= 78% Basosquamous= 71% Nodular, morphaeic & micronodular = 100%	p53 immunoreactivity both in low-risk and high-risk subtypes with no difference in staining pattern
Castanheira, A 2021	Porto, Portugal	157	Negative ≤10%	Approximately 2000 cells were counted	62 low-risk (56 nodular and 6 superficial) 51 high-risk (morphaeic, micronodular or mixed with high-risk component)	Proportion +: Nodular = 57.14% Infiltrative = 60.78% Superficial = 66.66% Mixed = 63.64%	No associations between p53 overexpression and the clinical and histological features, except for necrosis in which BCC showed significantly more frequent p53 overexpression). Indolent-type or infiltrative–type growth pattern displayed an equivalent frequency of p53 overexpression

Annexure 2.1: HREC Approval 2020

UNIVERSITY OF CAPE TOWN
Faculty of Health Sciences
Human Research Ethics Committee

Room G50- Old Main Building
Groote Schuur Hospital
Observatory 7925
Telephone [021] 406 6492
Email: hrec-enquiries@uct.ac.za
Website: www.health.uct.ac.za/fhs/research/humanethics/forms

15 July 2020

HREC REF: 398/2020

Dr R Roberts
Division of Anatomical Pathology
NHLS
Email: Riyaadh.roberts@uct.ac.za
Student: Rbljan001@myuct.ac.za

Dear Dr Roberts

PROJECT TITLE: AN IMMUNOHISTOCHEMICAL ASSESSMENT OF PROGNOSTIC MARKERS IN BASAL CELL CARCINOMAS -MASTERS CANDIDATE-DR JANET L DE STADLER

Thank you for submitting your study to the Faculty of Health Sciences Human Research Ethics Committee (HREC) for review.

It is a pleasure to inform you that the HREC has **formally approved** the above-mentioned study.

This approval is subject to strict adherence to the HREC recommendations regarding research involving human participants during COVID -19, dated 17 March 2020.

Approval is granted for one year until the 30 July 2021.

Please submit a progress form, using the standardised Annual Report Form if the study continues beyond the approval period. Please submit a Standard Closure form if the study is completed within the approval period.
(Forms can be found on our website: www.health.uct.ac.za/fhs/research/humanethics/forms)

The HREC acknowledge that the student: - Dr Janet de Stadler will also be involved in this study.

Please quote the HREC REF in all your correspondence.

Please note that the ongoing ethical conduct of the study remains the responsibility of the principal investigator.

Please note that for all studies approved by the HREC, the principal investigator **must** obtain appropriate institutional approval, where necessary, before the research may occur.

Yours sincerely

PROFESSOR M BLOCKMAN
CHAIRPERSON, FHS HUMAN RESEARCH ETHICS COMMITTEE

Federal Wide Assurance Number: FWA00001637.
Institutional Review Board (IRB) number: IRB00001938
NHREC-registration number: REC-210208-007

This serves to confirm that the University of Cape Town Human Research Ethics Committee complies to the Ethics Standards for Clinical Research with a new drug in patients, based on the Medical Research Council (MRC-SA), Food and Drug Administration (FDA-USA), International Council for Harmonisation of Technical Requirements for Pharmaceuticals for Human Use: Good Clinical Practice (ICH GCP), South African Good Clinical Practice Guidelines (DoH 2006), based on the Association of the British Pharmaceutical Industry Guidelines (ABPI), and Declaration of Helsinki (2013) guidelines. The Human Research Ethics Committee granting this approval is in compliance with the ICH Harmonised Tripartite Guidelines E6: Note for Guidance on Good Clinical Practice (CPMP/ICH/135/95) and FDA Code Federal Regulation Part 50, 56 and 312.

HREC 398/2020sa

Annexure 2.2 Annual ethics renewal 2021 and 2022

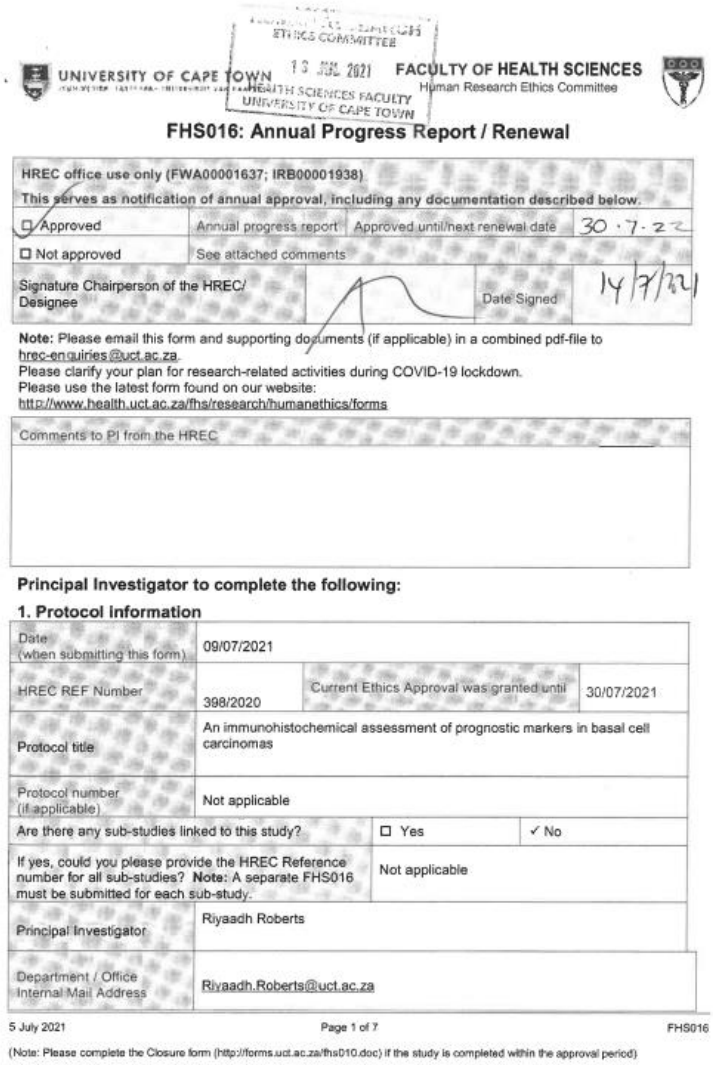

UNIVERSITY OF CAPE TOWN

HUMAN RESEARCH ETHICS COMMITTEE 13 JUL 2021 HEALTH SCIENCES FACULTY UNIVERSITY OF CAPE TOWN

FACULTY OF HEALTH SCIENCES
Human Research Ethics Committee

FHS016: Annual Progress Report / Renewal

HREC office use only (FWA00001637; IRB00001938)			
This serves as notification of annual approval, including any documentation described below.			
☑ Approved	Annual progress report	Approved until/next renewal date	30·7·22
☐ Not approved	See attached comments		
Signature Chairperson of the HREC/ Designee		Date Signed	14/7/2021

Note: Please email this form and supporting documents (if applicable) in a combined pdf-file to hrec-enquiries@uct.ac.za.
Please clarify your plan for research-related activities during COVID-19 lockdown.
Please use the latest form found on our website:
http://www.health.uct.ac.za/fhs/research/humanethics/forms

Comments to PI from the HREC

Principal Investigator to complete the following:

1. Protocol information

Date (when submitting this form)	09/07/2021		
HREC REF Number	398/2020	Current Ethics Approval was granted until	30/07/2021
Protocol title	An immunohistochemical assessment of prognostic markers in basal cell carcinomas		
Protocol number (if applicable)	Not applicable		
Are there any sub-studies linked to this study?	☐ Yes	✓ No	
If yes, could you please provide the HREC Reference number for all sub-studies? **Note:** A separate FHS016 must be submitted for each sub-study.	Not applicable		
Principal Investigator	Riyaadh Roberts		
Department / Office Internal Mail Address	Riyaadh.Roberts@uct.ac.za		

(Note: Please complete the Closure form (http://forms.uct.ac.za/fhs010.doc) if the study is completed within the approval period)

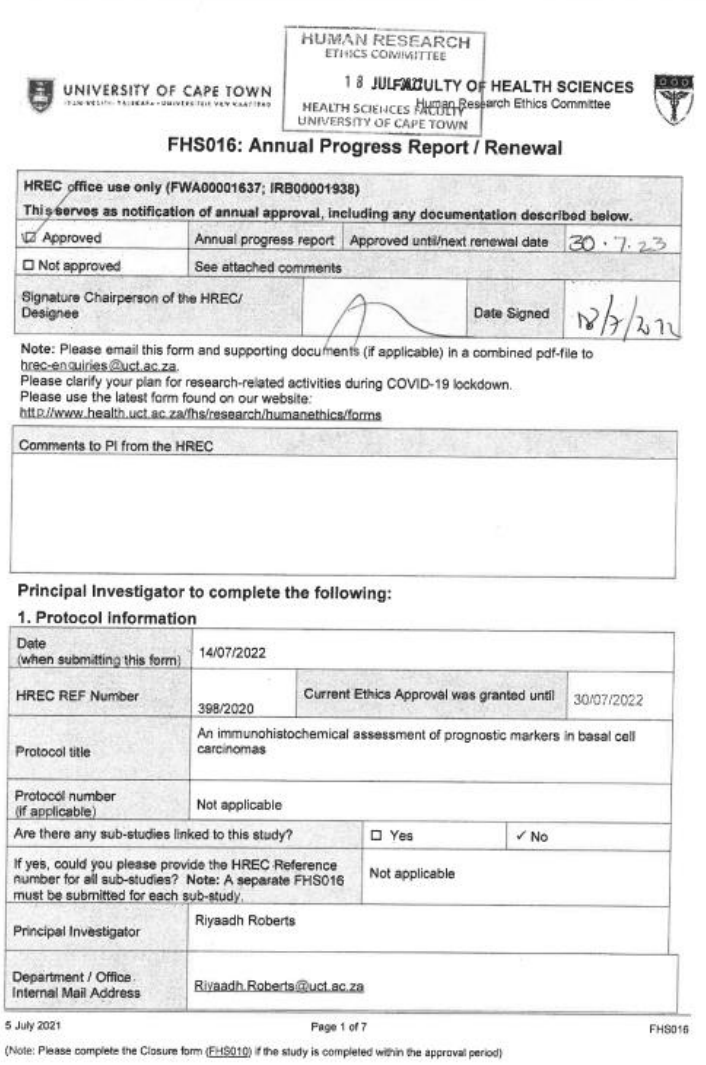

UNIVERSITY OF CAPE TOWN

HUMAN RESEARCH ETHICS COMMITTEE 18 JUL 2022 HEALTH SCIENCES FACULTY UNIVERSITY OF CAPE TOWN

FACULTY OF HEALTH SCIENCES
Human Research Ethics Committee

FHS016: Annual Progress Report / Renewal

HREC office use only (FWA00001637; IRB00001938)			
This serves as notification of annual approval, including any documentation described below.			
☑ Approved	Annual progress report	Approved until/next renewal date	30·7·23
☐ Not approved	See attached comments		
Signature Chairperson of the HREC/ Designee		Date Signed	18/7/2022

Note: Please email this form and supporting documents (if applicable) in a combined pdf-file to hrec-enquiries@uct.ac.za.
Please clarify your plan for research-related activities during COVID-19 lockdown.
Please use the latest form found on our website:
http://www.health.uct.ac.za/fhs/research/humanethics/forms

Comments to PI from the HREC

Principal Investigator to complete the following:

1. Protocol information

Date (when submitting this form)	14/07/2022		
HREC REF Number	398/2020	Current Ethics Approval was granted until	30/07/2022
Protocol title	An immunohistochemical assessment of prognostic markers in basal cell carcinomas		
Protocol number (if applicable)	Not applicable		
Are there any sub-studies linked to this study?	☐ Yes	✓ No	
If yes, could you please provide the HREC Reference number for all sub-studies? **Note:** A separate FHS016 must be submitted for each sub-study.	Not applicable		
Principal Investigator	Riyaadh Roberts		
Department / Office Internal Mail Address	Riyaadh.Roberts@uct.ac.za		

(Note: Please complete the Closure form (FHS010) if the study is completed within the approval period)

Annexure 2.3 Sample size calculations

BCL-2				
Bartoš et al	*Aggressive BCCs show low BCL-2 expression compared to non-aggressive BCCs*			
		BCL2-low	BCL2-high	Total
	Aggressive BCC	9	5	14
	Nonaggressive BCC	4	27	31
	Total	72	37	
	Sample size	46		

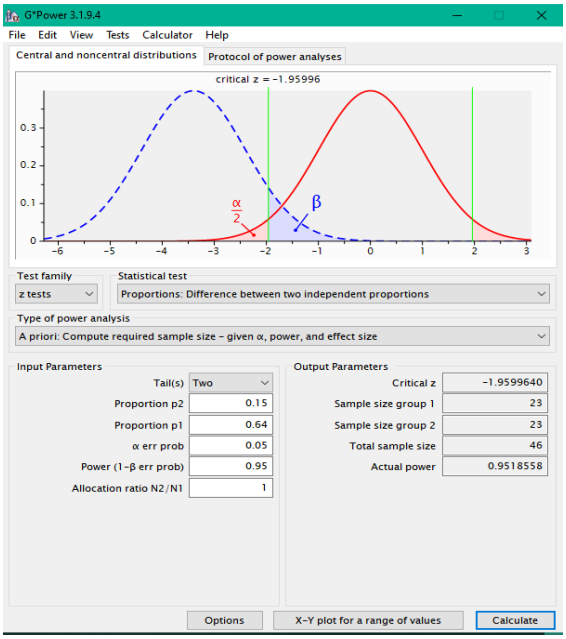

BCL-2 sample size

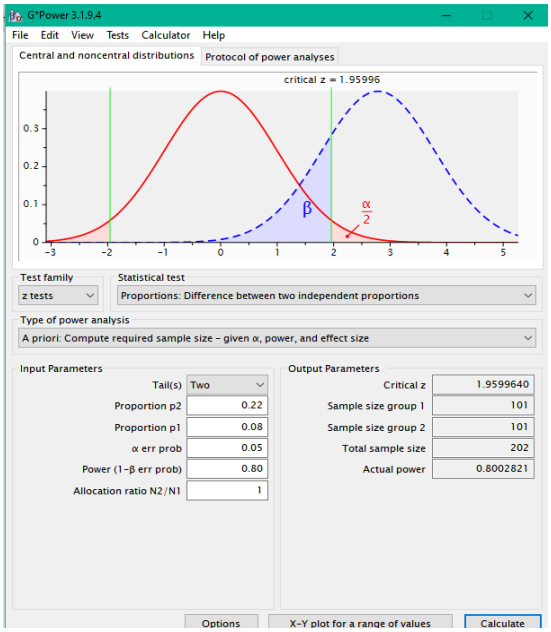

P53 sample size

P53

Demirkan et al	Aggressive BCCs show more diffuse p53 staining than non-aggressive BCCs			
		diffuse p53	non diffuse p53*	Total
	Aggressive BCC**	4	14	18
	Non-aggressive BCC	2	22	24
	Total	6	36	
	Sample size	202	(Dropping power to 80%)	
	Sample size	125	(Dropping power to 70%)	

- CD138

Barto et al	*Aggressive BCCs show an increased in peritumoral CD138 expression*			
	Stroma			
		CD138 pos	CD138 neg	Total
	Aggressive BCC	13	5	18
	Nonaggressive BCC	0	28	28
	Total	13	33	
	Sample size	14		
	Aggressive BCCs show reduced tumoral CD138 expression			
	Tumour cells			
		CD138 preserved	CD138 reduced*	Total
	Aggressive BCC	0	18	18
	Non-aggressive BCC	4	24	28
	Total	4	42	
	Sample size	140		*< 75% strongly stained

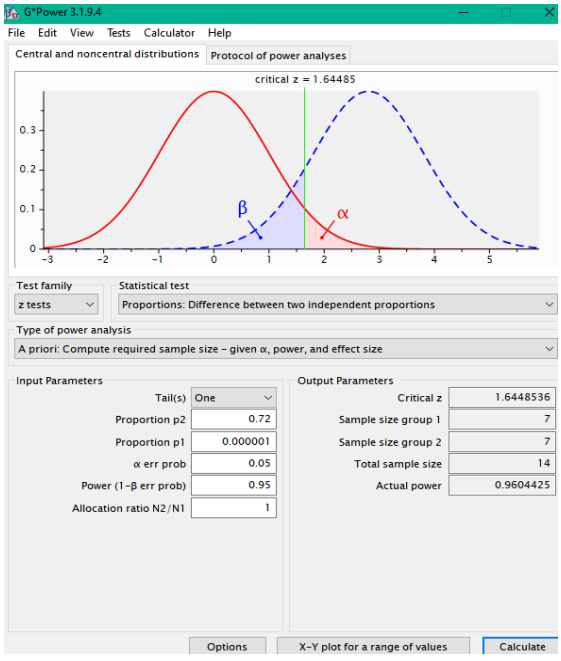

CD138 in stroma sample size

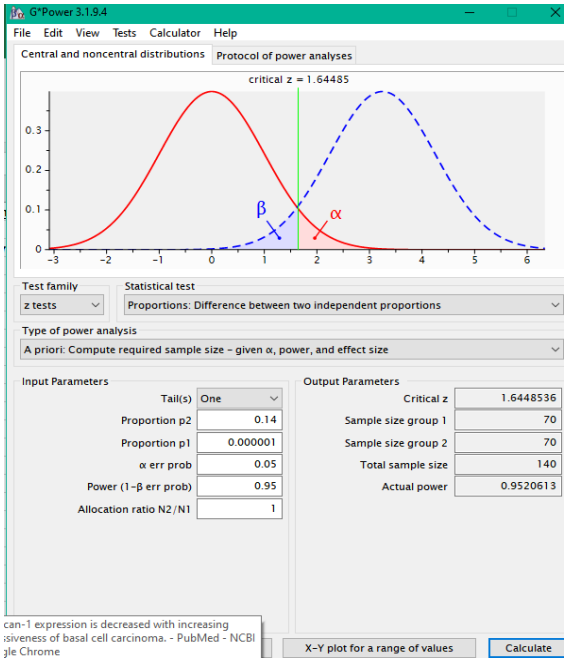

CD138 in tumour sample size

Annexure 2.4 Ventana XT Protocol Summary

Procedure: XT ultraView DAB v3 (v1.00.0000)

BenchMark XT IHC/ ISH

NHLS Histology Laboratory, Groote Schuur Hospital, Cape Town, South Africa

Protocol Number: 119

Version: 1

1. Paraffin
2. Deparaffinisation
3. Cell Conditioning: includes antigen retrieval
4. Conditioner
5. Mild CC1
6. Standard CC1
7. Titration
8. Hand apply primary antibody and incubate for 32 minutes
9. ultraWash
10. Apply haematoxylin counterstain
11. Coverslip

Annexure 2.5 QuPath scripts in groovy scripting language

1. BCL-2 tumour analysis

1 classify BCL2.groovy

```
setColorDeconvolutionStains('{"Name" : "H-DAB default", "Stain 1" : "Hematoxylin", "Values 1" : "0.65111 0.70119 0.29049 ",
"Stain 2" : "DAB", "Values 2" : "0.26917 0.56824 0.77759 ", "Background" : " 255 255 255 "}');
selectAnnotations();
runPlugin('qupath.imagej.detect.cells.PositiveCellDetection', '{"detectionImageBrightfield": "Optical density sum",
"requestedPixelSizeMicrons": 0.0, "backgroundRadiusMicrons": 12.0, "medianRadiusMicrons": 0.0, "sigmaMicrons": 1.5,
"minAreaMicrons": 2.0, "maxAreaMicrons": 400.0, "threshold": 0.1, "maxBackground": 2.0, "watershedPostProcess": true,
"excludeDAB": false, "cellExpansionMicrons": 4.0, "includeNuclei": true, "smoothBoundaries": true, "makeMeasurements":
true, "thresholdCompartment": "Cell: DAB OD mean", "thresholdPositive1": 0.19, "thresholdPositive2": 0.8,
"thresholdPositive3": 1.9, "singleThreshold": false}');
```

2 update image metadata for export.groovy

```
/**
* Update the image name in the ImageServer metadata to match with the image name in the project.
*
* This can be used (with caution!) to work around the fact that v0.2.x uses the name from the server
* in measurement tables when they are export - not the project.
*
* Using 'Run -> Run for project' to apply it to all images in a project.
* Best back up (as always) before doing anything that will change data files, but an additional
* safeguard here is that the original metadata can still be accessed via server.getOriginalMetadata(),
* and can be reset by double-clicking the 'Metadata changed' entry under the 'Image' tab.
*
* This behavior of the measurement export may change in future versions (it probably should).
*
* @author Pete Bankhead
*/

def name = getProjectEntry().getImageName()
def imageData = getCurrentImageData()
def server = getCurrentServer()
def metadata = server.getMetadata()
if (metadata.getName() == name) {
   println 'Name already correct for ' + name
   return
}
println 'Updating name from ' + metadata.getName() + ' to ' + name
def metadata2 = new qupath.lib.images.servers.ImageServerMetadata.Builder(metadata).name(name).build()
imageData.updateServerMetadata(metadata2)
```

3 export rendered image.groovy

```
/**
* Script to export a rendered (RGB) image in QuPath v0.2.0.
* @author Pete Bankhead
*/

import qupath.imagej.tools.IJTools
```

```
import qupath.lib.gui.images.servers.RenderedImageServer
import qupath.lib.gui.viewer.overlays.HierarchyOverlay
import qupath.lib.regions.RegionRequest

import static qupath.lib.gui.scripting.QPEx.*

// It is important to define the downsample!
// This is required to determine annotation line thicknesses
double downsample = 6.0

// Add the output file path here
String path = buildFilePath(PROJECT_BASE_DIR, 'bcl2-rendered', getProjectEntry().getImageName() + '.jpg')

// Request the current viewer for settings, and current image (which may be used in batch processing)
def viewer = getCurrentViewer()
def imageData = getCurrentImageData()

// Create a rendered server that includes a hierarchy overlay using the current display settings
def server = new RenderedImageServer.Builder(imageData)
  .downsamples(downsample)
  .layers(new HierarchyOverlay(viewer.getImageRegionStore(), viewer.getOverlayOptions(), imageData))
  .build()

// Write or display the rendered image
if (path != null) {
  mkdirs(new File(path).getParent())
  writeImage(server, path)
} else
  IJTools.convertToImagePlus(server, RegionRequest.createInstance(server)).getImage().show()
```

2. P53 tumour analysis

1 classify P53.groovy

```
setColorDeconvolutionStains('{"Name" : "H-DAB default", "Stain 1" : "Hematoxylin", "Values 1" : "0.65111 0.70119 0.29049 ",
"Stain 2" : "DAB", "Values 2" : "0.26917 0.56824 0.77759 ", "Background" : " 255 255 255 "}');
selectAnnotations();
runPlugin('qupath.imagej.detect.cells.PositiveCellDetection', '{"detectionImageBrightfield": "Optical density sum",
"requestedPixelSizeMicrons": 0.5,  "backgroundRadiusMicrons": 12.0,  "medianRadiusMicrons": 0.0,  "sigmaMicrons": 1.5,
"minAreaMicrons": 2.0,  "maxAreaMicrons": 400.0,  "threshold": 0.1,  "maxBackground": 2.0,  "watershedPostProcess": true,
"excludeDAB": false,  "cellExpansionMicrons": 4.0,  "includeNuclei": true,  "smoothBoundaries": true,  "makeMeasurements":
true,  "thresholdCompartment": "Nucleus: DAB OD mean",  "thresholdPositive1": 0.19,  "thresholdPositive2": 0.8,
"thresholdPositive3": 1.9,  "singleThreshold": false}');
```

2 update image metadata for export.groovy

```
/**
* Update the image name in the ImageServer metadata to match with the image name in the project.
*
* This can be used (with caution!) to work around the fact that v0.2.x uses the name from the server
* in measurement tables when they are export - not the project.
*
* @author Pete Bankhead
*/

def name = getProjectEntry().getImageName()
```

```
def imageData = getCurrentImageData()
def server = getCurrentServer()
def metadata = server.getMetadata()
if (metadata.getName() == name) {
   println 'Name already correct for ' + name
   return
}
println 'Updating name from ' + metadata.getName() + ' to ' + name
def metadata2 = new qupath.lib.images.servers.ImageServerMetadata.Builder(metadata).name(name).build()
imageData.updateServerMetadata(metadata2)
```

3 export rendered image.groovy

```
/**
* Script to export a rendered (RGB) image in QuPath v0.2.0.
* @author Pete Bankhead
*/

import qupath.imagej.tools.IJTools
import qupath.lib.gui.images.servers.RenderedImageServer
import qupath.lib.gui.viewer.overlays.HierarchyOverlay
import qupath.lib.regions.RegionRequest

import static qupath.lib.gui.scripting.QPEx.*

// It is important to define the downsample!
// This is required to determine annotation line thicknesses
double downsample = 6.0

// Add the output file path here
String path = buildFilePath(PROJECT_BASE_DIR, 'p53-rendered', getProjectEntry().getImageName() + '.jpg')

// Request the current viewer for settings, and current image (which may be used in batch processing)
def viewer = getCurrentViewer()
def imageData = getCurrentImageData()

// Create a rendered server that includes a hierarchy overlay using the current display settings
def server = new RenderedImageServer.Builder(imageData)
   .downsamples(downsample)
   .layers(new HierarchyOverlay(viewer.getImageRegionStore(), viewer.getOverlayOptions(), imageData))
   .build()

// Write or display the rendered image
if (path != null) {
   mkdirs(new File(path).getParent())
   writeImage(server, path)
} else
   IJTools.convertToImagePlus(server, RegionRequest.createInstance(server)).getImage().show()
```

3. CD138 tumour analysis

1 update image metadata for export.groovy

```
/**
* Update the image name in the ImageServer metadata to match with the image name in the project.
*
* This can be used (with caution!) to work around the fact that v0.2.x uses the name from the server
* in measurement tables when they are export - not the project.
*
* @author Pete Bankhead
*/


def name = getProjectEntry().getImageName()
def imageData = getCurrentImageData()
```

```
def server = getCurrentServer()
def metadata = server.getMetadata()
if (metadata.getName() == name) {
   println 'Name already correct for ' + name
   return
}
println 'Updating name from ' + metadata.getName() + ' to ' + name
def metadata2 = new qupath.lib.images.servers.ImageServerMetadata.Builder(metadata).name(name).build()
imageData.updateServerMetadata(metadata2)
```

2 remove all objects.groovy

```
toRemove = getAnnotationObjects().findAll()
removeObjects(toRemove, true)
```

3 positive cell detection CD138.groovy

```
setColorDeconvolutionStains('{"Name" : "H-DAB default", "Stain 1" : "Hematoxylin", "Values 1" : "0.65111 0.70119 0.29049 ",
"Stain 2" : "DAB", "Values 2" : "0.26917 0.56824 0.77759 ", "Background" : " 255 255 255 "}');
selectAnnotations();
runPlugin('qupath.imagej.detect.cells.PositiveCellDetection', '{"detectionImageBrightfield": "Hematoxylin OD",
"requestedPixelSizeMicrons": 0.5,  "backgroundRadiusMicrons": 8.0,  "medianRadiusMicrons": 3.0,  "sigmaMicrons": 1.5,
"minAreaMicrons": 2.0,  "maxAreaMicrons": 400.0,  "threshold": 0.01,  "maxBackground": 2.0,  "watershedPostProcess": true,
"excludeDAB": false,  "cellExpansionMicrons": 4.0,  "includeNuclei": true,  "smoothBoundaries": true,  "makeMeasurements":
true,  "thresholdCompartment": "Cytoplasm: DAB OD mean",  "thresholdPositive1": 0.19,  "thresholdPositive2": 0.8,
"thresholdPositive3": 1.9,  "singleThreshold": false}');
```

4 remove specific annotations.groovy

```
//Clean up bad objects
removal = getAnnotationObjects().findAll{it.getPathClass().toString().contains("+1")}
removeObjects(removal, true)
```

5 render region high-res annotation.groovy

```
//M6... may not work in most versions, but the expansions idea should be similar
//https://forum.image.sc/t/enlarging-images-around-relevant-masks-during-export/34220/8?u=research_associate
//@Pietro_Cicalese
/**
* Script to export binary masks corresponding to all annotations of an image,
* optionally along with extracted image regions.
*
* Note: Pay attention to the 'downsample' value to control the export             resolution!
*
* @author Pete Bankhead
*/

import qupath.lib.images.servers.ImageServer
import qupath.lib.objects.PathObject

import javax.imageio.ImageIO
import java.awt.Color
import java.awt.image.BufferedImage
```

```
// Get the main QuPath data structures
def imageData = getCurrentImageData()
def hierarchy = imageData.getHierarchy()
def server = imageData.getServer()

// Request all objects from the hierarchy & filter only the annotations
def annotations = hierarchy.getAnnotationObjects()

// Define downsample value for export resolution & output directory, creating directory if necessary
// The pad variable will add padding to both the image and mask output images (# of pixels)
def downsample = 2.0
pad = 75
def pathOutput = buildFilePath(QPEx.PROJECT_BASE_DIR, 'CD138-tumour-rendered-images')
mkdirs(pathOutput)

// Define image export type; valid values are JPG, PNG or null (if no image region should be exported with the mask)
// Note: masks will always be exported as PNG
def imageExportType = 'JPG'

// Export each annotation
annotations.each {
   saveImageAndMask(pathOutput, server, it, downsample, imageExportType)
}
print 'Done!'

/**
* Save extracted image region & mask corresponding to an object ROI.
*
* @param pathOutput Directory in which to store the output
* @param server ImageServer for the relevant image
* @param pathObject The object to export
* @param downsample Downsample value for the export of both image region & mask
* @param imageExportType Type of image (original pixels, not mask!) to export ('JPG', 'PNG' or null)
* @return
*/
def saveImageAndMask(String pathOutput, ImageServer server, PathObject pathObject, double downsample, String
imageExportType) {
   // Extract ROI & classification name
   def roi = pathObject.getROI()
   def pathClass = pathObject.getPathClass()
   def classificationName = pathClass == null ? 'None' : pathClass.toString()
   if (roi == null) {
      print 'Warning! No ROI for object ' + pathObject + ' - cannot export corresponding region & mask'
      return
   }
```

```
  // Create a region from the ROI
  def region = RegionRequest.createInstance(server.getPath(), downsample, (int)roi.getBoundsX()-pad, (int)roi.getBoundsY()-
pad, (int)roi.getBoundsWidth() + pad*2, (int)roi.getBoundsHeight() + pad*2, roi.getZ(), roi.getT())

  // Create a name
  String name = String.format('%s_%s',
        server.getMetadata().getName(),
        classificationName,
        region.getDownsample(),
        region.getX(),
        region.getY(),
        region.getWidth(),
        region.getHeight()
  )
  float thickness = 4
   // Request the BufferedImage
  def img = server.readBufferedImage(region)

  // Create a mask using Java2D functionality
  // (This involves applying a transform to a graphics object, so that none needs to be applied to the ROI coordinates)
  def shape = RoiTools.getShape(roi)
  def imgMask = new BufferedImage(img.getWidth(), img.getHeight(), BufferedImage.TYPE_BYTE_GRAY)
  def g2d = img.createGraphics()
  g2d.setColor(java.awt.Color.YELLOW)
  g2d.setStroke(new java.awt.BasicStroke((float)(thickness * downsample)))
  getAnnotationObjects().each { g2d.draw(it.getROI().getShape()) }
  g2d.scale(1.0/downsample, 1.0/downsample)
  g2d.translate(-region.getX(), -region.getY())
  //g2d.fill(shape)
  g2d.draw(shape)
  g2d.dispose()
  // Create filename & export
  if (imageExportType != null) {
     def fileImage = new File(pathOutput, name + '_outlines' + '.' + imageExportType.toLowerCase())
     ImageIO.write(img, imageExportType, fileImage)
  }
}
```

6 set annotation to be Tumour class.groovy

```
def tumor = getPathClass('Tumor')
getAnnotationObjects().eachWithIndex { annotation , i ->
    annotation.setPathClass(tumor)
}
fireHierarchyUpdate()
```

7 render region high-res detections.groovy

```
import qupath.imagej.tools.IJTools
import qupath.lib.gui.images.servers.RenderedImageServer
import qupath.lib.gui.viewer.overlays.HierarchyOverlay
```

```
import qupath.lib.regions.RegionRequest

import static qupath.lib.gui.scripting.QPEx.*

// It is important to define the downsample!
// This is required to determine annotation line thicknesses
double downsample = 3

// Add the output file path here
String path = buildFilePath(PROJECT_BASE_DIR, 'CD138-tumour-rendered-images', getProjectEntry().getImageName() +
'_detections' + '.jpg')

// Request the current viewer for settings, and current image (which may be used in batch processing)
def viewer = getCurrentViewer()
def imageData = getCurrentImageData()

//This code block will use individual viewer settings for each image
//- meaning you could turn off some channels in different images and the export would pick up on that
//Comment this block out and use the block below to use current viewer settings for all images
//////////////////////////////////////////////////////
def display = new qupath.lib.display.ImageDisplay(imageData)
// Create a rendered server that includes a hierarchy overlay using the current display settings
def server = new RenderedImageServer.Builder(imageData)
  .display(display)
  .downsamples(downsample)
  .layers(new HierarchyOverlay(viewer.getImageRegionStore(), viewer.getOverlayOptions(), imageData))
  .build()
//////////////////////////////////////////////////////

// Comment out the above code and use this code to use the SAME viewer settings as the current viewer
/************************************************
// Create a rendered server that includes a hierarchy overlay using the current display settings
def server = new RenderedImageServer.Builder(imageData)
  .downsamples(downsample)
  .layers(new HierarchyOverlay(viewer.getImageRegionStore(), viewer.getOverlayOptions(), imageData))
  .build()
************************************************/
// Write or display the rendered image
if (path != null) {
  mkdirs(new File(path).getParent())
  writeImage(server, path)
} else
  IJTools.convertToImagePlus(server, RegionRequest.createInstance(server)).getImage().show()
```

4. CD138 stroma analysis +1

1 update image metadata for export.groovy

```
/**
* Update the image name in the ImageServer metadata to match with the image name in the project.
```

```
*
* This can be used (with caution!) to work around the fact that v0.2.x uses the name from the server
* in measurement tables when they are export - not the project.
*
* @author Pete Bankhead
*/

def name = getProjectEntry().getImageName()
def imageData = getCurrentImageData()
def server = getCurrentServer()
def metadata = server.getMetadata()
if (metadata.getName() == name) {
   println 'Name already correct for ' + name
   return
}
println 'Updating name from ' + metadata.getName() + ' to ' + name
def metadata2 = new qupath.lib.images.servers.ImageServerMetadata.Builder(metadata).name(name).build()
imageData.updateServerMetadata(metadata2)
```

2 export rendered image.groovy

```
/**
* Script to export a rendered (RGB) image in QuPath v0.2.0.
* @author Pete Bankhead
*/

import qupath.imagej.tools.IJTools
import qupath.lib.gui.images.servers.RenderedImageServer
import qupath.lib.gui.viewer.overlays.HierarchyOverlay
import qupath.lib.regions.RegionRequest

import static qupath.lib.gui.scripting.QPEx.*

// It is important to define the downsample!
// This is required to determine annotation line thicknesses
double downsample = 6.0

// Add the output file path here
String path = buildFilePath(PROJECT_BASE_DIR, 'cd138-stroma-rendered', getProjectEntry().getImageName() + '.jpg')

// Request the current viewer for settings, and current image (which may be used in batch processing)
def viewer = getCurrentViewer()
def imageData = getCurrentImageData()

// Create a rendered server that includes a hierarchy overlay using the current display settings
def server = new RenderedImageServer.Builder(imageData)
   .downsamples(downsample)
   .layers(new HierarchyOverlay(viewer.getImageRegionStore(), viewer.getOverlayOptions(), imageData))
   .build()
```

```
// Write or display the rendered image
if (path != null) {
   mkdirs(new File(path).getParent())
   writeImage(server, path)
} else
   IJTools.convertToImagePlus(server, RegionRequest.createInstance(server)).getImage().show()
```

3 classify-intensity+1.groovy

```
setImageType('BRIGHTFIELD_H_DAB');
selectAnnotations();
createAnnotationsFromPixelClassifier("+1", 1.0, 1.0)
```

4 export rendered image and masks.groovy

```
/**
* Script to export a rendered (RGB) image in QuPath v0.2.0.
* @author Pete Bankhead
*/

/* Adapted by Jurgen */

import qupath.imagej.tools.IJTools
import qupath.lib.gui.images.servers.RenderedImageServer
import qupath.lib.gui.viewer.overlays.HierarchyOverlay
import qupath.lib.regions.RegionRequest

import static qupath.lib.gui.scripting.QPEx.*

// It is important to define the downsample!
// This is required to determine annotation line thicknesses
double downsample = 3.0

// Add the output file path here
String path = buildFilePath(PROJECT_BASE_DIR, 'cd138-stroma-positive-proportion-rendered', getProjectEntry().getImageName()
)

// Request the current viewer for settings, and current image (which may be used in batch processing)
def viewer = getCurrentViewer()
def imageData = getCurrentImageData()

// Create a rendered server that includes a hierarchy overlay using the current display settings
def server = new RenderedImageServer.Builder(imageData)
   .downsamples(downsample)
   .layers(new HierarchyOverlay(viewer.getImageRegionStore(), viewer.getOverlayOptions(), imageData))
   .build()

def annotationLabelServer = new LabeledImageServer.Builder(imageData)
   .backgroundLabel(0, ColorTools.WHITE) // Specify background label (usually 0 or 255)
   .addUnclassifiedLabel(2, ColorTools.YELLOW) // Specify unclassified annotations
```

```
    .addLabel('+1',1) //Each class requires a name and a number
    .downsample(downsample)    // Choose server resolution; this should match the resolution at which tiles are exported
    .multichannelOutput(false) // If true, each label refers to the channel of a multichannel binary image (required for multiclass probability)
    .build()

// Write or display the rendered image
if (path != null) {
    mkdirs(new File(path).getParent())
    writeImage(server, path + ".jpg")
    writeImage(annotationLabelServer, path + "-positive-stroma-area.png")
} else
    IJTools.convertToImagePlus(server, RegionRequest.createInstance(server)).getImage().show()
```

5. CD138 stroma analysis +2

1 update image metadata for export.groovy

```
/**
* Update the image name in the ImageServer metadata to match with the image name in the project.
*
* This can be used (with caution!) to work around the fact that v0.2.x uses the name from the server
* in measurement tables when they are export - not the project.
*
* @author Pete Bankhead
*/

def name = getProjectEntry().getImageName()
def imageData = getCurrentImageData()
def server = getCurrentServer()
def metadata = server.getMetadata()
if (metadata.getName() == name) {
    println 'Name already correct for ' + name
    return
}
println 'Updating name from ' + metadata.getName() + ' to ' + name
def metadata2 = new qupath.lib.images.servers.ImageServerMetadata.Builder(metadata).name(name).build()
imageData.updateServerMetadata(metadata2)
```

2 export rendered image.groovy

```
/**
* Script to export a rendered (RGB) image in QuPath v0.2.0.
*
* This is much easier if the image is currently open in the viewer,
* then see https://qupath.readthedocs.io/en/latest/docs/advanced/exporting_images.html
*
* The purpose of this script is to support batch processing (Run -> Run for project (without save)),
* while using the current viewer settings.
*
* Note: This was written for v0.2.0 only. The process may change in later versions.
```

```
*
* @author Pete Bankhead
*/

import qupath.imagej.tools.IJTools
import qupath.lib.gui.images.servers.RenderedImageServer
import qupath.lib.gui.viewer.overlays.HierarchyOverlay
import qupath.lib.regions.RegionRequest

import static qupath.lib.gui.scripting.QPEx.*

// It is important to define the downsample!
// This is required to determine annotation line thicknesses
double downsample = 6.0

// Add the output file path here
String path = buildFilePath(PROJECT_BASE_DIR, 'cd138-stroma-rendered', getProjectEntry().getImageName() + '.jpg')

// Request the current viewer for settings, and current image (which may be used in batch processing)
def viewer = getCurrentViewer()
def imageData = getCurrentImageData()

// Create a rendered server that includes a hierarchy overlay using the current display settings
def server = new RenderedImageServer.Builder(imageData)
  .downsamples(downsample)
  .layers(new HierarchyOverlay(viewer.getImageRegionStore(), viewer.getOverlayOptions(), imageData))
  .build()

// Write or display the rendered image
if (path != null) {
  mkdirs(new File(path).getParent())
  writeImage(server, path)
} else
  IJTools.convertToImagePlus(server, RegionRequest.createInstance(server)).getImage().show()
```

3 classify-intensity+2.groovy

```
setImageType('BRIGHTFIELD_H_DAB');
selectAnnotations();
createAnnotationsFromPixelClassifier("+2", 1.0, 1.0)
```

6. CD138 stroma analysis +3

1 update image metadata for export.groovy

```
/**
* Update the image name in the ImageServer metadata to match with the image name in the project.
*
* @author Pete Bankhead
*/

def name = getProjectEntry().getImageName()
```

```
def imageData = getCurrentImageData()
def server = getCurrentServer()
def metadata = server.getMetadata()
if (metadata.getName() == name) {
   println 'Name already correct for ' + name
   return
}
println 'Updating name from ' + metadata.getName() + ' to ' + name
def metadata2 = new qupath.lib.images.servers.ImageServerMetadata.Builder(metadata).name(name).build()
imageData.updateServerMetadata(metadata2)
```

2 export rendered image.groovy

```
/**
* Script to export a rendered (RGB) image in QuPath v0.2.0.
* @author Pete Bankhead
*/

import qupath.imagej.tools.IJTools
import qupath.lib.gui.images.servers.RenderedImageServer
import qupath.lib.gui.viewer.overlays.HierarchyOverlay
import qupath.lib.regions.RegionRequest
import qupath.lib.gui.viewer.OverlayOptions.DetectionDisplayMode
import static qupath.lib.gui.scripting.QPEx.*

// It is important to define the downsample!
// This is required to determine annotation line thicknesses
double downsample = 3.0

// Add the output file path here
String path = buildFilePath(PROJECT_BASE_DIR, 'CD138-stroma-proportion-stained-above+1', getProjectEntry().getImageName()
+'-overview.jpg')

// Request the current viewer for settings, and current image (which may be used in batch processing)
def viewer = getCurrentViewer()

def imageData = getCurrentImageData()

// Create a rendered server that includes a hierarchy overlay using the current display settings
def server = new RenderedImageServer.Builder(imageData)
   .downsamples(downsample)
   .layers(new HierarchyOverlay(viewer.getImageRegionStore(), viewer.getOverlayOptions(), imageData))
   .build()

// Write or display the rendered image
if (path != null) {
   mkdirs(new File(path).getParent())
   writeImage(server, path)
} else
```

```
IJTools.convertToImagePlus(server, RegionRequest.createInstance(server)).getImage().show()
```

3 classify-intensity+3.groovy

```
setImageType('BRIGHTFIELD_H_DAB');
selectAnnotations();
createAnnotationsFromPixelClassifier("+3", 1.0, 1.0)
```

7. CD138 stroma analysis classifying DAB intensity using OD

1 update image metadata for export.groovy

```
/**
* Update the image name in the ImageServer metadata to match with the image name in the project.
*
* @author Pete Bankhead
*/

def name = getProjectEntry().getImageName()
def imageData = getCurrentImageData()
def server = getCurrentServer()
def metadata = server.getMetadata()
if (metadata.getName() == name) {
  println 'Name already correct for ' + name
  return
}
println 'Updating name from ' + metadata.getName() + ' to ' + name
def metadata2 = new qupath.lib.images.servers.ImageServerMetadata.Builder(metadata).name(name).build()
imageData.updateServerMetadata(metadata2)
```

2 classify-intensity+1.groovy

```
setImageType('BRIGHTFIELD_H_DAB');
selectAnnotations();
createAnnotationsFromPixelClassifier("+1", 1.0, 1.0)
```

3 export rendered image.groovy

```
/**
* Script to export a rendered (RGB) image in QuPath v0.2.0.
* @author Pete Bankhead
*/

import qupath.imagej.tools.IJTools
import qupath.lib.gui.images.servers.RenderedImageServer
import qupath.lib.gui.viewer.overlays.HierarchyOverlay
import qupath.lib.regions.RegionRequest

import static qupath.lib.gui.scripting.QPEx.*

// It is important to define the downsample!
// This is required to determine annotation line thicknesses
double downsample = 7.0

// Add the output file path here
String path = buildFilePath(PROJECT_BASE_DIR, 'rendered-CD138-stroma-proportion-stained-above+1',
getProjectEntry().getImageName() + '.jpg')

// Request the current viewer for settings, and current image (which may be used in batch processing)
def viewer = getCurrentViewer()
def imageData = getCurrentImageData()

// Create a rendered server that includes a hierarchy overlay using the current display settings
def server = new RenderedImageServer.Builder(imageData)
  .downsamples(downsample)
  .layers(new HierarchyOverlay(viewer.getImageRegionStore(), viewer.getOverlayOptions(), imageData))
  .build()
```

```
// Write or display the rendered image
if (path != null) {
   mkdirs(new File(path).getParent())
   writeImage(server, path)
} else
   IJTools.convertToImagePlus(server, RegionRequest.createInstance(server)).getImage().show()
```

4 classify DAB intensity using OD.groovy

```
setColorDeconvolutionStains('{"Name" : "H-DAB default", "Stain 1" : "Hematoxylin", "Values 1" : "0.65111 0.70119 0.29049 ",
"Stain 2" : "DAB", "Values 2" : "0.26917 0.56824 0.77759 ", "Background" : " 255 255 255 "}');
selectAnnotations();
runPlugin('qupath.lib.algorithms.IntensityFeaturesPlugin', '{"pixelSizeMicrons": 0.345,  "region": "ROI",  "tileSizeMicrons": 25.0,
"colorOD": false,  "colorStain1": false,  "colorStain2": true,  "colorStain3": false,  "colorRed": true,  "colorGreen": false,
"colorBlue": false,  "colorHue": false,  "colorSaturation": false,  "colorBrightness": false,  "doMean": true,  "doStdDev": true,
"doMinMax": true,  "doMedian": true,  "doHaralick": false,  "haralickDistance": 1,  "haralickBins": 32}');
```

5 export rendered annotations.groovy

```
import qupath.lib.images.servers.LabeledImageServer
import qupath.lib.gui.images.servers.RenderedImageServer

// 1 is full resolution. You may want something more like 20 or higher for small thumbnails
downsample = 3
//remove the findAll to get all annotations, or change the null to getPathClass("Tumor") to only export Tumor annotations
annotations = getAnnotationObjects().findAll{it.getPathClass() == null}

def imageName = GeneralTools.getNameWithoutExtension(getCurrentImageData().getServer().getMetadata().getName())
def imageData = getCurrentImageData()
//Make sure the location you want to save the files to exists - requires a Project
//def pathOutput = buildFilePath(PROJECT_BASE_DIR, 'rendered-image-export')
//mkdirs(pathOutput)

def annotationLabelServer = new LabeledImageServer.Builder(imageData)
   .backgroundLabel(0, ColorTools.WHITE) // Specify background label (usually 0 or 255)
   .addLabel('+1',1) //Each class requires a name and a number
   .downsample(downsample)    // Choose server resolution; this should match the resolution at which tiles are exported
   .multichannelOutput(false) // If true, each label refers to the channel of a multichannel binary image (required for multiclass
probability)
   .build()


annotations.eachWithIndex{anno,x->
   roi = anno.getROI()
   def requestROI = RegionRequest.createInstance(getCurrentServer().getPath(), 1, roi)

   pathOutput = buildFilePath(PROJECT_BASE_DIR, 'rendered-CD138-stroma-proportion-stained-above+1', imageName)

   //Labeled images, either cells or annotations
   writeImageRegion(annotationLabelServer, requestROI, pathOutput+"-positive-stroma-above+1.png")

   //To get the image behind the objects, you would simply use writeImageRegion
  // writeImageRegion(getCurrentServer(), requestROI, pathOutput+"-original.jpg")
```

Annexure 2.6 QuPath intensity threshold parameters

1. Intensity threshold values per category

Intensity category	Threshold value	Colour
0	< 0.19	Blue
1+	0.19 to < 0.8	Yellow
2+	0.8 to < 1.9	Orange
Re3+	≥ 1.9	Red

2. Screenshot of data input for positive cell detection
   - Example of p53 nuclear detection with set thresholds inputted in the last category "Intensity threshold parameters"
   - Colours on the right correspond to the four threshold categories (see above table)

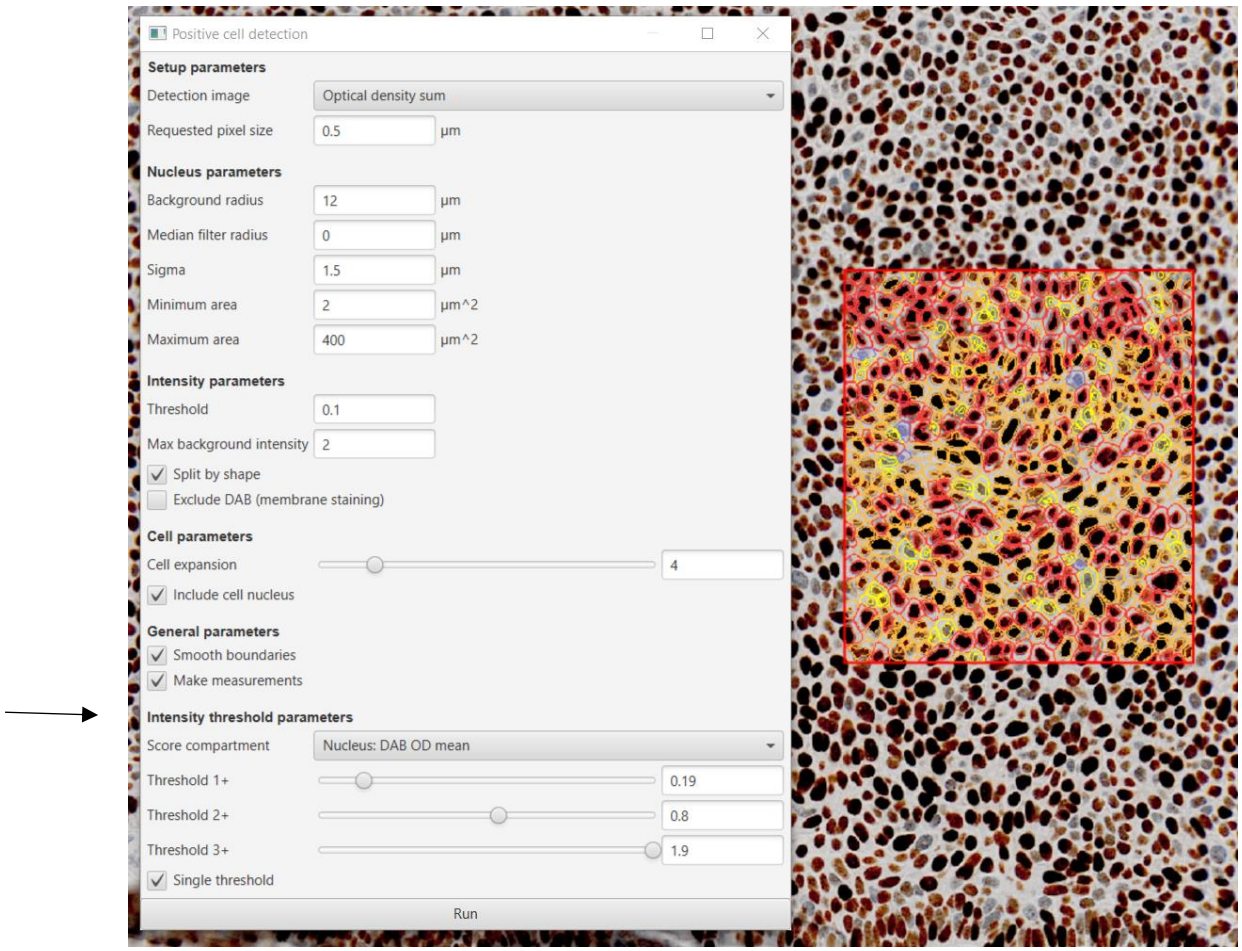

Annexure 2.7 Scoring systems utilised in our study

- BCL-2

1. Subcellular localisation interpreted: nuclear and cytoplasmic
2. Intensity based on QuPath intensity value cut-offs (Annexure 2.6):
   - 0 No staining
   - 1+ Weak staining
   - 2+ Moderate staining
   - 3+ Strong staining
3. Proportion: *based on Ramdial et al*
   - 0 – 5.0% Negative
   - 6.0 – 25% 1+
   - 26 – 50% 2+
   - 51 – 75% 3+
   - > 75% 4+

- P53

1. Subcellular localisation interpreted: nuclear only
2. Intensity based on QuPath intensity value cut-offs (Annexure 2.6): as above in BCL-2
3. Proportion: *based on Sungu et al* – as above in BCL-2

- CD138 in the tumour:

1. Subcellular localisation interpreted: membranous and cytoplasmic
2. Intensity based on QuPath intensity value cut-offs (Annexure 2.6): as above in BCL-2
3. Score: *based on Kind et al*

No staining	negative	
≤70% of cells	1+	Weakly positive
≤30% of cells	2+	
>70% of cells	1+	Moderately positive
30% to 70% of cells	2+	
≤30% of cells	3+	
>70% of cells	2+	Strongly positive
>30% of cells	3+	

- CD138 in the stroma

1. Localisation observed: cellular (lymphocytes, stromal cells), matrix or both
2. Intensity based on QuPath intensity value cut-offs (Annexure 2.6): as above in BCL-2
3. Proportion: percentage documented

Annexure 2.8 Example of data collection in the Redcap database

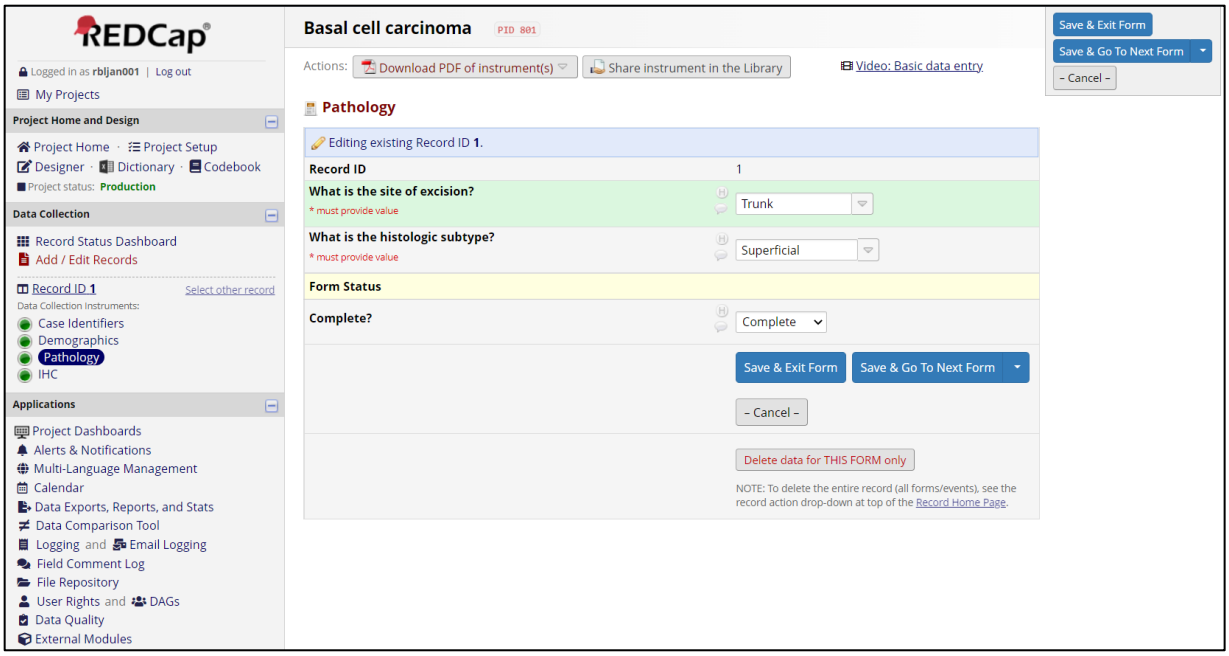

Screenshot of the "Pathology" section for data input for Record 1

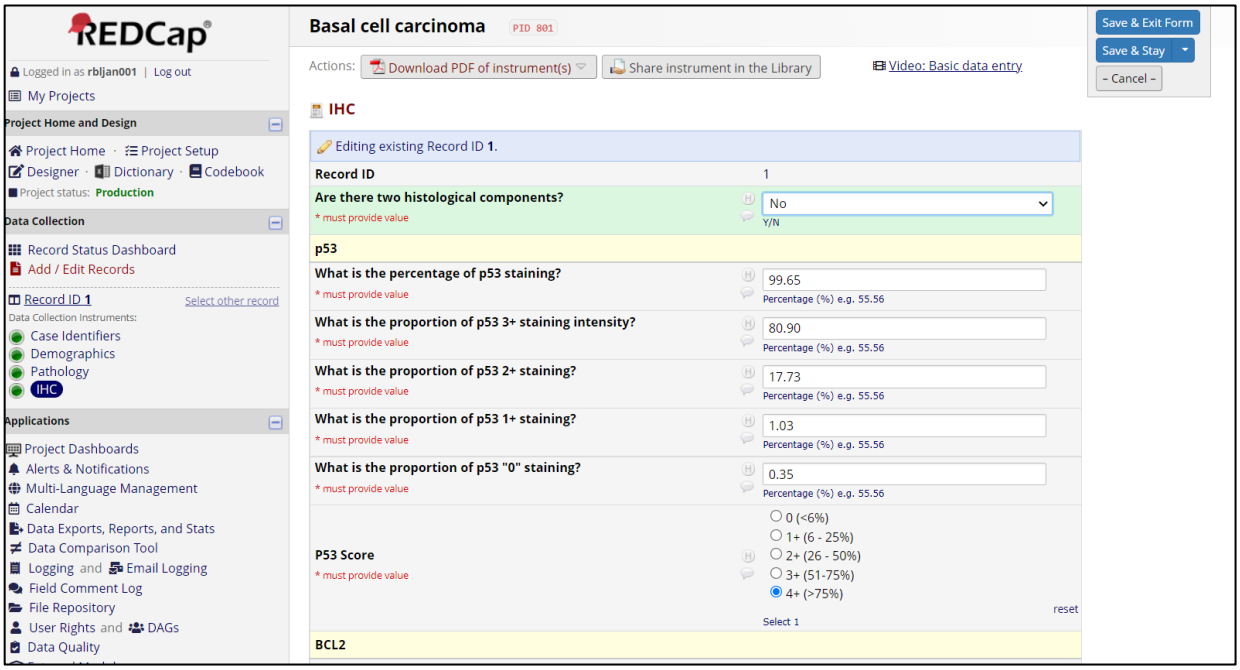

Screenshot of the "IHC – P53" section for data input for Record 1

Annexure 3.1 Anonymised raw data

Record ID	Duplicate	Age	Sex	Site	Region if on head and neck	Mixed versus nonmbed BCC	Histological subtype	Risk category	p53 IHC	Overall % p53	p53 3+ %	p53 2+ %	p53 1+ %	p53 '0' %	P53 Score	BCL2 IHC	Overall % BCL-2	BCL-2 3+ %	BCL-2 2+ %	BCL-2 1+ %	BCL-2 '0' %	BCL2 Score	Labelling
1	No	58	Female	Trunk	Not applicable	Non-mixed	Superficial	Low risk	Y	99,65	80,9	17,73	1,03	0,35	4	Y	89,75	0	11,53	78,23	10,25		H
2	No	76	Female	Missing	Not applicable	Non-mixed	Nodular	Low risk	Y	0,65	0	0,05	0,6	99,35	0	Y	1,23	0	0	1,23	98,78	0	
3	No	77	Male	Limbs	Not applicable	Non-mixed	Nodular	Low risk	Y	97,38	63,23	21,23	12,93	2,63	4	Y	1,33	0	0,03	1,3	98,68	0	
4	No	80	Female	Limbs	Not applicable	Non-mixed	Nodular	Low risk	Y	92,15	7,15	37,1	47,9	7,85	4	Y	86,08	0	11,83	74,25	13,93	4	H
5	No	48	Male	Head and Neck	Nose	Non-mixed	Superficial	Low risk	Y	1,93	0,03	0,58	1,33	98,08	0	Y	7,43	0	0,13	7,3	92,58	1	L
6	No	60	Male	Head and Neck	Scalp	Non-mixed	Nodular	Low risk	Y	91,7	60,63	15,73	15,35	8,3	4	Y	72,8	0	19,28	53,53	27,2	3	H
7	No	57	Male	Head and Neck	Lip	Non-mixed	Superficial	Low risk	Y	97,12	23,8	38,8	34,53	2,88	4	Y	57,15	0	0,05	57,1	42,85	3	H
8	No	74	Male	Head and Neck	Other	Non-mixed	Nodular	Low risk	Y	74,65	3,08	19,95	51,63	25,35	3	Y	94,1	0	7,85	86,25	5,9	4	H
9	No	84	Female	Limbs	Not applicable	Non-mixed	Nodular	Low risk	Y	28,9	2,25	10,86	15,79	71,1	2	Y	51,55	0	0,13	51,43	48,45	3	H
10	No	82	Male	Trunk	Not applicable	Non-mixed	Nodular	Low risk	Y	13,33	0,3	1,83	11,2	86,68	1	Y	6,65	0	0,03	6,63	93,35	1	L
11	No	60	Male	Limbs	Not applicable	Non-mixed	Nodular	Low risk	Y	55,07	37,48	11,48	6,13	44,93	3	Y	0,48	0	0	0,48	99,53	0	
12	No	47	Male	Missing	Not applicable	Non-mixed	Superficial	Low risk	Y	98,58	55,4	37,15	6,03	1,43	4	Y	7,35	0	0	7,35	92,65	1	L
13	No	44	Female	Trunk	Not applicable	Non-mixed	Superficial	Low risk	Y	95,25	6,43	25,5	63,33	4,75	4	Y	90,5	0,25	23,18	67,08	9,5	4	H
14	No	71	Male	Trunk	Not applicable	Non-mixed	Nodular	Low risk	Y	99,28	61,73	32,5	5,05	0,73	4	Y	1,43	0	0,03	1,4	98,58	0	
15	No	70	Male	Trunk	Not applicable	Non-mixed	Superficial	Low risk	Y	67,45	5,65	22,4	39,4	32,55	3	Y	42,88	0	0,13	42,75	57,13	2	L
16	No	49	Male	Trunk	Not applicable	Non-mixed	Nodular	Low risk	Y	81,95	5,35	19,9	56,7	18,05	4	Y	99,75	0,4	57,63	41,73	0,25	4	H
17	No	91	Female	Head and Neck	Ear	Non-mixed	Nodular	Low risk	Y	99,58	77,65	19,58	2,35	0,43	4	Y	66,67	0,03	5,35	61,3	33,33	3	H
18	No	75	Male	Trunk	Not applicable	Non-mixed	Superficial	Low risk	Y	99,94	83,03	14,08	2,83	0,06	4	Y	42,03	0	0,34	41,69	57,97	2	L
19	No	54	Female	Head and Neck	Face	Non-mixed	Nodular	Low risk	Y	99,91	85,09	13,62	1,21	0,09	4	Y	3,14	0	0	3,14	96,86	0	
20	No	56	Female	Limbs	Not applicable	Non-mixed	Nodular	Low risk	Y	93,45	33,15	39,35	20,95	6,55	4	Y	69,42	0	0,23	69,2	30,58	3	H
21	No	59	Male	Head and Neck	Neck	Non-mixed	Nodular	Low risk	Y	93,23	17,65	40,63	34,95	6,78	4	Y	71,23	0	11,15	60,08	28,78	3	H
22	No	73	Male	Head and Neck	Neck	Non-mixed	Nodular	Low risk	Y	79,6	2,78	15,45	61,38	20,4	4	Y	18,68	0	0	18,68	81,33	1	L
23	No	85	Female	Head and Neck	Neck	Non-mixed	Superficial	Low risk	Y	78,42	10,64	31,83	35,94	21,58	4	Y	94,61	0	19,53	75,07	5,39	4	H
24	No	68	Male	Head and Neck	Face	Non-mixed	Nodular	Low risk	Y	4,23	0	0,08	4,15	95,78	0	Y	35,52	0	3,9	31,63	64,48	2	L
25	No	59	Male	Head and Neck	Face	Non-mixed	Nodular	Low risk	Y	99,4	88,8	9,95	0,65	0,6	4	Y	23,88	0	0	23,88	76,13	1	L
26	No	87	Male	Limbs	Not applicable	Non-mixed	Nodular	Low risk	Y	86,28	35,83	37,15	13,3	13,73	4	Y	18,75	0	0	18,75	81,25	1	L

27	No	66	Female	Trunk	Not applicable	Non-mixed	Superficial	Low risk	Y	99,98	75,75	23,15	1,08	0,03	4	Y	17,7	0	0	17,7	82,3	1	L
28	No	89	Female	Head and Neck	Face	Non-mixed	Nodular	Low risk	Y	86,42	8,93	40,23	37,28	13,58	4	Y	4,13	0	0	4,13	95,88	0	
29	No	79	Female	Limbs	Not applicable	Non-mixed	Nodular	Low risk	Y	84,8	9	27,23	48,58	15,2	4	Y	0,45	0	0	0,45	99,55	0	
30	No	73	Male	Limbs	Not applicable	Non-mixed	Nodular	Low risk	Y	90,12	8,08	30,98	51,08	9,88	4	Y	4,68	0	0	4,68	95,33	0	
31	No	80	Female	Head and Neck	Nose	Non-mixed	Nodular	Low risk	Y	92,1	1,65	16,65	73,8	7,9	4	Y	10,25	0	0	10,25	89,75	1	L
32	No	82	Male	Head and Neck	Face	Non-mixed	Nodular	Low risk	Y	98,95	67,55	29,18	2,23	1,05	4	Y	10,42	0	0	10,42	89,58	1	L
33	No	78	Male	Trunk	Not applicable	Non-mixed	Nodular	Low risk	Y	0,28	0	0,05	0,23	99,73	0	Y	9,2	0	0,03	9,18	90,8	1	L
34	No	81	Male	Head and Neck	Neck	Non-mixed	Nodular	Low risk	Y	99,62	60,73	36,93	1,98	0,38	4	Y	66,17	0	1,78	64,4	33,83	3	H
35	No	67	Male	Head and Neck	Face	Non-mixed	Nodular	Low risk	Y	99,48	59,48	31,33	8,68	0,53	4	Y	8,73	0	0	8,73	91,28	1	L
36	No	76	Male	Head and Neck	Ear	Non-mixed	Superficial	Low risk	Y	98,9	86,75	10,68	1,48	1,1	4	Y	17,97	0	0	17,97	82,03	1	L
37	Yes	85	Female	Limbs	Not applicable	Mixed	Nodular	Low risk	Y	84,08	3,5	39,08	41,5	15,93	4	Y	4,23	0	0,03	4,2	95,78	0	
38	No	79	Male	Head and Neck	Nose	Non-mixed	Nodular	Low risk	Y	83,53	7,53	32,33	43,68	16,48	4	Y	2,2	0	0	2,2	97,8	0	
39	No	68	Female	Head and Neck	Nose	Non-mixed	Nodular	Low risk	Y	77,33	3,88	24,55	48,9	22,68	4	Y	27,75	0	0,65	27,1	72,25	2	L
40	No	72	Male	Trunk	Not applicable	Non-mixed	Nodular	Low risk	Y	99,98	86,9	12,55	0,53	0,03	4	Y	32,38	0	0,55	31,83	67,63	2	L
41	No	89	Female	Head and Neck	Nose	Non-mixed	Superficial	Low risk	Y	99,52	81,53	17,48	0,53	0,48	4	Y	5,1	0	0	5,1	94,9	0	
42	No	82	Male	Head and Neck	Nose	Non-mixed	Nodular	Low risk	Y	92,5	33,45	33,88	25,18	7,5	4	Y	24,05	0	0,13	23,93	75,95	1	L
43	No	50	Male	Limbs	Not applicable	Non-mixed	Nodular	Low risk	Y	90,2	18,53	39,58	32,1	9,8	4	Y	45,35	0	0	45,35	54,65	2	L
44	No	71	Male	Head and Neck	Nose	Non-mixed	Nodular	Low risk	Y	98,25	3,33	27,2	67,73	1,75	4	Y	64,58	0	4,55	60,03	35,43	3	H
45	Yes	68	Female	Trunk	Not applicable	Mixed	Nodular	Low risk	Y	99,75	90,7	8,4	0,65	0,25	4	Y	45,92	0,03	0,6	45,3	54,08	2	L
46	Yes	32	Male	Head and Neck	Neck	Mixed	Superficial	Low risk	Y	99,68	46,94	48,55	4,19	0,32	4	Y	39,04	0	1,91	37,13	60,96	2	L
47	No	72	Male	Trunk	Not applicable	Non-mixed	Nodular	Low risk	Y	96,2	29,18	55,25	11,78	3,8	4	Y	0,5	0	0	0,5	99,5	0	
48	No	78	Male	Limbs	Not applicable	Non-mixed	Nodular	Low risk	Y	96,5	22,55	50,68	23,28	3,5	4	Y	0	0	0	0	100	0	
49	No	54	Male	Head and Neck	Ear	Non-mixed	Infiltrating	High risk	Y	95,93	50,5	25,88	19,55	4,08	4	Y	21,88	0	0	21,88	78,13	1	L
50	No	72	Male	Limbs	Not applicable	Non-mixed	Basosquamous	High risk	Y	88,75	37,13	25,8	25,83	11,25	4	Y	13,23	0	0,03	13,2	86,78	1	L
51	No	39	Male	Head and Neck	Scalp	Non-mixed	Infiltrating	High risk	Y	19,02	0,03	1,28	17,73	80,98	1	Y	9,78	0	0,05	9,73	90,23	1	L
52	Yes	73	Male	Trunk	Not applicable	Mixed	Nodular	Low risk	Y	91,2	27,55	41,33	22,33	8,8	4	Y	93,7	0	3,83	89,88	6,3	4	H
53	No	67	Male	Head and Neck	Face	Non-mixed	Infiltrating	High risk	Y	99,38	86,25	11,6	1,53	0,63	4	Y	62,3	0	2,15	60,15	37,7	3	H
54	No	69	Male	Trunk	Not applicable	Non-mixed	Infiltrating	High risk	Y	96,55	44,33	46,58	5,65	3,45	4	Y	18,18	0	0,03	18,15	81,83	1	L
55	No	77	Female	Limbs	Not applicable	Non-mixed	Infiltrating	High risk	Y	98,75	56,85	35,45	6,45	1,25	4	Y	24,38	0	1,13	23,25	75,63	1	L

56	No	85	Male	Head and Neck	Ear	Non-mixed	Infiltrating	High risk	Y	96,85	42,58	31,2	23,08	3,15	4	Y	3,43	0	0	3,43	96,58	0	
57	No	76	Female	Head and Neck	Around the eye	Non-mixed	Infiltrating	High risk	Y	41,6	0,35	4,88	36,38	58,4	2	Y	22,4	0	0,13	22,28	77,6	1	L
58	Yes	71	Male	Head and Neck	Neck	Mixed	Nodular	Low risk	Y	2,63	0,08	0,78	1,76	97,38	0	Y	57,95	0	0,33	57,63	42,05	3	H
59	Yes	73	Female	Head and Neck	Ear	Mixed	Nodular	Low risk	Y	99,75	86,13	12,48	1,15	0,25	4	Y	7,75	0	0,05	7,7	92,25	1	L
60	Yes	70	Male	Head and Neck	Face	Mixed	Nodular	Low risk	Y	96,33	55,23	26,98	14,13	3,68	4	Y	13,1	0	0	13,1	86,9	1	L
61	No	71	Male	Head and Neck	Face	Non-mixed	Infiltrating	High risk	Y	99,08	69,7	25,55	3,83	0,93	4	Y	73,1	0	2,45	70,65	26,9	3	H
62	No	74	Male	Head and Neck	Ear	Non-mixed	Infiltrating	High risk	Y	99,83	85,35	14,2	0,28	0,18	4	Y	96,83	0,03	21,48	75,33	3,18	4	H
63	No	47	Female	Head and Neck	Around the eye	Non-mixed	Sclerosing/ morphoeic	High risk	Y	0,58	0	0,05	0,53	99,43	0	Y	2,83	0	0,03	2,8	97,18	0	
64	No	47	Male	Trunk	Not applicable	Non-mixed	Micronodular	High risk	Y	97,7	67,63	25,4	4,68	2,3	4	Y	8,18	0	0,08	8,1	91,83	1	L
65	No	94	Female	Head and Neck	Ear	Non-mixed	Infiltrating	High risk	Y	98,62	69,13	24,78	4,73	1,38	4	Y	32,8	0	7,43	25,38	67,2	2	L
66	No	55	Female	Head and Neck	Face	Non-mixed	Infiltrating	High risk	Y	98,47	66,62	28,01	3,85	1,53	4	Y	48,55	0	0,03	48,52	51,45	2	L
67	No	54	Male	Head and Neck	Neck	Non-mixed	Basosquamous	High risk	Y	52,55	3,18	13,9	35,48	47,45	3	Y	1,88	0	0	1,88	98,13	0	
68	Yes	65	Female	Head and Neck	Nose	Mixed	Nodular	Low risk	Y	99,95	86,9	13	0,05	0,05	4	Y	55,43	0	1,25	54,18	44,58	3	H
69	No	74	Male	Head and Neck	Face	Non-mixed	Infiltrating	High risk	Y	0,88	0,03	0,13	0,73	99,13	0	Y	2,55	0	0	2,55	97,45	0	
70	No	72	Female	Head and Neck	Face	Non-mixed	Infiltrating	High risk	Y	92,88	8,75	33,83	50,3	7,13	4	Y	4,78	0	0	4,78	95,23	0	
71	Yes	58	Male	Head and Neck	Neck	Mixed	Superficial	Low risk	Y	99,95	88,53	10,6	0,83	0,05	4	Y	5,33	0	0	5,33	94,68	0	
72	Yes	69	Male	Head and Neck	Face	Mixed	Nodular	Low risk	Y	99,48	75,95	20,68	2,85	0,53	4	Y	39,12	0	2,68	36,45	60,88	2	L
73	No	43	Male	Head and Neck	Face	Non-mixed	Infiltrating	High risk	Y	98,15	77,75	18,15	2,25	1,85	4	Y	34,9	0	0,2	34,7	65,1	2	L
75	No	42	Female	Head and Neck	Face	Non-mixed	Infiltrating	High risk	Y	33	0,5	5,48	27,03	67	2	Y	1,45	0	0	1,45	98,55	0	
76	No	81	Female	Trunk	Not applicable	Non-mixed	Infiltrating	High risk	Y	94,85	24,45	54,05	16,35	5,15	4	Y	63,95	0	1,53	62,43	36,05	3	H
77	Yes	78	Female	Head and Neck	Ear	Mixed	Nodular	Low risk	Y	85,42	13,13	35,28	37,03	14,56	4	Y	6,52	0	0	6,52	93,48	1	L
78	Yes	78	Male	Limbs	Not applicable	Mixed	Nodular	Low risk	Y	64,18	6,75	11,5	45,93	35,83	3	Y	53,15	0	1,68	51,48	46,85	3	H
79	Yes	96	Male	Head and Neck	Face	Mixed	Nodular	Low risk	Y	42,35	0,28	8,8	33,28	57,65	2	Y	63,45	0	0,18	63,28	36,55	3	H
80	No	84	Female	Other	Not applicable	Non-mixed	Infiltrating	High risk	Y	99,9	89,53	9,5	0,87	0,1	4	Y	1,99	0	0	1,99	98,01	0	
81	Yes	68	Male	Head and Neck	Face	Mixed	Nodular	Low risk	Y	5,2	0,05	1,03	4,13	94,8	0	Y	91,65	0	16,18	75,48	8,35	4	H
82	No	77	Male	Trunk	Not applicable	Non-mixed	Infiltrating	High risk	Y	99,42	93,4	5,35	0,68	0,58	4	Y	67,67	0	0,63	67,05	32,33	3	H
83	No	66	Female	Head and Neck	Nose	Non-mixed	Infiltrating	High risk	Y	98,85	70,18	26,6	2,08	1,15	4	Y	38,17	0	0,28	37,9	61,83	2	L
84	No	82	Female	Limbs	Not applicable	Non-mixed	Infiltrating	High risk	Y	98,45	55,05	30,88	12,53	1,55	4	Y	1,23	0	0	1,23	98,78	0	
85	Yes	79	Female	Head and Neck	Neck	Mixed	Nodular	Low risk	Y	98	67,23	26,68	4,1	2	4	Y	95,23	0,08	20,23	74,93	4,78	4	H

86	No	64	Female	Head and Neck	Around the eye	Non-mixed	Infiltrating	High risk	Y	95,9	39,68	40,15	16,08	4,1	4	Y	94,47	0	7,48	87	5,53	4	H
87	No	70	Male	Limbs	Not applicable	Non-mixed	Infiltrating	High risk	Y	99,12	76,75	21,25	1,13	0,88	4	Y	0,53	0	0	0,53	99,48	0	
88	Yes	77	Male	Head and Neck	Face	Mixed	Nodular	Low risk	Y	66,85	2,95	11,48	52,43	33,15	3	Y	21,25	0	0	21,25	78,75	1	L
89	Yes	81	Male	Head and Neck	Face	Mixed	Nodular	Low risk	Y	12,7	0,6	3,7	8,4	87,3	1	Y	8,48	0	0	8,48	91,53	1	L
90	No	68	Male	Head and Neck	Nose	Non-mixed	Micronodular	High risk	Y	98,95	72,95	20,58	5,43	1,05	4	Y	1	0	0	1	99	0	
91	No	82	Male	Head and Neck	Face	Non-mixed	Superficial	Low risk	Y	85,45	4,48	22,18	58,8	14,55	4	Y	45,15	0	1,68	43,48	54,85	2	L
92	No	83	Male	Head and Neck	Nose	Non-mixed	Nodular	Low risk	Y	72,6	7,53	25,13	39,95	27,4	3	Y	81,17	0	1,35	79,83	18,83	4	H
93	No	83	Male	Head and Neck	Neck	Non-mixed	Nodular	Low risk	Y	76,68	1,18	12,75	62,75	23,33	4	Y	82,17	0	3,23	78,95	17,83	4	H
94	No	49	Female	Head and Neck	Face	Non-mixed	Nodular	Low risk	Y	98,45	39,53	37,95	20,98	1,55	4	Y	72,52	0	4,48	68,05	27,48	3	H
95	Yes	86	Male	Head and Neck	Scalp	Mixed	Superficial	Low risk	Y	99,4	55,33	38,38	5,7	0,6	4	Y	0,83	0	0	0,83	99,18	0	
96	No	77	Male	Limbs	Not applicable	Non-mixed	Superficial	Low risk	Y	99,83	80,85	17,25	1,73	0,18	4	Y	19,38	0	0,08	19,3	80,63	1	L
97	No	58	Female	Head and Neck	Nose	Non-mixed	Superficial	Low risk	Y	37,9	2,18	15,75	19,98	62,1	2	Y	70,23	0	1	69,23	29,78	3	H
98	No	76	Male	Head and Neck	Ear	Non-mixed	Superficial	Low risk	Y	32,07	0,23	3,98	27,88	67,93	2	Y	6,75	0	0	6,75	93,25	1	L
99	No	67	Male	Head and Neck	Face	Non-mixed	Nodular	Low risk	Y	97,85	38,35	46,63	12,88	2,15	4	Y	13,83	0	0	13,83	86,18	1	L
100	No	60	Male	Trunk	Not applicable	Non-mixed	Nodular	Low risk	Y	81	19,25	34,78	26,98	19	4	Y	73,1	0	2,4	70,7	26,9	3	H
101	No	40	Male	Head and Neck	Face	Non-mixed	Nodular	Low risk	Y	43,75	1,8	7,65	34,3	56,25	2	Y	11,95	0	0	11,95	88,05	1	L
102	No	87	Male	Head and Neck	Ear	Non-mixed	Nodular	Low risk	Y	99,1	44,63	46,95	7,53	0,9	4	Y	23,97	0	0,38	23,6	76,03	1	L
103	No	86	Male	Trunk	Not applicable	Non-mixed	Nodular	Low risk	Y	0,95	0,03	0,3	0,63	99,05	0	Y	76,9	0,33	23,23	53,35	23,1	4	H
104	No	80	Male	Head and Neck	Ear	Non-mixed	Nodular	Low risk	Y	67,12	4,38	26,73	36,03	32,88	3	Y	98,55	0	5,8	92,75	1,45	4	H
105	No	71	Female	Head and Neck	Nose	Non-mixed	Nodular	Low risk	Y	97,97	47,13	40,7	10,15	2,03	4	Y	56,77	0	1,6	55,18	43,23	3	H
37a	Yes	85	Female	Limbs	Not applicable	Mixed	Infiltrating	High risk	Y	95,97	20,48	42,2	33,3	4,03	4	Y	36,88	0,03	0,95	35,9	63,13	2	L
45a	Yes	68	Female	Trunk	Not applicable	Mixed	Infiltrating	High risk	Y	98,45	85,63	10,9	1,93	1,55	4	Y	27,07	0	0,03	27,05	72,93	2	L
46a	Yes	32	Male	Head and Neck	Neck	Mixed	Infiltrating	High risk	N	missing	missing	missing	missing	missing	missing	N	missing	missing	missing	missing	missing	missing	
52a	Yes	73	Male	Trunk	Not applicable	Mixed	Infiltrating	High risk	Y	96,1	25,1	53,83	17,18	3,9	4	Y	84,78	0	1,5	83,28	15,23	4	H
58a	Yes	71	Male	Head and Neck	Neck	Mixed	Infiltrating	High risk	Y	0,6	0	0,1	0,5	99,4	0	Y	16,9	0	0,1	16,8	83,1	1	L
59a	Yes	73	Female	Head and Neck	Ear	Mixed	Infiltrating	High risk	Y	99,85	75,15	20,78	3,93	0,15	4	Y	15,4	0	0,03	15,38	84,6	1	L
60a	Yes	70	Male	Head and Neck	Face	Mixed	Infiltrating	High risk	N	missing	missing	missing	missing	missing	missing	Y	9,48	0	0	9,48	90,53	1	L
68a	Yes	65	Female	Head and Neck	Nose	Mixed	Sclerosing/ morphoeic	High risk	Y	99,35	75,13	20,83	3,4	0,65	4	Y	17,62	0	0	17,62	82,38	1	L
71a	Yes	58	Male	Head and Neck	Neck	Mixed	Infiltrating	High risk	Y	99,15	87,03	9,58	2,55	0,85	4	Y	6,98	0	0,08	6,9	93,03	1	L

72a	Yes	69	Male	Head and Neck	Face	Mixed	Infiltrating	High risk	Y	99,7	84,6	13,18	1,93	0,3	4	Y	10,5	0	0,03	10,48	89,5	1	L
77a	Yes	78	Female	Head and Neck	Ear	Mixed	Infiltrating	High risk	Y	71,55	0,63	8,35	62,58	28,45	3	N	missing	missing	missing	missing	missing	missing	
78a	Yes	78	Male	Limbs	Not applicable	Mixed	Sclerosing/ morphoeic	High risk	Y	91,27	10,28	25,43	55,58	8,73	4	Y	5,15	0	0	5,15	94,85	0	
79a	Yes	96	Male	Head and Neck	Face	Mixed	Infiltrating	High risk	Y	43,1	1,03	13,05	29,03	56,9	2	Y	20,38	0	0,1	20,28	79,63	1	L
81a	Yes	68	Male	Head and Neck	Face	Mixed	Infiltrating	High risk	Y	5,2	0,15	1,73	3,33	94,8	0	Y	59,13	0	2,08	57,05	40,88	3	H
85a	Yes	79	Female	Head and Neck	Neck	Mixed	Infiltrating	High risk	Y	97,08	36,13	48,7	12,25	2,93	4	Y	46,42	0	1	45,43	53,58	2	L
88a	Yes	77	Male	Head and Neck	Face	Mixed	Infiltrating	High risk	Y	57,4	5,28	22	30,13	42,6	3	Y	9,1	0	0,03	9,08	90,9	1	L
89a	Yes	81	Male	Head and Neck	Face	Mixed	Infiltrating	High risk	Y	50,22	2,48	9,03	38,73	49,78	2	Y	9,3	0	0	9,3	90,7	1	L
95a	Yes	86	Male	Head and Neck	Scalp	Mixed	Nodular	Low risk	Y	97,12	21,33	52,4	23,4	2,88	4	Y	8,88	0	0	8,88	91,13	1	L

Record ID	CD138 IHC tumour	Nuclear staining	Cytoplasmic staining	Membranous staining	Overall percentage CD138 in tumour	CD138 3+ percentage	CD138 2+ percentage	CD138 1+ percentage	CD138 '0' percentage	CD138 Scoring: as per table	CD138 IHC stroma	Stromal matrix	Stromal cells	Overall CD138 percentage stroma	CD138 3+ stroma percentage	CD138 2+ stroma percentage	CD138 1+ stroma percentage	CD138 '0' stroma percentage
1	Y	N	N	Y	100	32,37	66,03	1,6	0	Strongly positive	Y	N	Y	31,46	5,48	9,12	16,86	68,54
2	Y	N	N	Y	100	9,4	90,38	0,23	0	Strongly positive	Y	Y	Y	72,23	8,37	18,35	45,51	27,77
3	Y	N	N	Y	99,98	0,03	90,93	9,03	0,03	Strongly positive	Y	Y	Y	86,49	11,78	23,95	50,76	13,51
4	Y	N	N	Y	100	39,63	60,38	0	0	Strongly positive	Y	Y	Y	75,45	12,94	25,92	36,59	24,55
5	Y	N	N	Y	100	3,98	95,88	0,15	0	Strongly positive	Y	Y	Y	66,24	14,13	23,38	28,73	33,76
6	Y	N	N	Y	99,88	0,4	88,7	10,78	0,13	Strongly positive	Y	Y	Y	84,84	15,11	28,35	41,38	15,16
7	Y	N	N	Y	100	17,55	82,25	0,2	0	Strongly positive	Y	Y	Y	85,37	21,23	30,05	34,08	14,63
8	Y	Y	N	N	99,98	2,45	97,18	0,35	0,03	Strongly positive	Y	Y	Y	90,91	24,01	33,27	33,63	9,09
9	Y	N	N	Y	100	2,85	93,84	3,31	0	Strongly positive	Y	Y	Y	31,54	1,36	5,67	24,51	68,46
10	Y	Y	N	N	100	17,2	82,23	0,58	0	Strongly positive	Y	Y	Y	68,5	11,64	21,12	35,75	31,5
11	Y	N	N	Y	99,92	5,55	83,58	10,8	0,08	Strongly positive	Y	Y	Y	69,2	11,25	19,84	38,11	30,8
12	Y	N	N	Y	100	21,05	78,8	0,15	0	Strongly positive	Y	N	Y	67,6	13,89	21,43	32,28	32,4
13	Y	N	N	Y	100	89,24	10,66	0,1	0	Strongly positive	Y	N	Y	37,91	4,71	9,19	24,01	62,09
14	Y	N	N	Y	99,98	2,45	91,28	6,25	0,03	Strongly positive	Y	Y	Y	72,45	13,11	27,64	31,7	27,55
15	Y	N	N	Y	100	77,05	22,95	0	0	Strongly positive	Y	Y	Y	55,16	9,57	16,74	28,85	44,84
16	Y	N	N	Y	100	36,7	63,18	0,13	0	Strongly positive	Y	N	Y	8,63	0,25	1,16	7,21	91,37
17	Y	N	N	Y	100	12,88	86,7	0,43	0	Strongly positive	Y	Y	Y	87,52	18,85	33,53	35,14	12,48
18	Y	N	N	Y	97,13	0	61,7	35,43	2,87	Moderately positive	Y	Y	N	61,53	13,36	22,71	25,47	38,47

19	Y	N	Y	N	95,54	0	15,18	80,36	4,46	Moderately positive	Y	N	Y	6,86	0,37	1,08	5,41	93,14
20	Y	N	N	Y	100	11,55	81,1	7,35	0	Strongly positive	Y	Y	Y	78,8	13,45	26,22	39,13	21,2
21	Y	N	N	Y	100	41,23	58,78	0	0	Strongly positive	Y	Y	Y	80,12	17,92	25,7	36,5	19,88
22	Y	N	N	Y	100	0,5	99,43	0,08	0	Strongly positive	Y	Y	Y	74,41	6,78	20,4	47,23	25,59
23	Y	N	N	Y	100	79,9	19,59	0,51	0	Strongly positive	Y	N	Y	28,84	5,11	8	15,74	71,16
24	Y	N	N	Y	100	66,15	33,83	0,03	0	Strongly positive	Y	Y	Y	59,8	4,94	12,91	41,95	40,2
25	Y	N	N	Y	100	56,4	43,55	0,05	0	Strongly positive	Y	Y	Y	43,51	7,23	11,58	24,69	56,49
26	Y	N	N	Y	100	55,13	44,88	0	0	Strongly positive	Y	Y	Y	95,21	34,2	39,95	21,07	4,79
27	Y	N	N	Y	100	1,77	97,36	0,87	0	Strongly positive	Y	Y	Y	28,05	3,62	8,06	16,37	71,95
28	Y	N	N	Y	100	0,95	98,43	0,63	0	Strongly positive	Y	Y	Y	76,91	14,48	25,73	36,71	23,09
29	Y	N	N	Y	100	1,65	94,88	3,48	0	Strongly positive	Y	Y	Y	82,99	18,66	31,19	33,14	17,01
30	Y	N	N	Y	100	23,03	76,7	0,28	0	Strongly positive	Y	Y	Y	71,23	12,88	21,74	36,61	28,77
31	Y	N	N	Y	100	0,33	99,2	0,48	0	Strongly positive	Y	Y	Y	57,48	4,82	13,92	38,75	42,52
32	Y	N	N	Y	99,98	0,05	92,93	7	0,03	Strongly positive	Y	Y	Y	99,64	45,29	45,42	8,93	0,36
33	Y	N	N	Y	100	1,78	97,83	0,4	0	Strongly positive	Y	Y	Y	86,56	17,1	32,06	37,41	13,44
34	Y	N	N	Y	100	0	92,15	7,85	0	Strongly positive	Y	Y	Y	61,7	11,17	17,49	33,05	38,3
35	Y	N	N	Y	99,98	0,85	94,1	5,03	0,03	Strongly positive	Y	Y	Y	55,5	3,83	10,35	41,32	44,5
36	Y	N	N	Y	100	9,23	90,77	0	0	Strongly positive	Y	N	Y	58,47	13,16	19,97	25,35	41,53
37	Y	N	N	Y	100	15	84,5	0,5	0	Strongly positive	Y	Y	Y	71,91	11,25	21,68	38,98	28,09
38	Y	N	N	Y	100	1,45	96,85	1,7	0	Strongly positive	Y	Y	Y	60,57	3,22	10,36	47	39,43
39	Y	N	N	Y	100	0,53	97,9	1,58	0	Strongly positive	Y	Y	Y	60,13	4,86	12,12	43,15	39,87
40	Y	N	N	Y	100	42,05	57,9	0,05	0	Strongly positive	Y	Y	Y	70,27	13,69	23,96	32,62	29,73
41	Y	N	Y	N	100	5,13	94,85	0,03	0	Strongly positive	Y	Y	Y	88,09	19,66	31,78	36,65	11,91
42	Y	Y	N	N	100	10,1	89,18	0,73	0	Strongly positive	Y	Y	Y	95,41	30,02	38,56	26,83	4,59
43	Y	N	N	Y	100	0,45	94,13	5,43	0	Strongly positive	Y	Y	Y	83,77	12,89	26,5	44,38	16,23
44	Y	N	N	Y	100	26,68	72,7	0,63	0	Strongly positive	Y	Y	Y	92,16	18,92	31,67	41,57	7,84
45	Y	N	N	Y	99,98	18,28	79,88	1,83	0,03	Strongly positive	Y	Y	Y	47,21	5,6	10,77	30,84	52,79
46	Y	N	Y	N	99,43	9,82	68,42	21,19	0,57	Strongly positive	Y	Y	Y	22,41	1,16	3,47	17,77	77,59
47	Y	N	N	Y	100	1,5	98,2	0,3	0	Strongly positive	Y	Y	Y	92,94	19,87	36,28	36,79	7,06
48	Y	N	N	Y	100	0,43	97,75	1,83	0	Strongly positive	Y	N	Y	19,33	2,26	5,49	11,59	80,67

49	Y	N	N	Y	99,95	0,83	95,08	4,05	0,05	Strongly positive	Y	Y	Y	96	37,2	43,48	15,32	4
50	Y	N	Y	N	99,98	5,05	90,05	4,88	0,03	Strongly positive	Y	Y	N	90,39	27,82	34,37	28,2	9,61
51	Y	N	N	Y	100	3,25	87,65	9,1	0	Strongly positive	Y	Y	Y	82,61	21,59	29,69	31,33	17,39
52	Y	N	N	Y	100	5,53	92,35	2,13	0	Strongly positive	Y	Y	N	79,25	12,8	25,92	40,54	20,75
53	Y	N	N	Y	100	58,9	41	0,1	0	Strongly positive	Y	Y	Y	89,94	21,61	35,73	32,61	10,06
54	Y	N	N	Y	98,62	0,03	58,05	40,55	1,38	Moderately positive	Y	Y	N	90,49	28,18	38,24	24,07	9,51
55	Y	N	N	Y	99,98	5,13	94,18	0,68	0,03	Strongly positive	Y	Y	N	87,28	27,25	33,09	26,94	12,72
56	Y	Y	N	N	100	8,11	90,21	1,68	0	Strongly positive	Y	Y	Y	85,23	15,43	25,61	44,19	14,77
57	Y	N	N	Y	100	53,58	46,4	0,03	0	Strongly positive	Y	Y	Y	88	22,72	30,67	34,62	12
58	Y	N	N	Y	98,75	0	79,73	19,03	1,25	Strongly positive	Y	Y	Y	34,93	2,76	7,93	24,24	65,07
59	Y	N	N	Y	100	0	73,7	26,3	0	Strongly positive	Y	Y	Y	73,43	12,56	23,17	37,71	26,57
60	Y	N	N	Y	100	0,98	96,98	2,05	0	Strongly positive	Y	Y	Y	97,09	33,36	42,76	20,98	2,91
61	Y	Y	N	N	99,94	0,42	84,45	15,07	0,06	Strongly positive	Y	Y	Y	48,27	5,04	10,95	32,29	51,73
62	Y	N	N	Y	100	1,53	98,28	0,2	0	Strongly positive	Y	Y	Y	91,59	25,9	39,84	25,84	8,41
63	Y	Y	N	N	99,98	1,3	77,95	20,73	0,03	Strongly positive	Y	Y	Y	82,17	19,63	29,51	33,03	17,83
64	Y	N	Y	N	97,97	0	29,83	68,15	2,03	Moderately positive	Y	Y	Y	68,65	11,57	25,89	31,19	31,35
65	Y	N	N	Y	97,47	3,43	66	28,05	2,53	Moderately positive	Y	Y	Y	94,06	29,04	38,81	26,2	5,94
66	Y	N	N	Y	99,74	0,15	83,23	16,36	0,26	Strongly positive	Y	N	Y	52,3	5,91	14,05	32,34	47,7
67	Y	N	N	Y	95,65	0	24,68	70,98	4,35	Moderately positive	Y	Y	Y	69,03	6,34	19,2	43,5	30,97
68	Y	N	N	Y	100	57,7	42,28	0,03	0	Strongly positive	Y	N	Y	46,3	9,95	14,17	22,19	53,7
69	Y	N	N	Y	100	0,28	85,78	13,95	0	Strongly positive	Y	Y	Y	82,2	28,61	33,17	20,41	17,8
70	Y	N	N	Y	100	2,88	83,53	13,6	0	Strongly positive	Y	Y	Y	83,03	18,51	32,54	31,98	16,97
71	Y	N	N	Y	99,98	19,95	73,73	6,3	0,03	Strongly positive	Y	Y	Y	86,29	26,67	29,6	30,01	13,71
72	Y	N	N	Y	100	7,4	91,9	0,7	0	Strongly positive	Y	Y	Y	59,81	6,74	15,37	37,71	40,19
73	Y	Y	N	N	100	24,25	74,75	1	0	Strongly positive	Y	Y	Y	71,22	14,45	24,31	32,46	28,78
75	Y	Y	N	N	99,72	0,68	61,45	37,6	0,28	Moderately positive	Y	Y	Y	79,2	10,42	24,95	43,84	20,8
76	Y	N	N	Y	99,98	0,7	87,25	12,03	0,03	Strongly positive	Y	Y	Y	96,44	35,35	43,55	17,53	3,56
77	Y	N	N	Y	100	5,73	90,2	4,08	0	Strongly positive	Y	Y	Y	34,36	2,93	8,52	22,92	65,64
78	Y	N	N	Y	100	0,2	91,8	8	0	Strongly positive	Y	Y	Y	66,51	6,66	15,98	43,87	33,49
79	Y	N	N	Y	100	18,33	81,43	0,25	0	Strongly positive	Y	Y	Y	99,32	37,32	49,3	12,69	0,68

80	Y	N	N	Y	100	21,89	74,97	3,14	0	Strongly positive	Y	Y	Y	98,84	41,01	45,77	12,06	1,16
81	Y	N	N	Y	100	32,48	67,53	0	0	Strongly positive	Y	Y	Y	76,36	10,97	21,1	44,29	23,64
82	Y	N	N	Y	100	3,1	93,8	3,1	0	Strongly positive	Y	Y	Y	61,2	6,39	17,06	37,74	38,8
83	Y	N	N	Y	99,8	0,7	94,15	4,95	0,2	Strongly positive	Y	Y	Y	92,33	26,71	38,51	27,1	7,67
84	Y	N	N	Y	100	19,93	78,9	1,18	0	Strongly positive	Y	Y	Y	94,56	32,15	42,29	20,12	5,44
85	Y	N	N	Y	100	81,33	18,63	0,05	0	Strongly positive	Y	Y	Y	96,27	24,7	34,06	37,5	3,73
86	Y	N	N	Y	100	6,4	93,4	0,2	0	Strongly positive	Y	Y	Y	91,54	25,65	37,96	27,94	8,46
87	Y	N	N	Y	100	48,53	51,45	0,03	0	Strongly positive	Y	Y	Y	95,44	38	39,48	17,96	4,56
88	Y	N	N	Y	100	1,23	98,23	0,55	0	Strongly positive	Y	Y	Y	96,17	24,95	40,64	30,59	3,83
89	Y	N	N	Y	99,92	2,88	89,68	7,38	0,08	Strongly positive	Y	Y	Y	75,36	17,25	24,18	33,93	24,64
90	N	missing	missing	missing	missing	missing	missing	missing	missing	missing	N	missing	missing	missing	missing	missing	missing	missing
91	Y	Y	N	N	100	76,4	23,5	0,1	0	Strongly positive	Y	Y	Y	92,61	24,93	34,29	33,38	7,39
92	Y	N	N	Y	100	42,45	51,4	6,15	0	Strongly positive	Y	Y	Y	29,6	1,18	4,13	24,3	70,4
93	Y	N	N	Y	100	7,15	92,8	0,05	0	Strongly positive	Y	Y	Y	93,98	18,42	31,5	44,06	6,02
94	Y	N	N	Y	99,28	4,3	88,7	6,28	0,73	Strongly positive	Y	Y	Y	72,62	9,2	18,68	44,74	27,38
95	N	missing	missing	missing	missing	missing	missing	missing	missing	missing	Y	missing	missing	missing	missing	missing	missing	missing
96	Y	Y	N	N	100	23,23	76,68	0,1	0	Strongly positive	Y	Y	Y	69,9	13,91	20,24	35,76	30,1
97	Y	N	N	Y	99,98	2,18	86,55	11,25	0,03	Strongly positive	Y	N	Y	21,55	0,58	2,35	18,62	78,45
98	Y	N	N	Y	100	39,45	60,23	0,33	0	Strongly positive	Y	Y	Y	52,29	9,76	15,35	27,18	47,71
99	Y	N	N	Y	100	13,58	86,38	0,05	0	Strongly positive	Y	N	Y	51,97	6,84	13,94	31,2	48,03
100	Y	N	N	Y	100	43,78	56,18	0,05	0	Strongly positive	Y	N	Y	44,02	9,71	13,92	20,39	55,98
101	Y	N	N	Y	99,98	0,18	93,25	6,55	0,03	Strongly positive	Y	Y	Y	90,64	24,18	36,53	29,94	9,36
102	N	missing	missing	missing	missing	missing	missing	missing	missing	missing	N	missing	missing	missing	missing	missing	missing	missing
103	Y	Y	N	N	100	58,95	40,93	0,13	0	Strongly positive	Y	Y	Y	64,64	13,42	21,85	29,36	35,36
104	Y	N	N	Y	100	34,55	65,45	0	0	Strongly positive	Y	Y	Y	93,15	21,55	36,6	35	6,85
105	Y	N	N	Y	100	57,4	42,6	0	0	Strongly positive	Y	Y	Y	91,24	28,89	37,73	24,62	8,76
37a	Y	N	N	Y	100	9,28	90,28	0,45	0	Strongly positive	Y	Y	Y	90,93	20	35,4	35,53	9,07
45a	Y	Y	N	N	100	3,09	93,47	3,45	0	Strongly positive	Y	Y	Y	75,16	14,58	24,33	36,24	24,84
46a	N	missing	missing	missing	missing	missing	missing	missing	missing	missing	N	missing	missing	missing	missing	missing	missing	missing
52a	Y	N	Y	N	99,4	0,53	65,98	32,9	0,6	Moderately positive	Y	Y	N	79,85	18,42	29,76	31,67	20,15

58a	Y	N	N	Y	99,8	0,08	81,58	18,15	0,2	Strongly positive	Y	Y	Y	74,96	12,39	25,69	36,88	25,04
59a	Y	N	Y	N	100	4,38	93,7	1,93	0	Strongly positive	Y	Y	Y	89,76	21,21	35,24	33,31	10,24
60a	Y	N	N	Y	100	1,03	95,08	3,9	0	Strongly positive	Y	Y	Y	96,94	30,71	37,85	28,37	3,06
68a	Y	N	N	Y	100	22,05	77,83	0,13	0	Strongly positive	Y	Y	Y	93,37	27,84	39,41	26,12	6,63
71a	Y	N	N	Y	99,95	21,4	77,4	1,15	0,05	Strongly positive	Y	Y	Y	90,31	20,51	31,27	38,53	9,69
72a	Y	N	N	Y	99,98	0,13	90,18	9,68	0,03	Strongly positive	Y	Y	Y	52,77	5,6	13,69	33,48	47,23
77a	Y	N	N	Y	100	26,7	72,6	0,7	0	Strongly positive	Y	Y	Y	89,62	30,96	35,65	23,01	10,38
78a	Y	N	N	Y	99,95	0,15	96,73	3,08	0,05	Strongly positive	Y	Y	Y	99,81	42,55	51,2	6,06	0,19
79a	Y	N	N	Y	99,98	19,03	80,45	0,5	0,03	Strongly positive	Y	Y	Y	89,67	14,95	30,52	44,2	10,33
81a	Y	N	N	Y	100	2,83	96,73	0,45	0	Strongly positive	Y	Y	Y	93,02	20,81	35,61	36,6	6,98
85a	Y	Y	N	N	100	31,58	67,9	0,53	0	Strongly positive	Y	Y	Y	93,06	27,71	36,29	29,07	6,94
88a	Y	N	N	Y	100	6,6	91,5	1,9	0	Strongly positive	Y	Y	Y	88,8	21,19	35,05	32,57	11,2
89a	Y	N	Y	N	99,95	1,45	94,75	3,75	0,05	Strongly positive	Y	Y	Y	97,34	38,97	40,21	18,18	2,66
95a	Y	N	N	Y	100	45,58	54,35	0,08	0	Strongly positive	Y	N	Y	76,95	9,41	18,61	48,93	23,05